

Deformation and failure of polymer glasses

Citation for published version (APA):

Melick, van, H. G. H. (2002). *Deformation and failure of polymer glasses*. [Phd Thesis 1 (Research TU/e / Graduation TU/e), Mechanical Engineering]. Technische Universiteit Eindhoven.
<https://doi.org/10.6100/IR555099>

DOI:

[10.6100/IR555099](https://doi.org/10.6100/IR555099)

Document status and date:

Published: 01/01/2002

Document Version:

Accepted manuscript including changes made at the peer-review stage

Please check the document version of this publication:

- A submitted manuscript is the version of the article upon submission and before peer-review. There can be important differences between the submitted version and the official published version of record. People interested in the research are advised to contact the author for the final version of the publication, or visit the DOI to the publisher's website.
- The final author version and the galley proof are versions of the publication after peer review.
- The final published version features the final layout of the paper including the volume, issue and page numbers.

[Link to publication](#)

General rights

Copyright and moral rights for the publications made accessible in the public portal are retained by the authors and/or other copyright owners and it is a condition of accessing publications that users recognise and abide by the legal requirements associated with these rights.

- Users may download and print one copy of any publication from the public portal for the purpose of private study or research.
- You may not further distribute the material or use it for any profit-making activity or commercial gain
- You may freely distribute the URL identifying the publication in the public portal.

If the publication is distributed under the terms of Article 25fa of the Dutch Copyright Act, indicated by the "Taverne" license above, please follow below link for the End User Agreement:

www.tue.nl/taverne

Take down policy

If you believe that this document breaches copyright please contact us at:

openaccess@tue.nl

providing details and we will investigate your claim.

Deformation and failure of polymer glasses

CIP-DATA LIBRARY TECHNISCHE UNIVERSITEIT EINDHOVEN

Melick, Harold G.H. van

Deformation and failure of polymer glasses / by Harold G.H. van Melick. -
Eindhoven : Technische Universiteit Eindhoven, 2002.

Proefschrift. - ISBN 90-386-2923-0

NUGI 841

Trefwoorden: glasachtige polymeren / amorfe polymeren / deformatie / faalgedrag /
strain softening / strain hardening / crazing / craze-initiatie / localisatie

Subject headings: polymer glasses / amorphous polymers / deformation / failure /
strain softening / strain hardening / crazing / craze-initiation / localisation

Printed by the University Press Facilities, Eindhoven, the Netherlands.

Cover illustrations: Crazing in polystyrene; Necking in polystyrene at room temperature under superimposed pressure (6000 bars, performed at IRC Leeds); Remaining plastic indent with crazes after micro-indentation; Schematic representation of an RVE.

This research was financially supported by the Dutch Technology Foundation (STW) (Grant EWT.3766).

Deformation and failure of polymer glasses

PROEFSCHRIFT

ter verkrijging van de graad van doctor aan de
Technische Universiteit Eindhoven, op gezag van de
Rector Magnificus, prof.dr. R.A. van Santen, voor een
commissie aangewezen door het College voor
Promoties in het openbaar te verdedigen
op dinsdag 14 mei 2002 om 16.00 uur

door

Harold Geert Hendrik van Melick

geboren te Roermond

Dit proefschrift is goedgekeurd door de promotoren:

prof.dr.ir. H.E.H. Meijer

en

prof.dr.ir. F.P.T. Baaijens

Copromotor:

dr.ir. L.E. Govaert

Contents

Summary	vii
1 Introduction	1
References	4
2 Strain hardening behaviour of glassy polymers: influence of network density	5
2.1 Introduction	5
2.2 Materials and methods	8
2.3 Results	9
Dynamic Mechanical Thermal Analysis	9
Uniaxial compression tests	12
2.4 Discussion	14
2.5 Conclusions	16
References	17
3 Kinetics of ageing and re-embrittlement of mechanically rejuvenated polystyrene	19
3.1 Introduction	19
3.2 Experimental section	21
3.3 Results	23
Intrinsic behaviour	23
Predeformation	23
Creep tests	27
Density measurements	29
3.4 Discussion	30
References	32
4 Localisation phenomena in glassy polymers: influence of thermal and mechanical history	35
4.1 Introduction	35
4.2 Materials and Methods	37
4.3 Intrinsic deformation behaviour	38

Uniaxial compression tests	38
Numerical modelling	38
FEM model	42
4.4 Results	42
Deformation and localisation processes in polycarbonate	42
Deformation and localisation processes in polystyrene	48
4.5 Conclusions	53
References	53
5 Craze-initiation in glassy polymers: influence of strain rate, thermal history, and network density	57
5.1 Introduction	58
5.2 Materials and experimental methods	60
5.3 Numerical methods	62
5.4 Results	63
Materials characterisation	63
Indentation experiments	65
Identification of a craze-nucleation criterion	67
5.5 Conclusions	72
References	73
6 Near-surface mechanical properties of glassy polymers	77
6.1 Introduction	77
6.2 Numerical model	79
6.3 Materials and methods	82
6.4 Results and discussion	83
6.5 Conclusions	86
References	86
7 Prediction of brittle-to-ductile transitions in polystyrene	89
7.1 Introduction	90
7.2 Numerical modelling	91
7.3 Results	93
BDT induced by temperature	93
BDT induced by length-scale effects	97
7.4 Discussion and conclusions	99
References	101
8 Main conclusions	103
Samenvatting	105
Dankwoord	109
Curriculum Vitae	111

Summary

This thesis is composed of six papers in the field of deformation and failure of polymer glasses. Prediction of deformation and failure behaviour of polymers has become very important. In the last two decades considerable effort is addressed to the development of 3D constitutive models that were able to capture the visco-elastic and post-yield behaviour of glassy polymers. The compressible Leonov model, as developed in our group, proved to be a suitable model which provides an adequate description of this behaviour, including rate- and temperature-dependent yield, strain softening and strain hardening. However a failure criterion is still lacking.

Previous studies indicated that macroscopic deformation behaviour is dominated by the intrinsic post-yield behaviour. Improving the ductility should hence focus on avoiding localisation of strain by eliminating strain softening and promoting the contribution of the strain hardening. Although it is quite well established that strain hardening originates from the contribution of the entangled polymer network, the high strain hardening modulus compared to the rubber-modulus and its temperature dependence requires further investigation. The physical origin of strain softening is less well known, although it is reported that strain softening can be altered by thermal treatments and can even be eliminated by mechanical rejuvenation. The limited resistance to void nucleation and the build-up of high dilative stresses under certain loading conditions, show that decreasing strain softening and increasing strain hardening are not sufficient to achieve tough deformation behaviour. To circumvent these problems heterogeneity should be introduced in the structure to relieve the build-up of high hydrostatic stresses. For materials like polycarbonate and polyamide this results in a transition from crazing to shear yielding. For polystyrene this is only the case if the thickness of the ligaments within the structure are sufficiently small. The concept of a critical thickness suggests that an absolute length-scale is encountered. An absolute length-scale of the same order of magnitude as is found in mechanical tests, is also reported in polymer physics where a T_g -depression is found in thin polystyrene films.

In chapter 2 the influence of the network density on the strain hardening modulus is investigated. An increase in network density of polystyrene, achieved by cross-linking and blending with polyphenylene oxide results in a proportional increase in strain hardening modulus. It is discussed that the magnitude of the strain hardening modulus and its negative temperature dependence might originate from the time-scale of the stress-induced segmental mobility and that, on this time-scale, the secondary interac-

tions still play a significant role.

The transient deformation behaviour of mechanically rejuvenated polystyrene is studied in chapter 3. Although the recovery of yield stress and strain softening is independent of the molecular weight, the time to re-embrittlement proves to increase with increasing molecular weight. This is rationalised by the fact that the tensile strength of the material, and hence the recovered yield stress at which this strength is exceeded in a localised plastic zone, depends on the molecular weight.

The post-yield behaviour dominates the macroscopic deformation behaviour of amorphous polymers. In chapter 4 it is shown that polycarbonate with its moderate strain softening and strong strain hardening results in stable neck growth during deformation. By annealing the strain softening increases, leading to more severe localisation of strain and even brittle failure. The deformation mode can be predicted in a straight-forward manner using a stability analysis. The pronounced strain softening and weak strain hardening of polystyrene lead to extreme localisation of strain and explain that standard polystyrene can never be ductile. Elimination of strain softening by mechanical rejuvenation inhibits localisation of strain and results in (temporary) ductile deformation behaviour. Additional finite element simulations illustrate the route to improve ductility.

Since a failure criterion was still lacking in the finite element simulations employing the compressible Leonov model, micro-indentation experiments are used to generate crazes in a reproducible way. By evaluation of the local stress and strain distribution by finite element simulations, a critical hydrostatic stress of 40 MPa was found in polystyrene (provided that this event is preceded by plastic deformation) as a criterion for void nucleation. This criterion proved to be independent of thermal history and strain rate but proved to increase with network density.

By means of micro- and nano-indentations on polystyrene the influence of an absolute length-scale, as reported in other areas of polymer science, is investigated. For large indenters and indentation depth the experiments compare well to the length-scale independent finite element simulations, using bulk properties. For the smallest indenter (2.2 μm) and shallow indentation depth (100 nm) the resistance to indentation is much less than expected from the simulations, indicating that the mechanical properties near a free surface in polystyrene might differ from the bulk properties.

Using the criterion for void nucleation, as identified in chapter 5, brittle-to-ductile transitions (BDTs) were predicted by the deformation of a representative volume element (RVE). By increasing the temperature in the RVE, the overall stress level lowers in such a way that at 70°C the critical level of 40 MPa is not exceeded anymore in the simulations and hence a transition from crazing to shear yielding is achieved in polystyrene. The length-scale which is encountered experimentally and numerically in chapter 6 was incorporated in the RVE by assuming a gradient of increased temperature near free surfaces. At an interparticle distance of less than approximately 15 nm the critical value of 40 MPa is not exceeded anymore and crazing is hence inhibited. Both brittle-to-ductile transition compare well to experimental observations.

Chapter 1

Introduction

General introduction

With their ease of processing and fair mechanical and thermal properties, polymers offer an attractive compromise in many structural applications. Nowadays, numerical methods, like finite elements simulations, are commonly used in designing and optimising such applications. The reliability and suitability of numerical methods is determined by their ability to capture experimentally observed phenomena, giving understanding and yielding predictive capability.

In the past 15 years, considerable effort was directed towards the numerical simulation of deformation phenomena in polymers. The development of 3D constitutive models that were able to capture the non-linear visco-elastic and post-yield behaviour of glassy polymers started of with the work of Boyce and co-workers at MIT [1–4]. Her work was later followed by contributions of the group of van der Giessen [5, 6] and our group [7–15]. Tervoort *et al.* [7] developed the compressible Leonov model, a three dimensional constitutive equation which combines the the non-linear visco-elastic behaviour of an Eyring dashpot with the strain hardening behaviour of a neo-Hookean spring. Govaert *et al.* [8] extended this model by incorporating intrinsic strain softening, following the work of Hasan *et al.* [2]. This model is capable of describing the intrinsic deformation behaviour, including rate- and temperature dependent yield, strain softening and strain hardening, of glassy polymers like polystyrene, polycarbonate and polymethylmethacrylate under various loading conditions [8, 9].

A interesting application of the model is to use it in predicting the deformation behaviour of heterogeneous polymer systems, like e.g. polymer/rubber blends. Numerical studies on the evolution of deformation in micro-structures of various compositions are now well within reach and their consequences for macroscopic deformation behaviour is understood (see for instance the work of Smit *et al.* [13–15]). Application of this knowledge and understanding offers new opportunities for fast material evaluation and gives unique guidelines for further polymer development.

Limitations in applications of polymers often involves their low strain to break and impact toughness and hence a vast amount of experimental and numerical research was conducted in this area. Smit [15] proposed that toughness can only be improved, apart from by introducing heterogeneity to avoid crazing, by influencing the intrinsic post-yield behaviour; either by reducing strain softening, which does reduce the tendency for strain localisation, or by increasing the contribution of strain hardening which has a stabilising effect on the deformation behaviour. To influence those properties that are determined by processes on the molecular scale, a thorough knowledge of these processes is required. It is quite well established that strain hardening involves the cross-linked or entangled polymer network which is loaded at large strains. The exact relation between network density and strain hardening modulus is, however, still subject of discussion.

The physical origin of strain softening is much less established. It is known that it is dominated by the secondary interactions between polymer chains and hence influenced by temperature and strain rate in a similar way as the yield stress. Moreover, strain softening is known to be closely related to physical ageing. This can be witnessed from the fact that by thermal treatments (quenching and annealing) the amount of strain softening can be altered [16] and by mechanical treatments the strain softening can even be eliminated [17].

However, moderate strain softening and strong strain hardening does not imply tough deformation behaviour under all loading conditions. A well known example is the notch-brittleness of polycarbonate. Due to the confined development of the plastic zone underneath a notch, a build-up of high dilative stresses takes place in this region. At a sufficiently high hydrostatic stress, voids can nucleate in such a localised plastic zone which ultimately lead to crazing and macroscopic brittle failure. In polystyrene similar events can happen underneath a defect, making this polymer a brittle material.

For long it is recognised that the incorporation of a dispersed rubbery phase can relieve the build-up a high hydrostatic stresses within a structure, albeit on the expense of modulus and yield stress. This results in a transition from crazing to shear yielding and thus tough deformation behaviour in for instance polycarbonate and polyamide. For polystyrene, e.g high-impact polystyrene (HIPS), this ultimate mechanism is not reached and here the enhanced impact toughness is a result of the increase in the material volume participating in the deformation, by a process called *multiple crazing*, rather than the inhibition of crazing [18–20].

Wu [21] (for semi-crystalline) and van der Sanden [22] (for glassy polymers) proposed that a transition from crazing to shear yielding takes place if the ligaments within a filled polymer systems and the thickness in layered structures are reduced to below a critical value. Experimentally the existence of such a transition was found by van der Sanden [23] for highly filled polystyrene.

The concept of a critical interparticle distance relies on the explanation that an absolute length-scale is met in the material. Recently, also direct experimental evidence is reported on the existence of an absolute length-scale, and in thin polystyrene films a reduction of the glass-transition temperature (T_g) was found [24–26]. This phenomenon is rationalised by an enhanced segmental mobility of polymer chains near a free surface. This enhanced segmental mobility could, similar to thermally enhanced segmental mobility, induce in a reduction in yield stress and strain softening and result in more stable deformation behaviour.

Survey of this thesis

This thesis is composed of six chapters. The first two chapters investigate the intrinsic post-yield behaviour, with the emphasise on the influence of network density on strain hardening and the recovery of strain softening and its consequences the macroscopic deformation behaviour.

In chapter 2 the network density of polystyrene is increased by cross-linking and blending with polyphenylene oxide. By means of dynamic mechanical thermal analysis (DMTA) the network density is derived and compared to the strain hardening modulus measured in uniaxial compression tests. Moreover the influence of temperature on the strain hardening modulus is studied and discussed.

In chapter 3 the deformation of polystyrene after mechanical rejuvenation is investigated. Recovery of strain softening after mechanical rejuvenation and the temporary nature of the ductility enhancement are studied. The obvious question whether mechanical rejuvenation can be regarded as the ultimate thermal rejuvenation is investigated by analysing the creep behaviour of mechanically and thermally rejuvenated materials. All the experiments were performed on 3 grades of polystyrene with various molecular-weight distributions.

Next the consequences of intrinsic post-yield behaviour for the macroscopic deformation behaviour are demonstrated in chapter 4. Two (extreme) materials, polystyrene with a pronounced strain softening and weak strain hardening and polycarbonate with a moderate strain softening and strong strain hardening, are investigated by finite element simulations of a uniaxial tensile test. Thermo-mechanical treatments are used to tailor the amount of strain softening and monitor the influence on the macroscopic deformation. The necking process is analysed using a stability analysis analogous to the analysis proposed by Haward [27]. To conclude this chapter, finite element simulations are used to demonstrate to effect of temperature and incorporation of a rubbery phase on the deformation.

Although the compressible Leonov model in combination with finite element simulations [8, 13–15, 28] provide an excellent tool to study localisation of strain during deformation, a criterion to distinguish the onset of crazing and hence to predict brittle failure is still lacking. Therefore a craze initiation criterion is identified in chapter 5. By means of micro indentation, crazes are generated in a reproducible way. The local stress and strain distribution is evaluated by means of finite element simulations and used to identity a critical hydrostatic stress-based criterion for the nucleation of voids. This criterion is validated by investigating its dependence on thermal history, strain rate and network density.

The absolute length-scale, which is encountered in various fields of polymer engineering, is studied in chapter 6. Micro- and nano indentations, performed on distinct scales (mm to nm), are used to determine the force-displacement curves which are subsequently compared to finite element simulations of this test. The existence of an absolute length-scale could be confirmed.

Finally, in chapter 7, finite element simulations of the deformation of a representative volume element (RVE) are performed to investigate brittle-to-ductile transitions (BDTs) for polystyrene. The onset of crazing is evaluated using the criterion identified in chapter 5. The absolute length-scale found in chapter 6 is used. Both a temperature induced and length-scale induced BDT are indeed predicted, and are quantitatively in accor-

dance with experimental evidence.

Chapter 8 summarises some main conclusions of all previous chapters.

References

- [1] Boyce, M.C., Parks, D.M., Argon, A.S., *Mech. Mat.*, **7**, 15 (1988)
- [2] Hasan, O.A., Boyce, M.C., Li, X.S., Berko, S., *J. Pol. Sci., Part B: Pol. Phys.*, **31**, 185 (1993)
- [3] Arruda, E.M. and Boyce, M.C., *Int. J. Plast.*, **9**, 697 (1993)
- [4] Boyce, M.C., Arruda, E.M., Jayachandran, R., *Pol. Eng. Sci.*, **34**, 716 (1994)
- [5] Wu, P.D. and van der Giessen, E., *J. Mech. Phys. Solids*, **41**, 427 (1993)
- [6] Wu, P.D. and van der Giessen, E., *Int. J. Plast.*, **11**, 211 (1995)
- [7] Tervoort, T.A., Smit, R.J.M., Brekelmans, W.A.M., Govaert, L.E., *Mech. Time-depend. Mat.*, **1**, 269 (1998)
- [8] Govaert, L.E., Timmermans, P.H.M., Brekelmans, W.A.M., *J. Eng. Mat. Tech.*, **122**, 177 (2000)
- [9] Tervoort, T.A. and Govaert, L.E., *J. Rheol.*, **4**, 1263 (2000)
- [10] Tervoort, T.A., Klompen, E.T.J., Govaert, L.E., *J. Rheol.*, **40**, 779 (1996)
- [11] Smit, R.J.M., Brekelmans, W.A.M., Meijer, H.E.H., *Comp. Meth. Appl. Mech. Eng.*, **155**, 181 (1998)
- [12] Smit, R.J.M., Brekelmans, W.A.M., Meijer, H.E.H., *J. Mech. Phys. Sol.*, **47**, 201 (1999)
- [13] Smit, R.J.M., Brekelmans, W.A.M., Meijer, H.E.H., *J. Mat. Sci.*, **35**, 2855 (2000)
- [14] Smit, R.J.M., Brekelmans, W.A.M., Meijer, H.E.H., *J. Mat. Sci.*, **35**, 2869 (2000)
- [15] Smit, R.J.M., Brekelmans, W.A.M., Meijer, H.E.H., *J. Mat. Sci.*, **35**, 2881 (2000)
- [16] Hasan, O.A. and Boyce, M.C., *Polymer*, **34**, 5085 (1993)
- [17] Govaert, L.E.; Melick, H.G.H. van; Meijer, H.E.H., *Polymer*, **42**, 1271 (2001)
- [18] Bucknall, C.B., Rubber toughening, In: R.N. Haward and R.J. Young Eds., *The Physics of Glassy Polymers*, 2nd ed., Chapman & Hall, London 363-412 (1997)
- [19] Bucknall, C.B. and Smith, R.R., *Polymer*, **6**, 437 (1965)
- [20] Donald, A.M.; Kramer, E.J., *J. Mat. Sci.*, **17**, 2351 (1982)
- [21] Wu, S., *J. Appl. Pol. Sci.*, **35**, 549 (1988)
- [22] van der Sanden, M.C.M., Meijer, H.E.H., Lemstra, P.J., *Polymer*, **34**, 2148 (1993)
- [23] van der Sanden, M.C.M., de Kok, J.M.M., and Meijer, H.E.H., *Polymer*, **35**, 2995 (1994)
- [24] Keddie, J.L., Jones, R.A.L., and Cory, R.A., *Europhys. Lett.*, **27**, 59 (1994)
- [25] Forrest, J.A., and Mattsson, J., *Phys. Rev. E.*, **61**, R53 (2000)
- [26] Forrest, J.A., and Jones, R.A.L., In: A. Karim and S. Kumar Eds., *Polymer Surfaces, Interfaces, and Thin Films*, World Scientific Publishing, Singapore, 251-294 (2000)
- [27] Haward, R.N., *Polymer*, **28**, 1485 (1987)
- [28] van der Aa, M.A.H., Schreurs, P.J.G., Baaijens, F.P.T., *Mech. of Mat.*, **33**, 555 (2001)

Chapter 2

Strain hardening behaviour of glassy polymers: influence of network density

The influence of network density on the strain hardening behaviour of amorphous polymers is studied. The network density of poly-styrene is altered by blending with poly(2,6-dimethyl-1,4-phenylene-oxide) and by cross-linking during polymerisation. The network density is derived from the rubber-plateau modulus determined by Dynamic Mechanical Thermal Analysis. Subsequently uniaxial compression tests are performed to obtain the intrinsic deformation behaviour and, in particular, the strain hardening modulus. The strain hardening modulus proves to be proportional to the network density, irrespective of the nature of the network, i.e. physical entanglements or chemical cross-links.

2.1 Introduction

In principle all amorphous polymers are intrinsically tough, provided that their molecular weight is sufficiently high (typically 8 times the molecular weight between entanglements) to form a sufficiently strong entangled polymer network. However, under certain loading conditions the macroscopic response of these materials to deformation appears to be quite brittle, see figure 2.1a. Polystyrene (PS) and polymethylmethacrylate (PMMA) are considered as such materials which fracture at a few percent of strain under most loading conditions. In polystyrene crack-like defects, so-called crazes, appear in a tensile bar already in the apparent elastic region. With increasing load the crazes, which are bridged by fibrils, open up and macroscopic fracture occurs upon the

Reproduced from:

Influence of network density on the strain hardening behaviour of glassy polymers
H.G.H. van Melick, L.E. Govaert, H.E.H. Meijer, submitted to **Polymer**.

failure of these fibrils. That polystyrene is, though, intrinsically ductile can be witnessed from the fact that these fibrils consist of highly stretched material with draw ratios close to the maximum network draw ratio [1, 2]. Polycarbonate (PC), on the other hand, is generally considered to be a ductile material, although it does suffer notch-brittleness. During tensile deformation a stable neck is formed shortly after yielding. With ongoing strain the neck grows until ductile fracture occurs at approximately 100% macroscopic strain.

The intrinsic deformation behaviour can be determined in a test where localisation phenomena like necking and crazing are absent. Two examples are a video controlled tensile test [3] and an uniaxial compression test [4, 5]. The intrinsic stress-strain curve shows an initial (visco-) elastic region followed by yielding, intrinsic strain softening and strain hardening. Figure 2.1b illustrates that polystyrene, polycarbonate and polymethylmethacrylate exhibit remarkably similar intrinsic behaviour in compression. The initial elastic moduli equal approximately 3 GPa, the yield stresses range from 60 to 120 MPa and depend on strain rate and temperature. The main differences between these materials are found in their post-yield behaviour: (a) the drop in true stress after yielding (intrinsic strain softening or so-called 'yield-drop') and (b) the slope of strain hardening at large strains. This post-yield behaviour plays a key role in the macroscopic deformation behaviour in tension and determines whether a material is brittle or ductile.

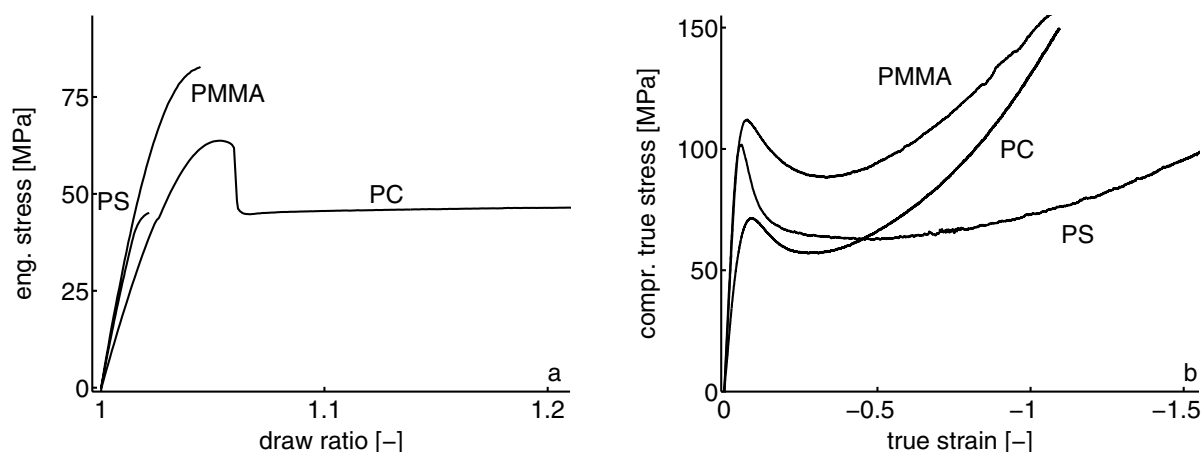


Figure 2.1: Deformation behaviour of three well known glassy polymers in tension (a) and compression (b).

Localisation of strain is induced by intrinsic strain softening and the evolution of this localised plastic zone depends on the stabilising effect of the strain hardening [6]. In polystyrene the substantial strain softening causes severe localisation of plastic strain, which can not be stabilised sufficiently due to the low value of strain hardening modulus. With ongoing deformation, localisation grows to extremes, resulting in void nucleation, craze formation and catastrophic failure. Polycarbonate, on the other hand, has limited strain softening only; the localisation induced is therefore moderate and can easily be stabilised by the stronger strain hardening. Polymethylmethacrylate has intermediate properties which leaves it on the edge between brittle and ductile.

The dominant influence of *strain softening* is convincingly demonstrated by the effects of thermal and mechanical histories on macroscopic deformation behaviour. For in-

stance, a quenched specimen exhibits less softening than a slowly cooled specimen in compression tests and, consequently, shows less localised deformation behaviour in tension. Cross and Haward [7] reported uniform deformation for quenched polyvinylchloride (PVC) samples, whereas slowly cooled samples exhibited necking. Various authors showed that by mechanical pre-conditioning or pre-deformation, the amount of strain softening can be reduced or even eliminated [8–11]. This pre-treatment results in uniform deformation of a polycarbonate tensile bar [10] and can induce ductile deformation behaviour of polystyrene in tension [11]. The crucial role which strain softening plays in the localisation of strain, and hence in the macroscopic deformation behaviour, request a thorough understanding of its molecular background. Despite research efforts [8, 12, 13], the physical origin of strain softening is not yet fully understood. A fair view point could be that the continuous increase in stress, with a change in slope at the yield point where strain hardening of the polymer network takes over, like it occurs after mechanical rejuvenation or fast quenching, is the natural response of polymers. By the process of physical ageing, the yield stress increases which, on its turn, is accompanied by what is measured as an increasing strain softening. Apparently further research is necessary long this line (see discussion section of [14])

The *strain hardening* behaviour of amorphous and semi-crystalline polymers is studied much more extensively. In modelling, effort has been put in numerical simulations of large strain deformation of amorphous, glassy polymers in particular. Most constitutive modelling of strain hardening behaviour is based on the concept of entanglements. Haward and Thackray [15] proposed a constitutive equation in which both a rubber-elastic response and finite extensibility are incorporated. This one-dimensional equation was extended by Boyce *et al.* [16, 17] into a 3-D finite strain formulation, now called the 'BPA-model'. The strain hardening response in this model is represented by a 'three chain' model [18]. The BPA-model was later refined by introducing a more realistic representation of the spatial distribution of molecular chains, resulting in the 'eight chain' model [19] and the 'full chain' model [20].

Haward [21] suggested that polymer coils do not approach a fully stretched condition and hence he proposed a neo-Hookean (Gaussian) relation. Studies of G'Sell [22] and Haward [21, 23] showed that for various semi-crystalline polymers this relation describes strain hardening behaviour very well. Tervoort and Govaert [24] investigated this behaviour during uniform deformation of 'pre-conditioned' polycarbonate tensile bars. By mechanical pre-conditioning, in this case torquing of cylindrical tensile bars to and fro over 720° , strain softening is eliminated and localisation of strain and necking inhibited. In tensile the strain hardening behaviour was well described by a neo-Hookean relation up to very high draw ratios ($\lambda = 3$). The authors incorporated subsequently a neo-Hookean description of the strain hardening behaviour in a Leonov model [25], consisting of a linear compressible spring and an Eyring dashpot [26]. This so-called compressible Leonov model was further extended by Govaert *et al.* [10] by incorporating intrinsic strain softening. Through finite element simulations of a necking polycarbonate specimen they showed that limited extensibility is not a prerequisite for stable neck-growth and that this can be simulated perfectly by an neo-Hookean relation.

In all models referred to above, strain hardening is modelled as a rubber-elastic spring, whether or not with finite extensibility, which suggests that an entangled polymer net-

work is involved. The physical relevance of this approach is demonstrated by the complete reversibility of plastic deformation when deformed polymers are brought above their glass transition temperature [27–30].

On the other hand, some data conflict with this entropic character. It was shown by Boyce and Haward [31], Arruda [32] and Tervoort [33] that the strain hardening modulus tends to decrease with temperature whereas the modulus of a true entropic spring would increase. Moreover, it was shown by Haward [15, 24] that the strain hardening modulus is orders of magnitude larger than could be expected from the network density determined in the melt.

This paper addresses this apparent contradiction and the role of the polymer network in the strain hardening behaviour. For this reason the network density of polystyrene is altered by blending with poly(2,6-dimethyl-1,4-phenylene oxide) (PPO) and by cross-linking during bulk polymerisation. The physical and chemical polymer networks are characterised in the rubbery state by Dynamic Mechanical Thermal Analysis (DMTA). From the dynamic modulus (E_d) in the rubbery state, the molecular weight between entanglements (M_e) and the network density (ν_e) are derived. In subsequent uniaxial compression tests, the intrinsic deformation behaviour is determined. The slope at large strains of the true stress-true strain curves represents the strain hardening modulus (G_R). Combination enables to investigate the relation between the network density and the strain hardening modulus.

Furthermore the validity of a neo-Hookean description of strain hardening behaviour is investigated by analytical and numerical tools, employing the previously mentioned compressible Leonov model [26]. Finally, the effect of temperature on the strain hardening modulus is investigated by performing uniaxial compression tests at various temperatures.

2.2 Materials and methods

The materials used were blends of polystyrene (Styron 638, Dow Chemical Company, The Netherlands) and poly(2,6-dimethyl-1,4-phenylene oxide) (PPO 803, General Electric Plastics, The Netherlands), and polystyrene cross-linked during polymerisation. These materials will be referred to as PS/PPO and XPS. Six blends of PS/PPO were compounded by General Electric Plastics, containing respectively 0, 20, 40, 60, 80, and 100% PPO. The granular material was compression moulded, step-wise, into plates of various thicknesses. Apart from pure PPO, for which a temperature of 260°C was used to prevent degradation, all material were pre-heated in a mould of 160x160 mm² at 80°C above their glass-transition temperature (T_g) for 15 minutes and subsequently compressed in the mould in 5 steps of increasing force (up to 300 kN) during 5 minutes. In between these steps, the pressure was released to allow for degassing. Next the mould was placed into a cold press and cooled to room temperature at a moderate force (100 kN). Rectangular samples used for DMTA were machined from a 1 mm thick plate with final dimensions of 30x4x1 mm³. From thick plates (160x160x9 mm³) rectangular bars with a cross-section of 9x9 mm² were cut, which were machined into cylindrical samples (\varnothing 6 mm x 6 mm) that were used in the uniaxial compression tests. Cross-linked polystyrene was prepared by bulk-polymerisation of styrene (Aldrich Chemical Company, The Netherlands) and various amounts of cross-linking agent (di-

(ethyl glycol)-dimethacrylate, DEGDMA; also from Aldrich). Amounts of 0, 2, 3, 4, and 5% DEGDMA were added to styrene in small glass tubes ($\varnothing 7$ mm x70 mm). Furthermore small amounts of initiator (tert-butyl proxy benzoate, Trigonox-C, Lamers and Plueger, The Netherlands) and chain transfer agent (dodecanethiol-98%, Aldrich) were added to obtain a desired molecular weight. After filling the tubes, the mixture was fluxed with argon gas to remove the oxygen and were sealed off to prevent evaporation of styrene. Next they were placed in a temperature-controlled silicon-oil bath from which the temperature was slowly raised from 85°C to 110°C in 5 steps of 5°C and one day duration each. This temperature profile was chosen to avoid auto-acceleration at low conversion rates and to enhance mobility during the propagation stage. Afterwards, the materials were post-cured (without cap) at 120°C (well above T_g) for 2 days to terminate all reactions and remove all remaining unused monomer. Both DMTA and compression samples were machined from these bars.

DMTA was performed on a Rheometrics Scientific MKIII Dynamic Analyser. A temperature sweep (from room temperature to 250°C) was used during a dynamic test (tensile setup) at 1Hz in order to determine the dynamic modulus (E_d) and the tangent of the phase lag ($\tan(\delta)$).

Compression tests were performed on a servo-hydraulic MTS Elastomer Testing System 810. Cylindrical specimens were compressed at a constant logarithmic strain rate of 10^{-2}s^{-1} between two parallel, flat steel plates. The friction between the sample and steel plates was reduced by an empirically optimised method: onto the sample a thin film of PTFE tape (3M 5480, PTFE skived film tape) was applied and the surface between steel and tape was lubricated by a soap-water mixture. During the compression test no bulging or buckling of the sample was observed, indicating that the friction was sufficiently reduced. The relative displacement of the steel plates was recorded by an Instron (2630-111) extensometer. Both displacement and force were recorded by data acquisition at an appropriate sample-frequency (depending on strain rate). This sampling frequency was adjusted in such a way that a least 1000 data points were collected per test. The setup for the uniaxial compression tests was placed in a temperature chamber with liquid-nitrogen cooling of which the temperature could be accurately controlled ($\pm 0.5^\circ\text{C}$). The tests were performed at 25, 45, 65, and 85°C. Approximately 15 minutes prior to testing the sample was mounted in the setup to assure thermal equilibrium.

2.3 Results

Dynamic Mechanical Thermal Analysis

The DMTA results for PS/PPO and XPS are given in figure 2.2. The dynamic modulus (E_d) as function of the temperature is shown in figures 2.2a and 2.2b. The PS/PPO blends exhibit the dynamic mechanical response which is characteristic for a thermoplastic material; at room temperature the storage modulus is relatively high, ranging from 2.5 GPa for PPO to 3.0 GPa for PS, and, with increasing temperature, this modulus gradually reduces. At the glass-transition temperature (T_g) a sharp decrease in dynamic modulus is observed, since here the polymer chains obtain full segmental mobility and their state changes from glassy to rubbery.

The phase lag between the input and output signal ($\tan(\delta)$, see figures and 2.2cd) shows a peak close to T_g , indicating that the contribution of the viscous part to the dynamic re-

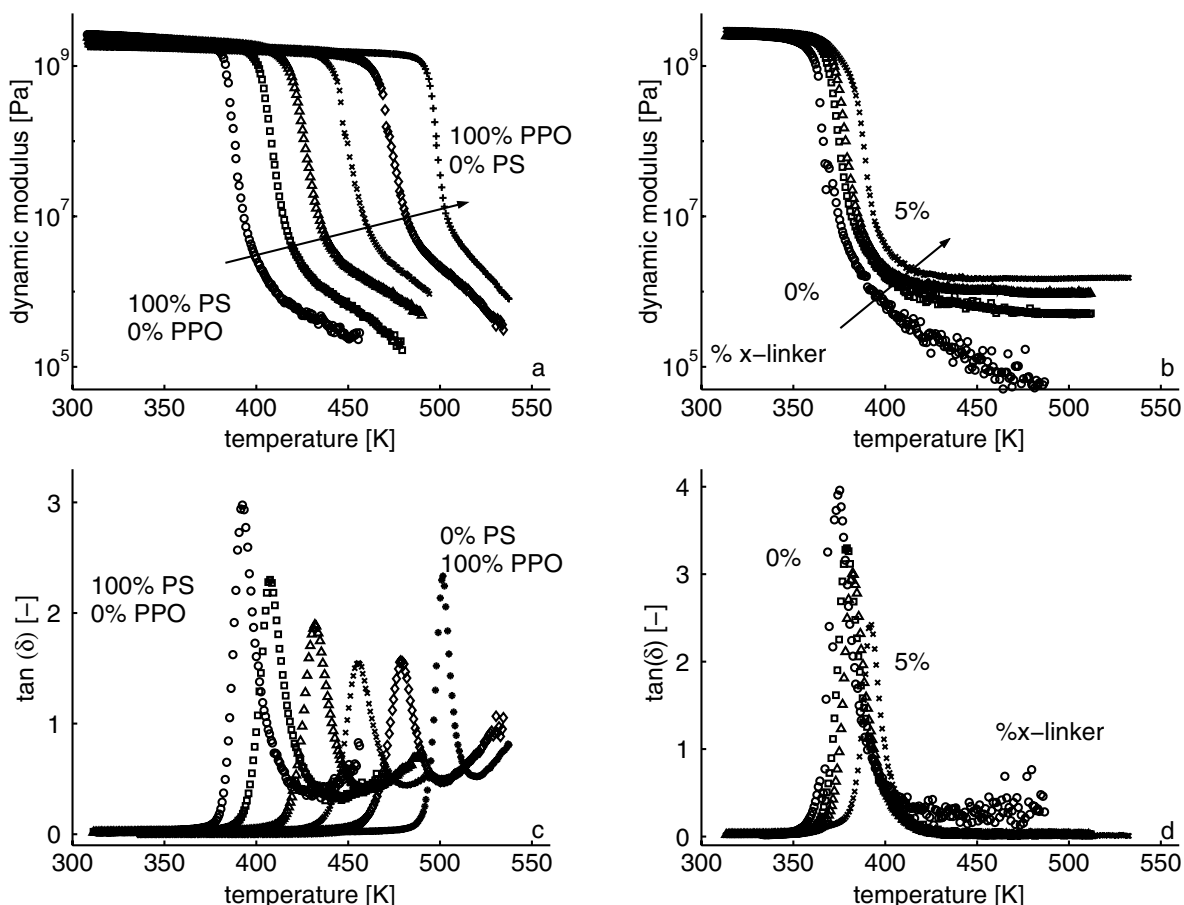


Figure 2.2: Results of the DMTA experiments; the dynamic modulus (E_d) and $\tan(\delta)$ as function of temperature for PS/PPO (a and c) and XPS (b and d).

response is relatively high in this temperature range. With increasing temperature $\tan(\delta)$ reduces again and the decay in modulus levels off, indicating that a more elastic region is reached, the so-called rubber plateau. In this rubber-elastic region, the polymer chains have full mobility and the properties are determined by the entangled network. Although the rubber plateau for thermoplastics is not as distinct as for thermosets, the rubber plateau modulus (G_N^0) is defined in this region, as the 'most elastic' dynamic modulus found at the minimum of $\tan(\delta)$ (see figure 2.2c and table 2.1). Upon further heating the polymer starts to disentangle and the dynamic modulus decays further out of the measurable range. In this temperature range the onset of a second 'viscous' peak is observed in $\tan(\delta)$, which indicates that the material becomes liquid-like. The rubber plateau moduli G_N^0 show a continuous increase with PPO content. Values found are similar to values reported in literature [23, 34].

The T_g 's of the blends increase with increasing PPO fraction, ranging from 378K for pure PS to 484K for pure PPO (see table 2.1), in good accordance with previously reported data (both DSC and DMTA) on similar blends [34–37]. The fact that only one clear glass-to-rubber transition is observed in the DMTA runs confirms that PS and PPO are miscible on a molecular level and form a compatible mixture.

The response of the in-situ polymerised and cross-linked materials is shown in figure 2.2b and 2.2d. PS with 0% cross-linking agent behaves similar to the commercial PS, although some minor differences in modulus and T_g can be caused from differences

in molecular weight (distribution) [38]. The cross-linked materials behave like typical thermoset. Above T_g a clear rubber-elastic plateau is reached due to the chemically entangled network. At this plateau the rubber-elastic modulus is defined.

%-PPO	T_g [K]	T_g [K] ref. [35]	G_N^0 [MPa] @ min. $\tan(\delta)$	x-linker[%]	T_g [K]	G_N^0 [MPa]
0	378	378	0.16	0	362	0.15
20	393	391	0.26	2	368	0.19
40	415	410	0.49	3	372	0.31
60	435	427	0.57	4	377	0.36
80	458	449	0.66	5	383	0.51
100	484	487	0.79			

Table 2.1: Glass-transition temperatures and rubber plateau moduli for the PS/PPO blends (left) and XPS (right).

The T_g increases slightly with cross-link density from 362K for material with 0% cross-linker to 382K for the material with 5% cross-linker and rubber-plateau modulus increases with cross-link density and their values are given in table 2.1.

The rubber(-plateau) moduli, as function of PPO fraction or added amount of cross-linker, are given in figure 2.3 (solid lines to guide the eye). At low amounts of cross-linker the rubber modulus does not increase. A reasonable explanation would be that at small amounts of cross-linker the additional cross-links hardly contribute to the rubber modulus and therefore the rubber modulus departs from a plateau (see figure 2.3b).

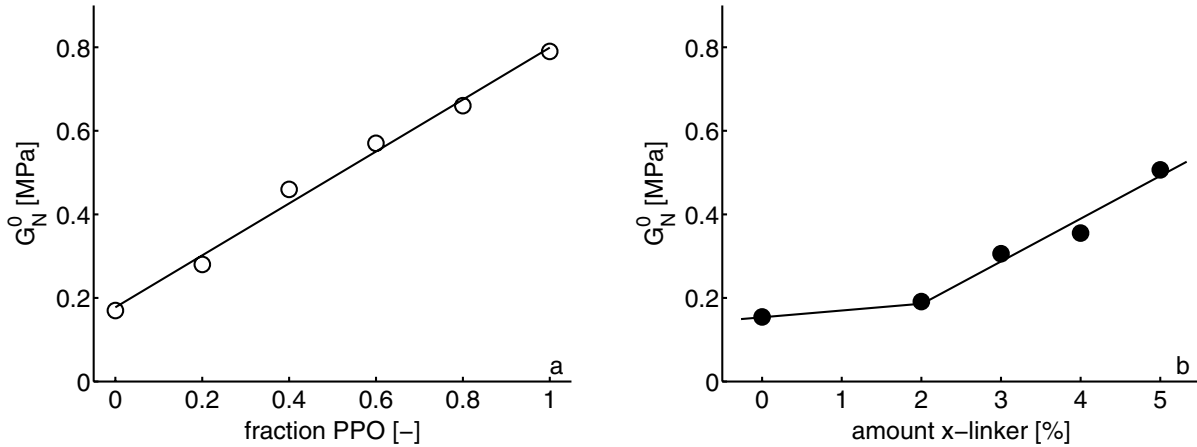


Figure 2.3: The rubber(-plateau) moduli as function of fraction PPO (a) and percentage cross-linker (b).

Moduli can be transformed into network densities using the following equations [39]:

$$G_N^0 = \rho_r \frac{RT}{M_e} \quad (2.1)$$

where ρ_r is the density of the polymer in the rubbery state, R the molar gas constant and T the absolute temperature. The molecular weight between entanglements M_e , is

inversely proportional to the network density (ν_e) according to:

$$\nu_e = \frac{\rho_g N_A}{M_e} \quad (2.2)$$

where ρ_g is the density of the polymer in the glassy state and N_A the Avogadro number. Zoller and Hoehn [40] performed an extensive investigation of the pressure-volume-temperature properties of PS, PPO and their blends. Their values for the specific volume in the rubbery and glassy state are used here to calculate the network density. For XPS the specific volume of pure PS is used.

Since the variations in density of the PS/PPO blends are small, it is reasonable to anticipate that the relationship between the network density and the rubber-plateau modulus is linear. As a result the network density also proves to be proportional to the PPO content in the blends (see figure 2.4a). The solid line is the best fit on the experimental data, while the dashed line is derived from the model Prest and Porter [41] used, which states that the molecular weight between entanglements for PS/PPO blends, $M_e(\chi)$ depends solely on the M_e of PS and the fraction (χ) PPO present in blend:

$$M_e(\chi) = \frac{M_e(PS)}{1 + 3.2\chi} \quad (2.3)$$

Only at high PPO fractions some discrepancy is observed between their model and our experimental data.

In figure 2.4b it is shown that with an increasing amount of cross-linker added during polymerisation, the network density increases. Similar to the results of figure 2.3b the influence of small amount of cross-linker on the network density is low and therefore it is reasonable to assume that the network density also departs from a plateau, represented by the solid line in figure 2.4b.

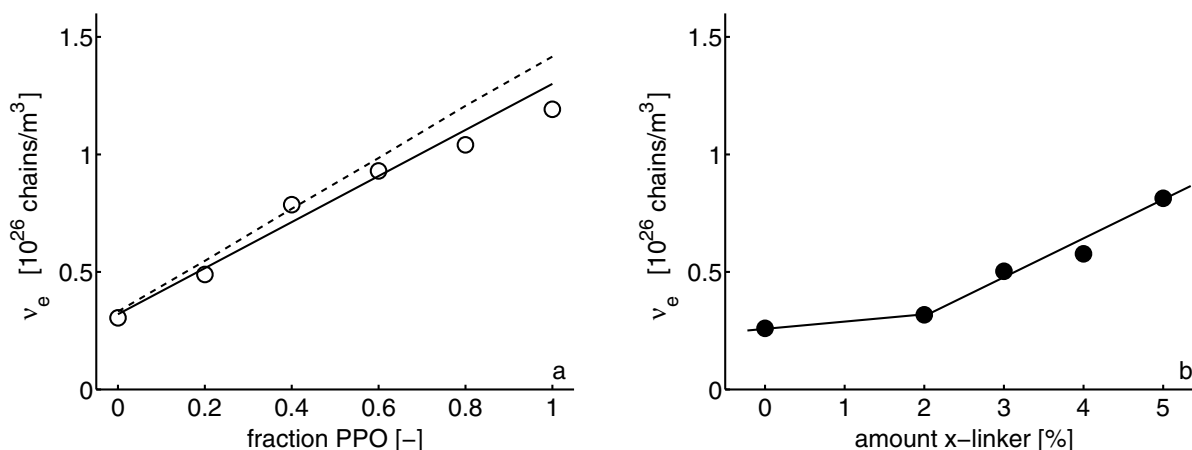


Figure 2.4: Network density as function of fraction PPO in PS/PPO (a) and added amount of cross-linker in XPS (b).

Uniaxial compression tests

The effects of an increased network density on the post-yield behaviour was investigated by uniaxial compression tests. Since localisation phenomena like crazing and necking

are absent in such tests, a true stress-true strain curve is obtained, see figure 2.5. From these results it can be concluded that the post-yield behaviour is strongly influenced by a change in network density. For increasing network density, i.e. increasing PPO fraction or increasing the amount of cross-linker, the strain hardening modulus clearly rises, while the yield stress, which is mainly determined by the secondary interactions between the polymer chains, remains largely unaffected. The fact that strain softening, which is also governed by secondary interactions, decreases with increasing network density must be attributed to the stabilising contribution of the polymer network, that shows a noticeable effect at small strains. Hence the true stress can not drop as much as in a looser network.

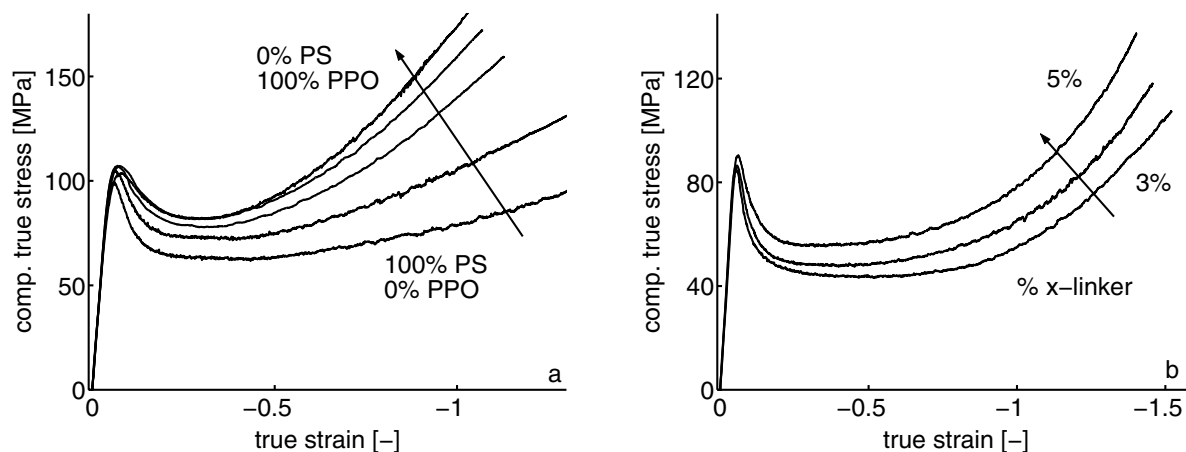


Figure 2.5: Compressive behaviour of PS/PPO (a) and XPS (b) at room temperature and at a strain rate of 10^{-2} s^{-1} .

From the uniaxial compression curves at large strains, the strain hardening moduli were determined. From the strain energy function, first proposed by Mooney [42], for rubber-elastic materials, it can be derived that the true stress is proportional to $\lambda^2 - \lambda^{-1}$. If a neo-Hookean description is valid for the strain hardening behaviour of these materials, the true stress should be proportional to this strain measure. In figure 2.6a it is shown that for the PS/PPO blends the true stress is indeed linear in $\lambda^2 - \lambda^{-1}$. The strain hardening modulus is defined as the slope at large strains, which is schematically represented by the dashed line in figure 2.6a. An identical procedure is followed to determine the strain hardening moduli of XPS.

The validity of a neo-Hookean description of the large strain behaviour of these materials is illustrated by numerical simulations, performed with MARC (MSC Software) employing the compressible Leonov model [10, 26, 43] with a neo-Hookean relation representing the large strain behaviour. In figure 2.6b it is shown that the simulations provide a good description of the uniaxial compression tests, indicating that the strain hardening behaviour can indeed adequately be described by a neo-Hookean relation. Finally, combining the results of the DMTA experiments and the uniaxial compression tests yields the relation sought between the network density and the strain hardening modulus. In the table of figure 2.7 the values for the network density and strain hardening modulus of the various materials are given, while in figure the strain hardening modulus is plotted versus the network density (the open circles represent the PS/PPO blends, the filled circles XPS). Similar to rubber-elastic behaviour the strain hardening modulus proves to be proportional to the network density, irrespective of the nature of the polymer network, i.e. physical entanglements or chemical cross-links.

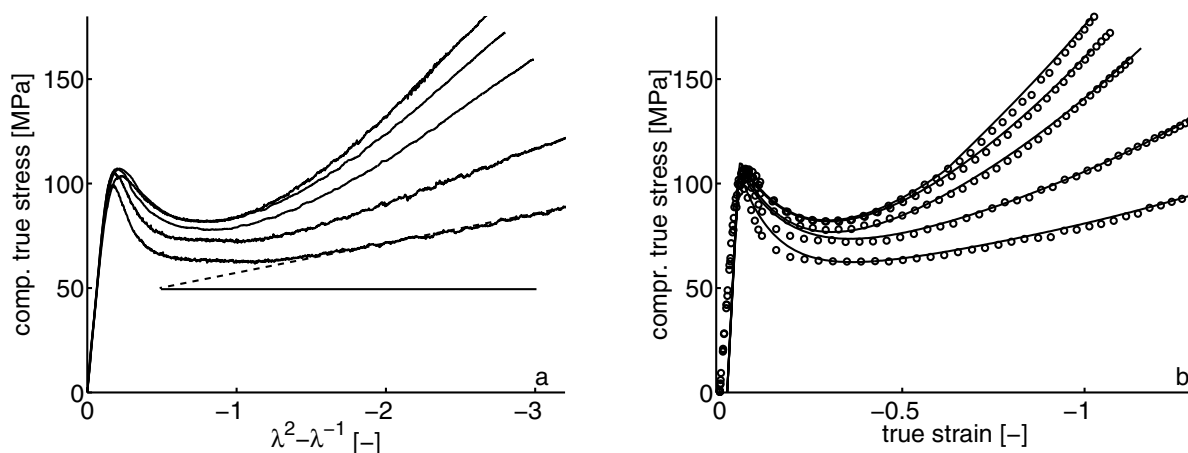


Figure 2.6: A neo-Hookean relation can adequately describe the strain hardening behaviour as is shown by analytical (a) and numerical methods (b).

		ν_e [10^{26} chains/ m^3]	G_R [MPa]
PS/PPO	100/0	0.30	13
	80/20	0.49	25
	60/40	0.79	48
	40/60	0.93	58
	20/80	1.04	65
	0/100	1.19	75
XPS	0%	0.26	13
	2%	0.32	23
	3%	0.50	27
	4%	0.58	33
	5%	0.81	45

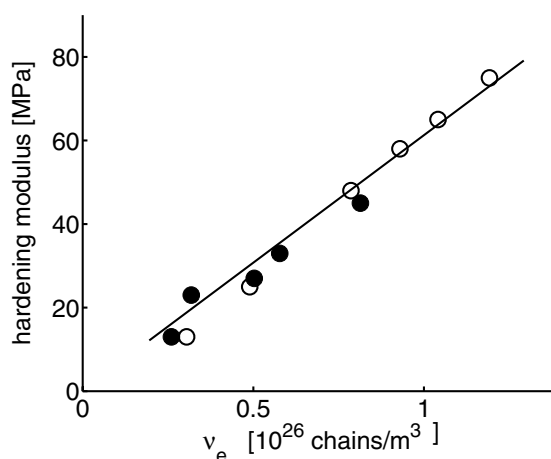


Figure 2.7: Strain hardening modulus, G_R , versus the network density, ν_e , for all materials investigated.

So far the experimental and numerical results indicate a neo-Hookean relation to provide an adequate description of the strain hardening behaviour of amorphous polymers. However, as was already shown by several authors [31–33], the strain hardening modulus decreases with temperature. In figure 2.8a the strain hardening modulus of the PS/PPO blends is given as function of temperature. Obviously the strain hardening moduli are inversely proportional to the temperature (the lines are drawn as a guide to the eye) and this becomes more pronounced at high PPO fractions in the blend.

Representing the strain hardening modulus as function of network density, which is a characteristic of each blend, gives a bundle of straight lines with proportionality constant c , see figure 2.8b, according to:

$$G_R = c(T) \nu_e \quad (2.4)$$

2.4 Discussion

In case of an entropic spring a proportionality constant equal to ρRT would be expected, and hence an increasing modulus with temperature. This clearly indicates that strain

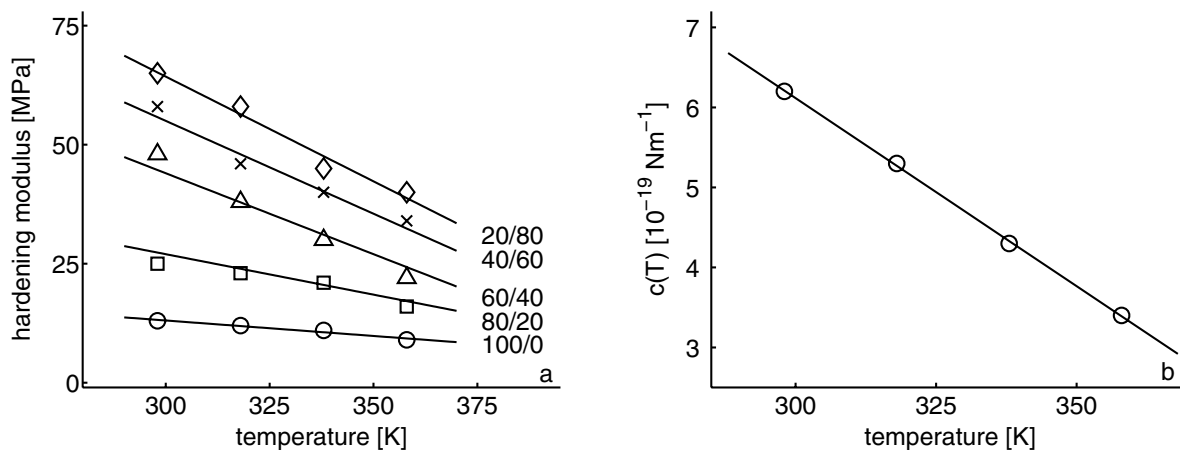


Figure 2.8: The strain hardening modulus, G_R , for the PS/PPO blends (a) and the proportionality constant, $c(T)$ (equation 2.4), as function of temperature.

hardening behaviour is not unambiguously of an entropic nature. As can be concluded from figure 2.7, the strain hardening modulus is related, and even proportional, to the rubber-plateau modulus measured in the melt. One could argue that the trend of the increasing strain hardening modulus with increasing PPO content can be fully addressed to the changes in secondary interactions caused by the differences in chemical structure of polystyrene and polyphenylene-oxide. However, the increasing strain hardening modulus with cross-link density proves that the density of the polymer network governs the large strain behaviour. This relationship between the strain hardening modulus and the rubber-plateau modulus seems to suggest that these phenomena have a common (micro-)structural background.

It is well known that in the melt, where the rubber-plateau modulus is determined, polymer chains have full main-chain segmental mobility which is thermally induced. The dynamic response, measured in this region, is fully dependent on the molecular network as on this time-scale the contribution of secondary interactions is negligible. The time and temperature dependent behaviour in this region has been subject to many studies in the past and the validity of the reptation theory is quite well established, see e.g. [44, 45]. The response in this region is governed by entropy elasticity and relaxation, which implies that both time and temperature play an important role.

During plastic deformation in the glassy state, polymer chains also obtain a certain degree of mobility, albeit of different nature: stress-induced instead of temperature-induced main-chain segmental mobility. That this mobility does activate a contribution of the molecular network can be witnessed from the fact that chemical cross-linking does have a significant effect on the strain hardening modulus and that plastic deformation is fully reversible by bringing the polymer above its glass-transition temperature [27–30].

The higher values of the strain hardening modulus, compared to the rubber-plateau modulus, might originate from the difference in nature of the mobility obtained. Although the material is deformed in the glassy state, it is reasonable to assume that under the influence of the applied stress, the polymer molecules only obtain a limited degree of mobility. Several experimental studies showed that mobilisation of chains occurs under influence of stress at the crack tip during crazing and that the model of reptation might be used in certain cases in the glassy state [46–48]. Numerical simulations by Tervoort *et al.* [49] suggested that yielding in glassy polymers can be regarded as a

stress-induced glass-to-rubber transition. A natural assumption would be that the time-scale of the stress-induced main-chain segmental mobility during yielding is equal to the time-scale on which the experiment is performed. It is well known that the time-scale of main-chain segmental mobility in, for instance, a dynamic mechanical thermal analysis is influenced by temperature. In the glassy state, far below T_g , the time-scale of main-chain segmental mobility is much longer than the time-scale of the experiment, whereas in the rubbery state, far above T_g , the time-scale of main-chain segmental mobility is much shorter than the time-scale of the experiment. In a way one could regard the stress-induced main-chain segmental mobility during yielding analogous to a dynamic mechanical thermal analysis at a temperature at which the time-scale of the thermally-induced main-chain segmental mobility is equal to the excitation frequency, i.e. right at the glass transition temperature. So one could qualify the main chain segmental mobility, induced by yielding, as partial main-chain segmental mobility with a significant contribution of the secondary interactions which are not fully relaxed. Similar to a thermodynamic glass-to-rubber transition, the modulus measured in this region is higher than the rubber-plateau modulus in the melt but still the entangled polymer network does contribute to the response.

Moreover, one could imagine that on top of this stress-induced main-chain segmental mobility a thermally-induced segmental mobility can be superposed. Testing at an elevated temperature could result in a higher overall segmental mobility and therefore lead to a lower strain hardening modulus.

2.5 Conclusions

In this paper the role of the network density on the strain hardening behaviour of amorphous polymers has been investigated. The network density of glassy polystyrene was altered by blending with polyphenylene oxide and by cross-linking. The blends of PS and PPO are fully compatible in all mixing ratios and form a mixture on a molecular scale. This can be witnessed from the fact that in DMTA only one glass transition temperature is observed. From these tests it was also concluded that the glass transition temperature and the rubber modulus (dynamic modulus determined in the rubbery state) increase with increasing PPO fraction in the blend. The DMTA experiments of cross-linked polystyrene (XPS) show, besides a slight increase in T_g , an increased rubber-plateau modulus with an increasing amount of added cross-linking agent. From the rubber(-plateau) moduli the network density was derived using equations from the rubber-elastic theory. Experimentally determined network densities correlate well with the model proposed by Prest and Porter [41].

Uniaxial compression tests showed minor changes in the elastic and yield behaviour of the PS/PPO blends; the main differences were found in the strain hardening behaviour. With increasing PPO fraction in PS/PPO and an increasing amount of cross-linker in XPS the strain hardening modulus increases. Numerical and analytical approaches demonstrated that the strain hardening behaviour can be adequately described by a neo-Hookean relation.

Representing the strain hardening modulus as function of the network density, obtained from DMTA experiments, yields the conclusion that the strain hardening modulus is proportional to the network density, irrespective of the nature of the entangled polymer network, i.e. physical entanglements or chemical cross-links .

However, the strain hardening modulus measured in uniaxial compression tests as function of temperature contradicts the similarity with rubber-elastic behaviour. With increasing temperature the strain hardening modulus decreases whereas for an entropic spring it is expected to rise. It was discussed that after yielding, which can be interpreted as a stress-induced rubbery state, the polymer network is addressed but that relaxation mechanisms might also play an important role. In the temperature dependence of the strain hardening behaviour, relaxation might overrule the entropic character of the polymer network and lead to an decreasing trend.

Acknowledgements

The authors wish to acknowledge Theo Tervoort for his valuable contribution to the discussion and the financial support provided by the Dutch Technology Foundation (STW) (Grant EWT.3766).

References

- [1] Donald, A.M. and Kramer, E.J., *Polymer*, **23**, 451 (1982)
- [2] Donald, A.M. and Kramer, E.J., *J. Pol. Sci., Pol. Phys. Ed.*, **20**, 1129 (1982)
- [3] G'Sell, C., Hiver, J.M., Dahouin, A., Souahi, A., *J. Mat. Sci.*, **27**, 5031 (1992)
- [4] Arruda, E.M. and Boyce, M.C., *Int. J. Plast.*, **9**, 697 (1993)
- [5] Boyce, M.C., Arruda, E.M., Jayachandran, R., *Pol. Eng. Sci.*, **34**, 716 (1994)
- [6] Meijer H.E.H., Govaert L.E., Smit R.J.M., A Multi-Level Finite Element Method for Modeling Rubber-Toughened Amorphous Polymers, In: R. Pearson, Ed., *Toughening of Plastics*, American Chemical Society, Boston, 50-70 (1999)
- [7] Cross, A. and Haward, R.N., *Polymer*, **19**, 677 (1978)
- [8] G'Sell C., Plastic deformation of glassy polymers: constitutive equations and macromolecular mechanisms. In: H.J. Queens *et al.*, Eds. *Strength of metals and alloys*, Pergamon Press, Oxford, 1943-1982 (1986)
- [9] Bauwens, J.C., *J. Mat Sci.*, **13**, 1443 (1978)
- [10] Govaert, L.E., Timmermans, P.H.M., Brekelmans, W.A.M., *J. Eng. Mat. Tech.* **122**, 177 (2000)
- [11] Govaert, L.E., Melick, H.G.H. van, Meijer, H.E.H., *Polymer*, **42**, 1271 (2001)
- [12] Aboulfaray M., G'Sell C., Mangelinck D., McKenna G.B., *J. Non-Cryst. Solids* **172-174**, 615 (1994)
- [13] Hasan, O.A. and Boyce, M.C., *Polymer*, **34**, 5085 (1993)
- [14] van Melick, H.G.H., Govaert, L.E., Raas, B., Nauta, W.J., Meijer, H.E.H., Kinetics of ageing and re-embrittlement of mechanically rejuvenated polystyrene, *Polymer*, submitted
- [15] Haward, R.N. and Thackray, G., *Proc. Roy. Soc. London A*, **302**, 453 (1967)
- [16] Boyce, M.C., Parks, D.M., Argon, A.S., *Mech. Mat.*, **7**, 15 (1988)
- [17] Boyce, M.C. and Arruda, E.M., *Pol. Eng. Sci.*, **30**, 1288 (1990)
- [18] James, H.M. and Guth, E., *J. Chem. Phys*, **11**, 455 (1943)
- [19] Arruda, E.M. and Boyce, M.C., *J. Mech. Phys. Solids*, **41**, 389 (1993)
- [20] Wu, P.D. and van der Giessen, E., *J. Mech. Phys. Solids*, **41**, 427 (1993)

- [21] Haward, R.N., J. Pol. Sci., part B: Pol. Phys., **33**, 1481 (1995)
- [22] G'Sell, C., Boni, S., Shrivastava, S. J. Mat. Sci., **18**, 903 (1983)
- [23] Haward, R.N., Macromolecules, **26**, 5860 (1993)
- [24] Tervoort, T.A. and Govaert, L.E., J. Rheo., **44**, 1263 (2000)
- [25] Leonov, A., Rheologica Acta, **15**, 85, (1976)
- [26] Tervoort, T.A., Smit, R.J.M., Brekelmans, W.A.M., Govaert, L.E., Mech. Time-Dep. Mat., **1**, 269 (1998)
- [27] Gurevich, G. and Kobeko, P., Rubber Chem. Tech., **13**, 904 (1940)
- [28] Haward, R.N., Trans. Faraday Soc., **38**, 394 (1942)
- [29] Hoff, E.A.W., J. Appl. Chem., **2**, 441 (1952)
- [30] Haward, R.N., Murphy, B.M., White, E.F.T., J. Pol. Sci., Part A2, **9**, 801-14 (1971)
- [31] Boyce, M.C. and Haward, R.N., The post-yield deformation of glassy polymers, In: R.N. Haward and R.J. Young, Eds., *The Physics of Glassy Polymers*, 2nd edn., Chapman&Hall, London, 213-293 (1997)
- [32] Arruda, E.M., *Charaterization of the strain hardening response of amorphous polymers*, PhD thesis, Massachusetts Institute of Technology (1992)
- [33] Tervoort, T.A., *Constitutive Modelling of Polymer Glasses, finite, nonlinear viscoelastic behaviour of polycarbonate*, PhD thesis, Eindhoven University of Technology (1996)
- [34] Wu, S., J. Pol. Sci., Part B: Pol. Phys., **25**, 2511 (1987)
- [35] Creton, C., Halary, J.-L., Monnerie, L., Polymer, **40**, 199 (1998)
- [36] Cowie, J.M.G., Harris, S., Gómez Ribelles, J.L., Meseguer, J.M., Romero, F., Torregrosa, C., Marcomol., **34**, 4430 (1999)
- [37] Robertson, C.G. and Wilkes, G.L., Polymer, **41**, 9191 (2000)
- [38] Kumar, A. and Gupta, R.K., *Fundamentals of Polymers*, McGraw-Hill, London (1998)
- [39] Treloar, L.R.G., *The Physics of Rubber Elasticity*, 3rd edn., Clarendon Press, Oxford, UK (1975)
- [40] Zoller, P. and Hoehn, H.H., J. Pol. Sci., Pol. Phys. Ed., **20**, 1385 (1982)
- [41] Prest jr., W.M. and Porter, R.S., Pol. Sci. Eng., Part A2, **10**, 1639 (1972)
- [42] Mooney, M., J. Appl. Phys., **11**, 582 (1940)
- [43] van der Aa, M.A.H., Schreurs, P.J.G., Baaijens, F.P.T., Mech. Mat, **33**, 555 (2001)
- [44] de Gennes, P.G., J. Chem. Phys., **55**, 572 (1971)
- [45] Doi, M. and Edwards, S.F., *The Theory of Polymer Dynamics*, Oxford University Press (1986)
- [46] Prentice, P., Polymer, **24**, 344 (1983)
- [47] Evans, K.E., J. Pol. Sci, Part B: Pol. Phys., **25**, 353 (1987)
- [48] McLeish, T.C.B., Plummer, C.J.G., Donald, A.M., Polymer, **30**, 1651 (1989)
- [49] Tervoort, T.A., Klompen, E.T.J., Govaert, L.E., J. Rheo., **40**, 779 (1996)

Chapter 3

Kinetics of ageing and re-embrittlement of mechanically rejuvenated polystyrene

Pre-deforming polystyrene by rolling results in elimination of strain softening and induces ductile deformation behaviour in a subsequent tensile test. However, both yield stress and strain softening recover in time as a result of ageing, resulting in renewed brittle failure behaviour. The kinetics of this process is addressed in this paper. Although the process of recovery of yield stress and strain softening shows no molecular weight dependence, the time-scale of renewed brittle fracture after rejuvenation does. Any localisation of strain can only be stabilised if the molecular network can transfer sufficient load. For a relatively low molecular-weight polystyrene, the load bearing capacity is already exceeded at short ageing times, whereas for higher molecular-weight grades this takes longer. Since the creep compliance and shift-rate of mechanically rejuvenated polystyrene shows a pronounced increase as compared to thermally rejuvenated polystyrene, the segmental mobility in the mechanically rejuvenated samples has increased, despite a lower free volume. This indicates that a new explanation for ageing should be postulated, which is discussed.

3.1 Introduction

Crazing, shear yielding, and necking are the mechanisms which generally dominate the macroscopic deformation behaviour of glassy polymers. Which of these localisation phenomena prevails is determined by the post-yield behaviour of the polymer, i.e.

Reproduced from:

Kinetics of ageing and re-embrittlement of mechanically rejuvenated polystyrene

H.G.H. van Melick, L.E. Govaert, B. Raas, W.J. Nauta, H.E.H. Meijer, submitted to **Polymer**.

the strain softening and the strain hardening. Most striking example here is the difference in macroscopic behaviour of polystyrene and polycarbonate. Polystyrene exhibits substantial strain softening and only a weak contribution of the strain hardening. Localisations of strain, induced during the initial stage of deformation, can not be stabilised and evolve almost without limits. As a result this extreme strain localisation leads to the initiation of crazes, as postulated by Kramer [1] and, ultimately, macroscopic failure. Polycarbonate, on the other hand, exhibits only a moderate amount of strain softening and a stronger contribution of the strain hardening. Localised plastic deformation zones, induced by strain softening, can be stabilised and transfer deformation to other regions in the material. As a result a larger volume participates in the deformation and shear yielding and stable necking are observed in a tensile test. Despite, also polycarbonate will initiate crazes if a more severe localisation is introduced by changing the geometry of the test, e.g. by adding a notch.

The amount of strain softening can be altered by thermal treatments, like quenching and annealing. Small changes in yield stress can have major consequences for the macroscopic deformation behaviour. For instance, a subtle increase in strain softening, induced by annealing, leads to severe localisation of strain and brittle fracture in a relatively low molecular weight polycarbonate [2, 3]. Other examples include the observations of Cross and Haward [4], who showed that by rapid cooling of PVC a reduction in the strain softening results in homogeneous deformation in a subsequent tensile test whereas slowly cooled samples exhibit necking.

The most effective way to influence strain softening is by pre-deformation. Bauwens [5] demonstrated that by alternating bending of PVC samples, prior to tensile testing, necking was suppressed. Similar experimental observations were reported by G'Sell [6] for epoxy and Aboulfaraj *et al.* [7] for polycarbonate, respectively. Mechanical pre-conditioning of polycarbonate was also performed by Govaert *et al.* [8] and Tervoort *et al.* [9]. Cylindrical tensile bars were torqued to and fro, and subsequently subjected to a tensile test. The original moderate amount of strain softening was virtually eliminated by this pre-conditioning and localisation of strain was prevented, resulting in homogeneous deformation without neck-formation. Pre-deformation can also be performed by rolling, as was reported first by Gruenwald [10], who observed a remarkable increase in toughness for polycarbonate, which could again be erased upon annealing at temperatures below T_g . Broutman and co-workers adapted this procedure and performed similar studies on a number of amorphous polymers [11–13], excluding polystyrene. In these studies a sharp increase in Izod impact strength was found at an optimum degree of thickness reduction (PC \approx 5%, PVC \approx 30%), while at larger reductions, the impact strength decreased again. The authors claimed the slight molecular orientation and the residual stresses induced to be the origin of this toughness enhancement. However, the fact that annealing well below the glass transition temperature did erase the toughness enhancement whereas the molecular orientation did not disappear [13], questions their explanation. The influence of residual stresses remained unclear since during annealing a correlation between the relaxation of the residual stresses and the sudden transition from ductile to renewed brittle fracture was not observed.

A similar rolling procedure was followed by Govaert *et al.* [14] to pre-deform glassy polystyrene. Consistent with the previous studies, a remarkable increase in ductility was observed after a thickness reduction of approximately 30%. The tremendous reduction in strain softening, observed after rolling, was made responsible for the prevention of

strain localisation in a subsequent tensile test. This interpretation is consistent with observations of pre-conditioning of polycarbonate by torquing [8, 9] and the observations of Broutman that the ratio yield stress (maximum in stress) and draw stress (stress at which the polymer is drawn) approaches unity after a certain degree of rolling [11].

A common factor in these studies is the transient nature of the toughness enhancement. In time, either at room temperature or at elevated temperatures (below T_g), the ductility or impact strength decreased again. Govaert *et al.* [14] showed that the renewed brittle fracture in polystyrene occurred at the same time scale as the recovery of the yield stress and strain softening. For polycarbonate a similar recovery was observed although on a much longer time-scale [15, 16]. Since the factors that influence this transient behaviour are unknown, the actual study was designed. Tensile bars of polystyrene were pre-deformed by rolling and, subsequently, subjected to a uniaxial tensile test after certain periods in time (ageing times) after mechanical rejuvenation, allowing to examine the kinetics of the recovery of the yield stress and strain softening. At each ageing time step, 50 tensile tests were performed to determine the probability to failure as function of the ageing time.

Moreover, to investigate any differences in the state after thermal rejuvenation and mechanical rejuvenation by rolling, the creep behaviour was studied.

3.2 Experimental section

Materials

The materials used were three commercial grades of polystyrene, N5000 (Shell), Styron 648 and 660 (Dow Chemical). Gel permeation chromatography (GPC) was performed to determine their molecular weights and molecular-weight distributions. In figure 3.1 the weight fraction of the $\log(\text{molecular weight})$ is given as function of the molecular weight.

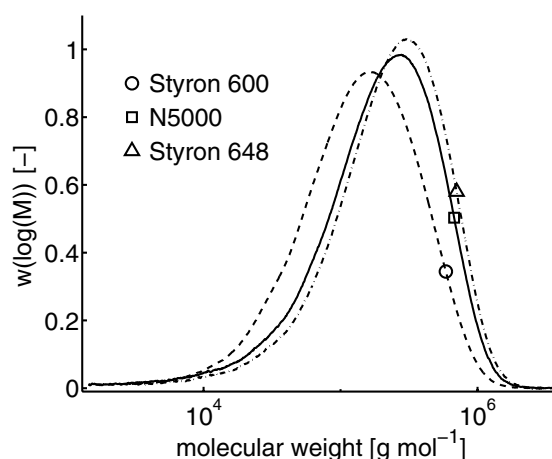


Figure 3.1: Molecular-weight distribution of the PS grades used in this study.

The weight-averaged and number-averaged molecular weights, given in table 3.1, increase in the sequence of Styron 660, N5000 and Styron 648. The dispersities of the Styron grades are similar, around 3, whereas for the N5000 grade it is slightly higher: 3.5.

	M_w [g mol ⁻¹]	M_n [g mol ⁻¹]	$\frac{M_w}{M_n}$
Styron 660	203,401	65,822	3.09
N5000	281,461	79,968	3.52
Styron 648	318,490	107,215	2.97

Table 3.1: Weight-averaged and number-averaged molecular weights of the PS grades used in this study.

For the uniaxial compression tests, cylindrical samples ($\varnothing 6$ mm x 6 mm) were machined from plates (160x160x9 mm³), that were compression moulded from granular material at a temperature of 190°C. First, the materials were heated for 15 minutes and next compressed during 5 minutes in 5 steps of increasing force, up to 300 kN. In between the steps, the force was released to allow for degassing. Afterwards the mould was placed in a cold press and cooled to room temperature at a moderate force (100 kN). All tensile specimens were prepared via injection moulding, shaped according to ISO 527.

Treatments

Quenching of tensile bars was performed after heating of the samples in an oven at 110°C (just above T_g) for half an hour and, subsequently, rapid cooling in liquid nitrogen. Mechanical pre-deformation of the tensile bars was performed by rolling along the length axis on a two-roll mill (diameter of 45 mm), more extensively described in Govaert *et al.* [14]. During rolling, a thickness reduction of approximately 32% was achieved while the length of the tensile bars increased by 36%. Since the rolling procedure induced a temperature rise of approximately 35°C, cooling of the samples to room temperature was allowed prior to testing.

Mechanical testing

In uniaxial compression, performed on a servo-hydraulic MTS Elastomer Testing System 810, cylindrical specimens were compressed, under strain control, at a constant logarithmic strain rate of 10^{-2} s⁻¹ between two parallel, flat steel plates. The friction between the sample and steel plates was reduced by an empirically optimised method. Onto the sample a thin film of PTFE tape (3M 5480, PTFE skived film tape) was applied and the surface between steel and tape was lubricated by a soap-water mixture. During the test no bulging or buckling of the sample was observed, indicating that the friction was sufficiently reduced.

Tensile test were performed on a Zwick Z010 tensile tester, at a constant linear strain rate of 10^{-3} s⁻¹, at distinct ageing times after pre-deformation. At each ageing time, 50 tensile tests were performed for each grade to obtain statistically relevant data. Besides the stress-strain curve, the yield stress and draw ratio at which fracture (ductile or brittle) occurred, were recorded. In this respect 'ductile' is defined when a tensile bar exceeding 6% macroscopic strain (well beyond the yield point). The tensile creep experiments were performed at TNO Industrial Technology on an in-house built tester [17]. Since the requirements for the tensile creep specimens differ from ISO standards, only

the waisted sections of the pre-deformed tensile bars were used. Loading, following the procedure described by Struik [17], was performed at distinct ageing times after mechanical or thermal rejuvenation. The shortest ageing time was 1350 sec, doubled every next ageing time till 21600 sec in the last time step. During the tests the creep compliance was measured at a constant temperature of 40°C.

Density measurements

The density of the materials was measured before and after the pre-deformation on a Davenport density gradient column filled with a NaBr/water solution kept at a temperature of 23°C. Calibration spheres were used and the density gradient over the column was 0.020 g cm⁻³ (ranging from 1.040 to 1.060 g cm⁻³) over a length of 700 mm. Since the reading accuracy is at least 1mm, the resolution on the density measurements is 3·10⁻⁵ g cm⁻³. The samples used for these measurements were cut from the tensile bars and polished to prevent adhesion of air bubbles to the surface, which could influence the results.

3.3 Results

Intrinsic behaviour

In uniaxial compression the intrinsic deformation behaviour, i.e. deformation without localisation phenomena like shear banding, necking and crazing, was determined. As expected, see figure 3.2, the molecular-weight (distribution) has no significant influence on the intrinsic behaviour. However, properties that are influenced by the molecular weight are related to failure. Following Flory's [18] approach, Merz *et al.* [19] and McCormick *et al.* [19, 20] reported that the tensile strength of polystyrene increases with increasing M_n . Since fracture phenomena are absent in uniaxial compression tests, this influence could not be observed.

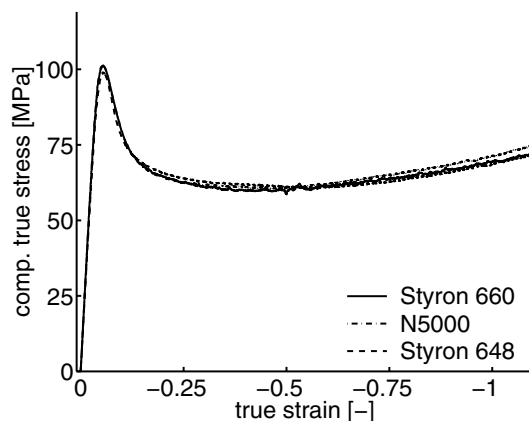


Figure 3.2: Intrinsic deformation behaviour of the three PS grades, measured in compression.

Pre-deformation

Pre-conditioning or pre-deformation has major consequences on both the intrinsic properties and macroscopic deformation behaviour of amorphous polymers [10, 11, 14]. In

figure 3.3, the deformation behaviour of polystyrene N5000 in tension, compression, and after rolling are presented. In this figure the absolute values of the stress and strain are plotted on the axis to enable comparison of both tensile and compression tests. When injection-moulded bars of polystyrene are subjected to a uniaxial tensile test, they exhibit crazing and brittle macroscopic fracture already in the apparent elastic region. Strains and stresses, which are typically reached in such a test, are in the order of 1-2% and 40-50 MPa. The intrinsic behaviour of polystyrene, represented by the compression curve, is characterised by a high yield stress, a pronounced strain softening and weak strain hardening. The effect of pre-deformation is quite clear from figure 3.3: strain softening is virtually eliminated and ductile deformation behaviour is observed, even in a tensile test, reaching macroscopic strains of 30%.

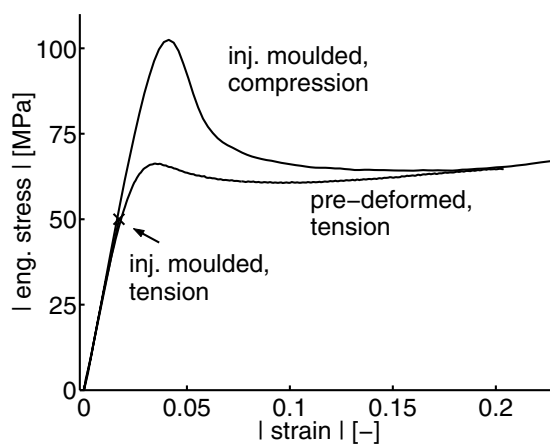


Figure 3.3: Deformation of PS in tension, compression and pre-deformed in tension.

Although the samples are slightly oriented as a result of the pre-deformation, the observed ductility of polystyrene originates from the reduction in strain softening and not from the molecular orientation. This conclusion is substantiated by two facts. First, Broutman *et al.* [11,12] showed, using an identical rolling procedure on polycarbonate, that the improved impact toughness is only slightly influenced by the relative angle of the rolling direction and the test direction. Second, the enhanced ductility is of a transient nature, see below, whereas the induced molecular orientation is permanent at room temperature on this time scale.

To investigate the transient behaviour of ductility, tensile tests are performed at distinct ageing times, see figure 3.4. In these tests, apart from the stress-strain curve, the yield stress and strain to break are recorded. In time, the yield stress increases, see figure 3.5, and strain softening is, consequently, restored, whereas the large strain behaviour remains unchanged. Approximately two days after pre-deformation, renewed brittle fracture is observed for the PS N5000 grade.

The yield stress increases linearly on a logarithmic time scale with ageing time, see figure 3.5. Each marker represents the average value of 50 tensile tests. Since recovery of the yield stress, and thus of strain softening, displays a behaviour similar to physical ageing and proves to be independent of molecular weight, it can be ascribed to relaxation of the polymer chains on a segmental scale.

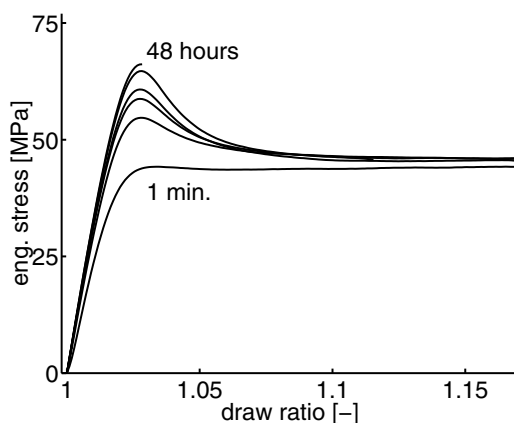


Figure 3.4: Sequence of tensile tests on PS N5000 at distinct ageing times after rolling: renewed brittle fracture after 48 hours is observed.

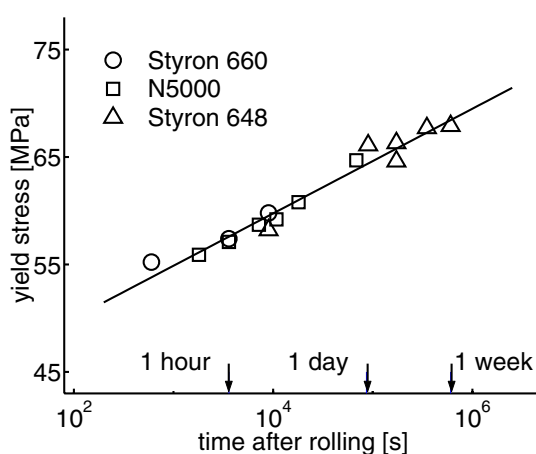


Figure 3.5: Kinetics of the yield stress recovery after pre-deformation.

The obtainable draw ratio is strongly dependent on the ageing time, illustrated in figure 3.6 for PS N5000. The majority of the tensile bars exhibits ductile deformation behaviour ($\lambda > 1.06$) up to 5 hours after pre-deformation, whereas after 48 hours every single tensile bar fractures in a brittle manner.

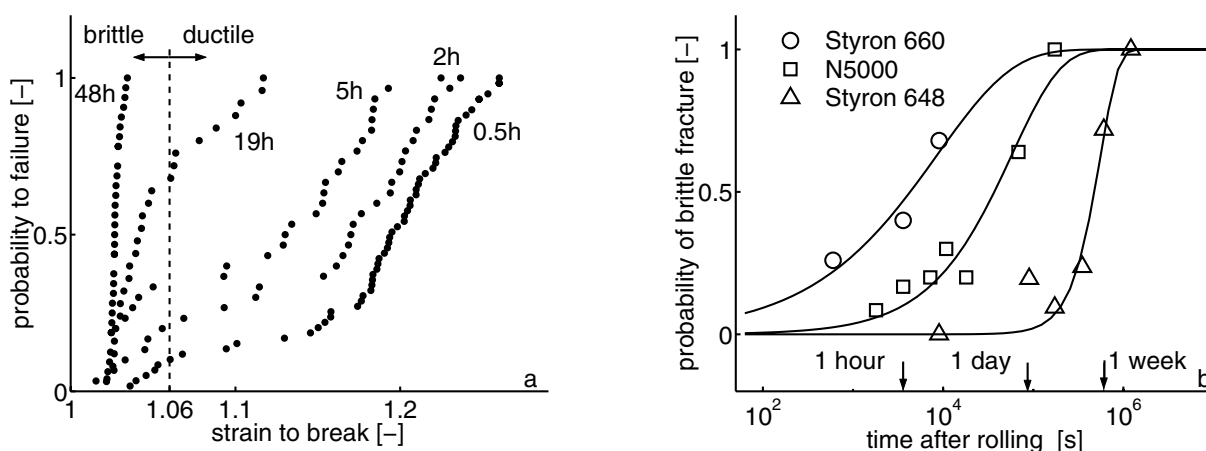


Figure 3.6: Probability to brittle failure: decreasing strain to break for N5000 with increasing ageing time (a) and influence of molecular weight (b).

From figure 3.6a, the fraction of brittle fractures (defined here as the fraction of bars

with a draw ratio smaller than 1.06) observed, are determined at each ageing time. Following an identical procedure for the other grades, and representing these data versus the ageing times, gives the probability to brittle fracture as function of ageing time (figure 3.6b). This probability to failure proves to be dependent on the molecular weight. For the low molecular weight grade, the majority of the tensile bars displays brittle fracture at relative short ageing times, i.e. after 1 hour. With increasing molecular weight, the renewed brittle fracture is postponed: it takes 2 days for N5000 and 1 week for Styron 648 respectively.

Since the intrinsic behaviour, figure 3.2, and the kinetics of yield stress and strain softening recovery with ageing, figure 3.5, are identical for all grades, the difference in macroscopic deformation behaviour after ageing must originate from the influence of molecular-weight, more specifically M_n on breaking stress, Merz *et al.* [19] and McCormick *et al.* [20]. In figure 3.7 the influence of M_n on the deformation behaviour is illustrated.

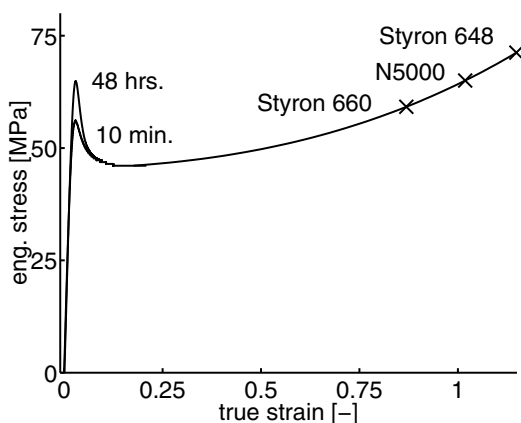


Figure 3.7: Schematic representation of the intrinsic tensile response of the three PS grades at 10 min and 48 hrs after rolling.

Localisations of strain, induced by an increased strain softening, evolve in the same way for all materials. Strain localisation can only be stabilised if the stress, or the force, which can be transferred by the polymer network in the localised plastic zone is sufficiently high in order to exceed the yield stress of the surrounding material. However, the polymer network can only be loaded up to a limited stress, the tensile strength. Hence, after a certain ageing time, the stress in the local plastically deformed zone required to surpass the recovered yield stress in the, yet, hardly undeformed regions, exceeds the tensile strength. Since this tensile strength is related to M_n , both the recovering yield stress and the time-scale, at which fracture occurs, are dependent on M_n .

That intrinsic strain softening is dominant in the macroscopic response of polymers, provides another verification possibility, since strain softening is rate dependent [15, 21]. Therefore, also a rate dependency of the ductile-to-brittle transition is expected, see figure 3.8. At 10 minutes after rolling, the specimen deformed at a strain rate of 10^{-4} s^{-1} exhibits no strain softening. Increasing the strain rate by 1 and 2 decades, results in an increase of yield stress and strain softening with 10 and 20 MPa respectively, see figure 3.8a.

Figure 3.8b shows that the probability to failure at lower draw ratios is unambiguously higher at a strain rate of $5 \cdot 10^{-3} \text{ s}^{-1}$ compared to 10^{-3} s^{-1} at an ageing time of 10

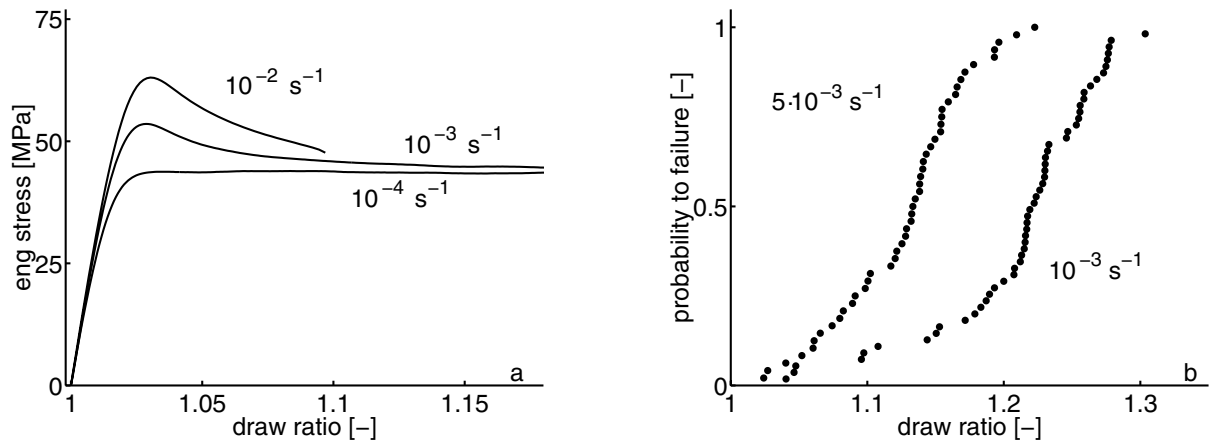


Figure 3.8: PS N5000: influence of strain rate on the tensile behaviour at 10 min after rolling (a) and the accompanying distribution of draw ratios (b).

minutes. This can be rationalised by the fact that at a higher strain rate, resulting in more strain softening, the maximum tensile strength of the polymer network is earlier exceeded, confirming the explanation given above.

Creep tests

The kinetics of recovery of the yield stress and strain softening are independent of the molecular weight and resembles the kinetics of an ageing process. The question rises whether the typical time-scale of this progressive ageing equals that of physical ageing after thermal rejuvenation and whether mechanical rejuvenation can be interpreted as an ultimate quenching procedure.

It is well known that physical ageing and the accompanying structural rearrangements of the molecules, have consequences for the small-strain visco-elastic and time-dependent behaviour of amorphous polymers [17, 22]. Therefore, creep tests are performed at distinct ageing times after rejuvenation (both thermal and mechanical).

During the creep tests, the compliance of the samples is measured. For creeping materials the compliance rises as time passes. The evolution of this compliance was described by a stretched exponent [17] and reads:

$$D(t) = D_0 \exp\left(\frac{t}{a_e \tau}\right)^\gamma \quad (3.1)$$

where D_0 is the initial compliance, t the creep time, τ the relaxation time and a_e the shift factor. As shown by Struik [17], the creep curves are super-imposable and hence the shape of the curves is not influenced by physical ageing. This super-imposability and the fact that the creep curves stretch over many decades, suggest that the process of creep can be described by a spectrum of relaxation times. This has led to the introduction of a shift factor (a_e) by which the relaxation time is multiplied. It was shown that many polymers age in a similar way and that ageing can be characterised by a double-logarithmic shift rate, μ , which is defined as:

$$\mu = -\frac{d \log a_e}{d \log t_e} \quad (3.2)$$

where t_e is the ageing time.

Figure 3.9a and 3.9b, show the creep behaviour of thermally and mechanically rejuvenated polystyrene (N5000), respectively. During creep at constant force, the strain increases in time resulting in an increase in creep compliance. For the quenched material the creep compliance increases slightly from 0.396 to 0.465 GPa^{-1} for the shortest ageing time, i.e. 1350 sec after quenching. As the ageing time rises, a shift along the logarithmic time axis to longer creep times is observed, consistent with observations reported in literature for many amorphous polymers [17].

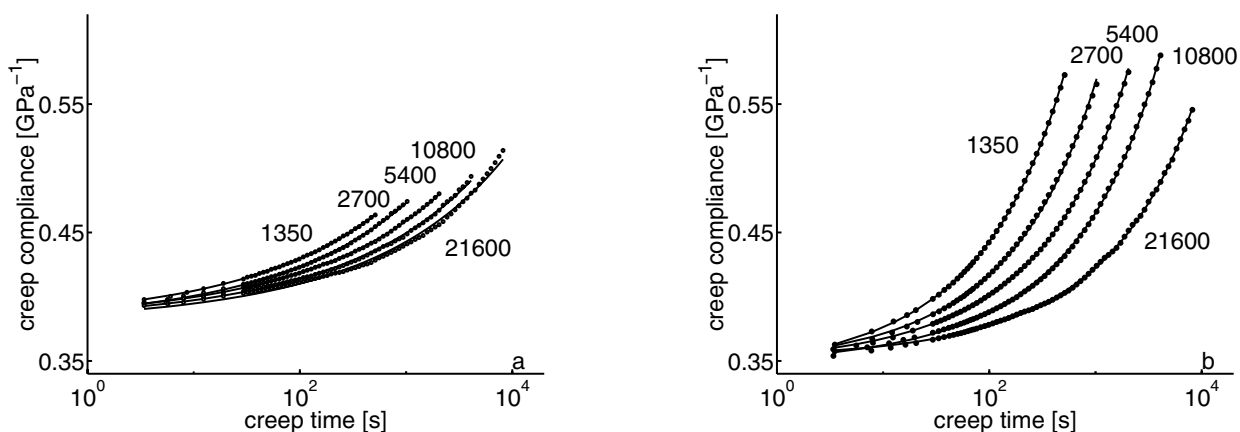


Figure 3.9: Creep compliance of PS N5000 as function of creep time at distinct ageing times (in sec) for thermally rejuvenated PS (a) and mechanically rejuvenated PS (b).

The creep compliance curves for rolled polystyrene, represented in figure 3.9b, deviate considerably from the curves of the quenched material. Initially a lower creep compliance is measured, indicating that the stiffness for the samples after pre-deformation was initially higher, which can be rationalised by the fact that slight orientation of the polystyrene molecules during the rolling procedure occurred. Moreover, as was shown by Broutman *et al.* and will also be shown later in this paper, the macroscopic density increased after rolling, resulting in a closer packing of the chains.

The creep compliance of the pre-deformed samples increases faster with creep time; for the shortest ageing time an increase from 0.363 to 0.573 GPa^{-1} is observed, which is 3 times as much than for the quenched material. This pronounced creep behaviour indicates that the segmental mobility of the polymer chains in the mechanically rejuvenated material is relatively large compared to that of the quenched material. This does not necessarily imply that rejuvenated state of both materials is different, since it is expected that the elimination of strain softening is accompanied by a higher degree of segmental mobility.

A characteristic feature of creep curves is the horizontal shift factor by which they can be shifted along the logarithmic time axes to form a master curve. As shown in figure 3.10, these shift factors prove to be quite different for the thermally and mechanically rejuvenated materials. The shift factor is proportional to the ageing time for both materials but their slopes, a characteristic measure for creep, differ quite remarkably. The shift rate for the pre-deformed material is 50% larger than for the quenched material, that has a shift rate of 0.69, consistent with values reported by Struik [17].

These results suggest that the mechanically rejuvenated state achieved by pre-deformation is quite different from the state reached after thermal quenching. This also gives rise

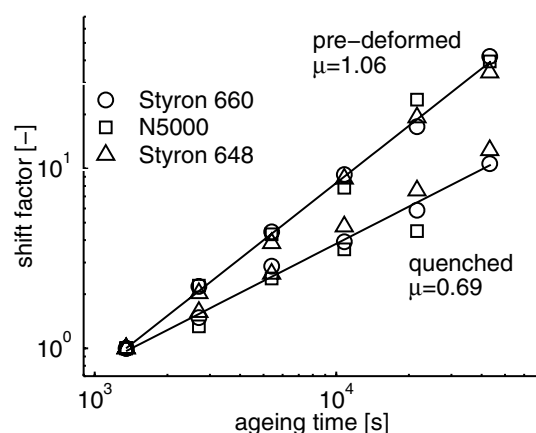


Figure 3.10: Shift factor of thermally rejuvenated and mechanically rejuvenated PS N5000 as function of ageing time.

to the question whether the relaxations on a molecular scale, involved in progressive ageing after pre-deformation, are different from those after quenching. Answering this question, requires knowledge of the processes active on a molecular scale while strain softening evolves during ageing.

Density measurements

Classically the process of physical ageing, and the accompanying changes in properties, are attributed to changes in free volume. This is explained by the fact that a reduced free volume lowers the mobility on segmental scale, and results in, for instance, an increased modulus and yield stress [17]. Since yield stress and strain softening are inherently coupled, this would imply that in a rejuvenated state of reduced strain softening the free volume should be higher and thus the macroscopic density should be lower. To investigate this, the densities of the PS grades are measured, before and after mechanical rejuvenation. Interestingly, these measurements show an opposite effect, summarised in table 3.2, and the density after mechanical rejuvenation is higher than prior to this treatment for all grades. Although the differences are small, they are certainly significant taking into account the accuracy of the density gradient column used (the differences are 10 to 40 times as large as the accuracy of the measurement).

	density before [g cm^{-3}]	density after [g cm^{-3}]
Styron 660	1.05112	1.05145
N5000	1.05118	1.05137
Styron 648	1.04968	1.05080

Table 3.2: Density of PS grades before and after pre-deformation.

Similar observations were done by Broutman *et al.* [11, 12]. They applied an identical procedure for the pre-deformation of various other polymers, like PC, ABS and PVC, and reported an increase in density after rolling of their specimens. Consistent in this respect are the results reported by Xie *et al.* [23], who found an increased density, measured by means of positron annihilation lifetime spectroscopy (PALS), during compression

tests. For such a test it is known that the strain softening is strongly reduced and even eliminated [24].

3.4 Discussion

During processing of polymers, generally rapid cooling from above the rubbery to the glassy state takes place. When passing the glass transition temperature, the segmental mobility of the polymer chains is drastically reduced and hence molecules are not in thermal equilibrium anymore and their occupied volume is larger than the actual equilibrium volume. In time, with ageing of the material, the limited segmental mobility which the molecules possess, causes volume relaxation and thus reduction of the free volume. Due to physical ageing also an increase of the yield stress and concurrent strain softening is observed. The question is, however, whether the classical free volume theory can account for all these effects.

If with physical ageing the reduction in free volume leads to a reduced segmental mobility and, consequently, changes in properties, this would imply that in a rejuvenated state the mobility is enhanced and the density decreased due to an increase in free volume. The density measurements presented here, which are consistent with similar experiments of Broutman [11, 12], show an increased density after mechanical rejuvenation, the treatment that results in the most extreme, reversible reduction of the yield stress. These observations are supported by those of Xie *et al.* [23] and Hasan *et al.* [24]. These experimental observations question the mechanism proposed by Struik that free volume is the governing parameter in physical ageing [17].

The question remains what the physical origin of strain softening is and how it relates to physical ageing. Therefore, a possible explanation that could account for the experimental observations is discussed. Since glassy polymers are in a non-equilibrium state after rapid cooling, in time these materials will pursue a state closer to the equilibrium state. This strive for an energetically more favourable state, driven by primary and secondary interactions of the polymer chains, is accompanied by changes in physical properties. The interactions of the inter- and intra-molecular forces between the polymer molecules can be captured in a concept of a potential energy landscape [25]. This potential energy landscape is defined as a distribution of valleys (energy minima), mountains (energy maxima) and mountain passes (saddle points) [26]. Since polymer chains still possess a certain degree of mobility on a segmental scale in the glassy state, this landscape is not static, but subject to dynamic processes dominated by vibrations within local minima and relaxation between local minima [26]. These dynamic processes lead to local reconfigurations of chain segments and, consequently, a slow loss of energy, deepening the valleys already present in the landscape. Malandro and Lacks [26] investigated by molecular dynamics simulation the influence of shear stress on this potential energy landscape of ductile glasses. They concluded that changes in the potential energy landscape, induced by shear, implied the disappearance of local energy minima, resulting in mechanical instabilities and discontinuous local stress drops. On a macroscopic level this stress drop becomes continuous and can be identified as intrinsic strain softening. Despite the simplicity of the model, it can account for the macroscopic stress-strain response of an amorphous glass in a qualitative way, including its temperature dependence.

Atomistic simulations of Utz *et al.* [27] confirmed this view point and showed that by

ageing the macroscopic stress-drop increases. Moreover, they showed that plastic deformation can 'reverse' these ageing effects. Straining of an aged polymer glass therefore requires more energy than all the minima in the potential energy have to be overcome. Since by ageing these minima become deeper, more energy is required to establish yielding and hence the material exhibits more strain softening. The energy required to draw the material at large strains remains of course identical, as was shown in these atomistic simulations. After this 'pre-deformation' a renewed process of relaxation and strive for local minimisation of potential energy takes place and local minima in potential energy evolve again.

The enhanced mobility, observed in the creep experiments of figure 3.9, can be rationalised by the fact that by pre-deformation the material is taken to a higher energy state. If the minima in the potential energy landscape are leveled out, the chains possess more mobility and creep is facilitated. With ageing, the strive for minimisation of energy reduces the mobility and increases the yield stress and automatically the strain softening. Therefore, considering the intrinsic behaviour of amorphous polymers, a fair view point could be that the stress at which the network contribution takes over during deformation, observed in rapidly quenched samples (PVC) [4] or mechanically rejuvenated samples (see e.g. figure 3.3), can be regarded as the natural response of polymers. Thus, in time increasing yield stress, and, consequently, strain softening, should be regarded as the natural increase in resistance to flow of the polymer chains due to an increasing number of deeper energy minima in the potential energy landscape.

The strive for local energy minimisation must be interrelated to structural rearrangements of polymer chains. Since crystallisation is an effective way to reduce potential energy, some degree of local order in non-crystallisable polymers is not beyond imagination. From the early scattering studies local order in glassy polymers is subject of controversy. Although the scattering patterns of glassy polymers like polystyrene and polycarbonate are very distinct, Mitchell and co-workers stated that any parallelism between chain segments must be minimal [28, 29]. Recent studies, employing techniques like NMR, (FT)IR and atomistic simulations, do suggest the presence of some local order, however, on a much smaller scale [30–39]. It was shown by NMR studies that a preferential packing of molecules exists for glassy polycarbonate which consists of planar alignments of phenylene groups and parallel or perpendicular alignment of carbonate groups [33]. The presence of small-scale order in polystyrene is less well documented and most studies on NMR for polystyrene involve conformation changes [34, 35, 40–43]. Considering the structure of the polymer chains, a local order would certainly involve the (re-)arrangement of phenylene rings. As these rings in the side groups of polystyrene are quite mobile compared to the rings situated in the backbone of polycarbonate, this accounts for the differences in kinetics of the yield stress and strain softening recovery between polystyrene and polycarbonate, see [15].

Further studies, using molecular modelling and the application of these experimental techniques on extreme materials, such as the mechanically rejuvenated polystyrene presented in this study, will be needed to substantiate the present discussion.

Acknowledgements

The authors wish to acknowledge the financial support provided by the Dutch Technology Foundation (STW) (Grant EWT.3766).

References

- [1] Kramer, E.J., In: Kausch, H.H., Ed., *Adv. Pol. Sci.*, Springer, Berlin, **52/53**, 1-56 (1983)
- [2] Legrand. D.G., *J. Appl. Pol. Sci.*, **13**, 2129 (1969)
- [3] Hill, A.J., Heater, K.J., Agrawal, C.M., *J. Pol. Sci.: Part B: Pol. Phys.* **28**, 387 (1990)
- [4] Cross, A., Haward, R.N. Mills, N.J., *Polymer*, **20**, 288 (1979)
- [5] Bauwens-Crowet, C., Bauwens, J.C., Homès, G., *J. Pol. Sci., Part A2*, **7**, 735 (1969)
- [6] G'Sell C., Plastic deformation of glassy polymers: constitutive equations and macromolecular mechanisms. In: H.J. Queens *et al.*, eds. *Strength of metals and alloys*, Pergamon Press, Oxford, 1943-1982 (1986)
- [7] Aboulfaraj, M., G'Sell C., Mangelinck D., McKenna G.B., *J. Non-Cryst. Solids* **172-174**, 615 (1994)
- [8] Govaert, L.E., Timmermans, P.H.M., Brekelmans, W.A.M., *J. Eng. Mat. Tech.* **122**, 177 (2000)
- [9] Tervoort, T.A. and Govaert, L.E., *J. Rheo.*, **44**, 1263 (2000)
- [10] Gruenwald, G., *Modern Plastics*, **37**, 137 (1960)
- [11] Broutman, L.J. and Patil, R.S., *Pol. Eng. Sci.*, **11**, 165 (1971)
- [12] Broutman, L.J. and Krishnakumar, S.M., *Pol. Eng. Sci.*, **14**, 249 (1971)
- [13] Thakkar, B.S. and Broutman, L.J., *Pol. Eng. Sci.*, **20**, 1214 (1980)
- [14] Govaert, L.E.; Melick, H.G.H. van; Meijer, H.E.H., *Polymer*, **42**, 1271 (2001)
- [15] van Melick, H.G.H., Govaert, L.E., Meijer, H.E.H., Localisation phenomena in glassy polymers: influence of thermal and mechanical history, *Polymer*, submitted
- [16] Klompen, E.T.J., *Deformation behaviour of glassy polymers : consequences of thermorheological complex behaviour*, Institute for Continuing Education, Eindhoven University of Technology (1996)
- [17] Struik, L.C.E., *Physical aging in amorphous polymers and other materials*, Elsevier, Amsterdam (1978)
- [18] Flory, P.J., *J. Am. Chem. Soc.*, **67**, 2048 (1945)
- [19] Merz, E.H., Nielsen, L.E., Buchdahl, R., *Ind. Eng. Chem.*, **43**, 1396 (1951)
- [20] McCormick, H.W., Brower, F.M., Kin, L., *J. Pol. Sci.*, **39**, 87 (1959)
- [21] A Multi-Level Finite Element Method for Modeling Rubber-Toughened Amorphous Polymers, In: R. Pearson, Ed., *Toughening of Plastics*, American Chemical Society, Boston, 50-70 (1999)
- [22] Hutchinson, J.M., *Prog. Pol. Sci.*, **20**, 703, (1995)
- [23] Xie, L., Gidley, D.W., Hristov, H.A., Yee, A.F., *J. Pol. Sci., Part B: Pol. Phys.*, **33**, 77, (1995)
- [24] Hasan, O.A. and Boyce, M.C., *Polymer*, **34**, 5085 (1993)
- [25] Stillinger, F.H., *Science*, **267**, 1935 (1995)
- [26] Malandro D.L. and Lacks, D.J., *J. Chem. Phys.*, **110**, 4593 (1999)
- [27] Utz, M., Debenedetti, P.G., Stillinger, F.H., *Phys. Rev. Lett.*, **84**, 1471 (2000)
- [28] Mitchell, G.R. and Windle, A.H., *Polymer*, **25**, 906 (1984)
- [29] Mitchell, G.R., Rosi-Schwartz, B., Ward, D.J., Local order in polymer glasses, In: A. Keller, M. Warner and A.H. Windle, Eds., *Self-order and form in polymeric materials*, Chapman&Hall, London, 93-113 (1995)

- [30] Utz, M., Tomaselli, M., Ernst, R.R., Suter, U.W., *Macromolecules*, **29**, 2909 (1996)
- [31] Utz, M., Atallah, A.S., Robyr, P., Widmann, A.H., Ernst, R.R., Suter, U.W., *Macromolecules*, **33**, 6191 (1999)
- [32] Dybal, J., Schmidt, P., Baldrain, J., Kratochvil, J., *Macromolecules*, **31**, 611 (1998)
- [33] Robyr, P., Gan, Z., Suter, U.W., *Macromolecules*, **31**, 6199 (1998)
- [34] Dunbar, M.G., Novak, B.M., Schmidt-Rohr, K., *Solid State Nuclear Magnetic Resonance*, **12**, 119 (1998)
- [35] Dunbar, M.G., Sanstroem, D., Schmidt-Rohr, K., *Macromolecules*, **33**, 6017 (2000)
- [36] Kozlov, G.V. and Novikov, V.U., *Physics Uspekhi*, **44**, 681 (2001)
- [37] Wang, Y., Shen, D., Qian, R., *J. Pol. Sci.: Part B: Pol. Phys.*, **36**, 783 (1998)
- [38] McGonigle, E.-A., Daly, J.H., Gallagher, S., Jenkins, S.D., Liggat, J.J., Olson, I., Pethrick, R.A., *Polymer*, **40**, 4977 (1999)
- [39] Kaji, H., Horii, E., *J. Chem Phys.*, **109**, 4651 (1998)
- [40] Robyr, P., Gan, Z., Suter, U.W., *Macromolecules*, **31**, 8918 (1998)
- [41] Robyr, P., Mueller, M., Suter, U.W., *Macromolecules*, **32**, 8681 (1999)
- [42] Xu, Z., Jasse, B., Monnerie, L., *J. Pol. Sci. part B: Pol. Phys.*, **27**, 355 (1989)
- [43] Theodorou, M., Jasse, B., Monnerie, L., *J. Pol. Sci. part B: Pol. Phys.*, **23**, 445 (1985)

Chapter 4

Localisation phenomena in glassy polymers: influence of thermal and mechanical history

The macroscopic deformation behaviour of amorphous polymers is dominated by localisation phenomena like necking and crazing. Finite element simulations show that the details of the intrinsic post-yield behaviour, strain softening and strain hardening, determine the severity of strain localisations. In order to perform these numerical simulations an accurate constitutive model is required. The compressible Leonov model is, for this purpose, extended to include temperature effects. Experimentally it is demonstrated that by a small increase in strain softening (by annealing of polycarbonate) or substantial decrease (by mechanical rejuvenation of polystyrene), transitions from ductile to brittle and, respectively, brittle to ductile can be realised. An analytical stability analysis is performed that predicts stable or unstable neck growth dependent on the ratio between yield stress and hardening modulus. The extensive simulations and experimental results lead to the conclusion that in order to macroscopically delocalise strain, and thus improve toughness, one has to reduce strain softening or enhance strain hardening, either by improving the intrinsic behaviour of polymers, or by creating an optimised micro-structure.

4.1 Introduction

The macroscopic deformation behaviour of amorphous polymers is generally dominated by localisation phenomena like shear-band formation, necking and crazing. Which

Reproduced from:

Localisation phenomena in glassy polymers: influence of thermal and mechanical history
H.G.H. van Melick, L.E. Govaert, H.E.H. Meijer, submitted to **Polymer**.

mechanism prevails during deformation is determined by the post-yield behaviour, specifically the balance between strain softening and strain hardening. Although all glassy polymers show a similar intrinsic post-yield behaviour, their macroscopic behaviour is quite different. Polystyrene is, for instance, an extremely brittle material. In tension, crack-like defects appear already in the apparent elastic region. These lens-shaped defects, so-called *crazes*, are no actual cracks but the faces are still bridged with highly stretched fibrillar material [1, 2], which provide them some load-bearing capacity. Ultimately, one of the crazes breaks up and loses its load-bearing capacity, resulting in macroscopic failure. Polycarbonate on the other hand, is a ductile material. In tension, upon yielding, a stable neck is formed that proceeds along the tensile bar and fails at elongations exceeding a draw ratio of approximately 2.

The marked difference in macroscopic behaviour between polystyrene and polycarbonate can be rationalised in terms of subtle differences in strain softening and strain hardening [3]. In polystyrene localisation of strain is severe due to pronounced strain softening and, since its strain hardening is weak, these strain localisations evolve to extremes, leading to crazing and brittle fracture. The moderate strain softening of polycarbonate does induce strain localisations that are, however, easily stabilised by its strong strain hardening contribution.

Many examples are known considering the influence of strain hardening on the macroscopic deformation behaviour. It is now well established that strain hardening is a stress contribution of the entangled polymer network [4–6], the strongest arguments being that it can be enhanced by increasing the network density. For polystyrene this can be achieved by cross-linking [6, 7] or by blending with polyphenylene oxide (PPO) [6, 8]. The increase of strain hardening eventually leads to macroscopically ductile deformation behaviour in polystyrene, for instance, Henkee and Kramer [7] reported that cross-linking of polystyrene [7] induced a transition from crazing to shear yielding in a tensile test. Similar results were reported for blends of polystyrene and polyphenylene oxide (PPO) with high fractions of PPO [9–13].

Although the exact physical origin of strain softening is not really clear, it is known to be strongly related to physical ageing [14, 15]. Physical ageing is often explained by the free volume theory [15], despite the fact that there is evidence which questions this relation. During mechanical treatments or tests, in which the material is rejuvenated and strain softening is reduced, the macroscopic density increased and thus free volume must have decreased [16–18]. Furthermore it is known that strain softening depends on the thermal and mechanical history and the testing conditions. Quenched samples exhibit less strain softening than slowly cooled specimens [17, 19, 20], strain softening can be drastically reduced, or even eliminated, by mechanical pre-conditioning or pre-deformation [5, 17, 21–25] and, similar to the yield stress, strain softening is sensitive to temperature, strain rate and pressure [26–29].

In this paper the influence of post-yield behaviour on localisation of strain during deformation is investigated by numerical and experimental methods. Finite element simulations, employing the compressible Leonov model, are performed to show the consequences of differences in intrinsic behaviour on macroscopic deformation behaviour of polystyrene and polycarbonate. Only localisation of strain is considered and failure mechanisms which occur in this process [30–32] are not incorporated. The influence of thermal and mechanical treatments on strain softening and the consequences for macroscopic deformation behaviour are investigated. Finally, finite element simulations

are used to illustrate the influence of temperature and a supporting rubber layer on the macroscopic deformation behaviour of polystyrene in tension.

4.2 Materials and Methods

Materials

The materials used were a commercial grade of polystyrene, N5000 (supplied by Shell) and two commercial grades of polycarbonate, Lexan 101^R (supplied by General Electric Plastics) and Makrolon CD2000 (supplied by Bayer Co.). For the uniaxial compression tests, cylindrical samples ($\varnothing 6$ mm x 6 mm) were machined from thick plates (160x160x9 mm³), which were compression moulded from granular material at a temperature 90°C above their T_g . First the material was heated for 15 minutes in the mould and compressed during 5 minutes in 5 steps of increasing force, up to a maximum force of 300 kN. In between the steps, the force was released to allow for degassing. Afterwards the mould was placed in a cold press and cooled to room temperature at a moderate force (100 kN). The specimens for the uniaxial tensile tests were made via injection moulding, according to ISO 527. Prior to processing, all materials were dried in an oven at 70°C for three days.

Mechanical tests

Uniaxial compression and tensile tests were performed on a servo-hydraulic MTS Elastomer Testing System 810. In compression tests, specimens were loaded between two parallel, steel compression plates. Friction between sample and plates was reduced by an empirically optimised method: onto the sample a thin film of PTFE tape (3M 5480, PTFE skived film tape) was applied and the surface between steel and tape was lubricated by a soap-water mixture. During compression tests no bulging or buckling of the sample was observed, indicating that the friction was sufficiently reduced. The compression tests were performed, in strain control, at constant logarithmic strain rates ranging from 10^{-4} to 10^{-2} s⁻¹ whereas uniaxial tensile tests were performed at a constant linear strain rate of 10^{-3} s⁻¹. A temperature chamber was used to allow accurate control of the temperature ($\pm 0.5^\circ\text{C}$). Approximately 15 minutes prior to testing the samples were mounted in the setup to ensure thermal equilibrium at the desired temperature.

Thermo-mechanical treatments

Two thermal treatments were used: quenching and annealing. Quenching was performed by heating of the samples in an oven at 15°C above their glass transition temperature for half an hour and, subsequently, rapidly cooling in ice-water. The annealing was done by a heating period of three days at 20°C below the glass transition temperature, followed by slow cooling (1 day) to room temperature. The mechanical treatment of polystyrene (rolling) is extensively described in Govaert *et al.* [25].

4.3 Intrinsic deformation behaviour

Uniaxial compression tests

Since localisation phenomena like necking and crazing are suppressed in uniaxial compression tests, these tests are used here to determine the intrinsic deformation behaviour of polystyrene and polycarbonate. Figure 4.1 presents the true-stress/true-strain curves at a temperature of 20°C and a logarithmic strain rate of 10^{-3} s^{-1} (circles). The differences in intrinsic behaviour between polystyrene and polycarbonate are unambiguously shown. Besides a slight difference in elastic modulus and yield stress, the main difference is found in the amount of strain softening, or yield drop, and in the value of the strain hardening modulus. Polystyrene exhibits a yield drop of approx-

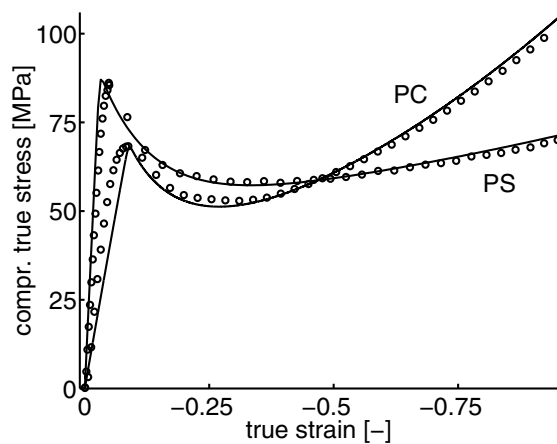


Figure 4.1: True-stress/true-strain curves for PS and PC in compression: experimental data (circles) and numerical simulations (solid lines), using the compressible Leonov model with the parameters given in table 4.1.

imately 30 MPa, whereas for polycarbonate this drop is only 19 MPa under identical testing conditions. The strain hardening modulus, defined as the slope of the stress-strain curve (true stress versus $\lambda^2 - \lambda^{-1}$) at large strains, is more than twice as large for polycarbonate as for polystyrene, 29 MPa versus 11 MPa.

Numerical modelling

In the numerical model used, the generalised compressible Leonov model [24, 33], a distinction is made between the contribution of secondary interactions between polymer chains, that determine the (visco-) elastic properties at small deformations and the yield behaviour, and the entangled polymer network that governs the large strain behaviour. The total Cauchy stress (σ) is decomposed in a driving stress (s) and a hardening stress (r), according to:

$$\sigma = s + r \quad (4.1)$$

The driving stress is subsequently decomposed into a deviatoric part (s^d) and hydrostatic part (s^h):

$$s^d = G\tilde{B}_e^d \quad \text{and} \quad s^h = \kappa(J - 1)\mathbf{I} \quad (4.2)$$

where G is the shear modulus, $\tilde{\mathbf{B}}_e^d$ the deviatoric part of the isochoric elastic left Cauchy-Green deformation tensor, κ the bulk modulus, J the volume change factor and \mathbf{I} the unity tensor. The superscripts d and h denote the *deviatoric* and the *hydrostatic* part respectively, the subscripts e , p , and eq indicate that an *elastic*, *plastic*, and *equivalent* quantity is used. The relative volume change and the isochoric elastic left Cauchy-Green deformation tensor $\tilde{\mathbf{B}}_e$ are given by the evolution equations:

$$\dot{J} = J \text{tr}(\mathbf{D}) \quad (4.3)$$

$$\overset{\circ}{\tilde{\mathbf{B}}}_e = (\mathbf{D}^d - \mathbf{D}_p) \cdot \tilde{\mathbf{B}}_e + \tilde{\mathbf{B}}_e \cdot (\mathbf{D}^d - \mathbf{D}_p) \quad (4.4)$$

where $\overset{\circ}{\tilde{\mathbf{B}}}_e$ is the Jaumann rate of $\tilde{\mathbf{B}}_e$, \mathbf{D}^d the deviatoric part of the rate of deformation tensor and \mathbf{D}_p the plastic part of the rate of deformation tensor.

The hardening behaviour is described by a neo-Hookean relation for the hardening stress \mathbf{r} :

$$\mathbf{r} = G_R \tilde{\mathbf{B}}^d \quad (4.5)$$

where G_R is the strain hardening modulus. As proposed by Tervoort *et al.* [33] a Newtonian flow rule with a stress dependent Eyring viscosity is used to relate the plastic deformation rate tensor, \mathbf{D}_p , to the deviatoric driving stress tensor, \mathbf{s}^d :

$$\mathbf{D}_p = \frac{\mathbf{s}^d}{2\eta(\tau_{eq}, D, p)} \quad (4.6)$$

The viscosity, η , is strongly dependent on the equivalent stress, τ_{eq} , and was originally described by an Eyring relationship [34]. Govaert *et al.* [24] extended the model by incorporating pressure dependence (μ) and intrinsic strain softening (D) in the viscosity function:

$$\eta(\tau_{eq}, D, p) = A(D, p) \tau_0 \frac{\frac{\tau_{eq}}{\tau_0}}{\sinh\left(\frac{\tau_{eq}}{\tau_0}\right)} \quad (4.7)$$

where the equivalent stress, τ_{eq} , is defined as:

$$\tau_{eq} = \sqrt{\frac{1}{2} \text{tr}(\mathbf{s}^d \cdot \mathbf{s}^d)} \quad (4.8)$$

and

$$A = A_0 \exp\left(\frac{\Delta H}{RT}\right) \exp\left(\frac{\mu p}{\tau_0} - D\right) \quad (4.9)$$

$$\tau_0 = \frac{RT}{V} \quad (4.10)$$

$$p = -\frac{1}{3} \text{tr}(\boldsymbol{\sigma}) = -\frac{1}{3} \text{tr}(\mathbf{s}) \quad (4.11)$$

where A_0 is a constant pre-exponential factor, R is the gas constant, and T the absolute temperature. In the evolution of the softening, originally proposed by Hasan *et al.* [35],

the softening parameter D is initially set to zero. In time, this parameter evolves to the softening limit D_∞ according to:

$$\dot{D} = \left(1 - \frac{D}{D_\infty}\right) \dot{\gamma}_p \quad (4.12)$$

where the equivalent plastic strain rate, $\dot{\gamma}_p$, equals:

$$\dot{\gamma}_p = \sqrt{2\text{tr}(\mathbf{D}_p \cdot \mathbf{D}_p)} \quad (4.13)$$

From equation 4.6 a condensation in equivalent quantities can be performed using equations 4.8 and 4.13, under the assumption that during yielding the equivalent strain rate equals the equivalent plastic strain rate:

$$\dot{\gamma}_{eq} = \frac{\tau_{eq}}{\eta(\tau_{eq}, D, p)} \quad (4.14)$$

Combining this equation with equation 4.7 yields the well-known Eyring expression for the equivalent strain rate as function of the equivalent stress [34]:

$$\dot{\gamma}_{eq} = \frac{1}{A} \sinh\left(\frac{\tau_{eq}}{\tau_0}\right) \quad (4.15)$$

If the argument of the hyperbolic sine function is large, it can be replaced by an exponential function. Some rearranging of equations 4.9 and 4.15 (at yield point $D = 0$), results in an equation for the equivalent stress, expressed in the equivalent strain rate:

$$\tau_{eq} = \tau_0 \left[\ln 2A_0 \dot{\gamma}_{eq} + \frac{\Delta H}{RT} + \frac{\mu p}{\tau_0} \right] \quad (4.16)$$

This expression can be used directly to fit the parameters on the experimental data, the macroscopic yield stresses (σ_y) and the logarithmic strain rates ($\dot{\epsilon}$). Using equations 4.8 and 4.13 in a uniaxial compression test, at the yield point, equivalent quantities can be expressed as function of stress and strain rate:

$$\tau_{eq} = \frac{1}{\sqrt{3}} \sigma_y \quad \text{and} \quad \dot{\gamma}_{eq} = \sqrt{3} \dot{\epsilon} \quad (4.17)$$

In figure 4.2a, the experimentally obtained equivalent yield stresses, τ_{eq} , (markers), as function of temperature and equivalent strain rate, $\dot{\gamma}_{eq}$, are presented. From the slope of these curves the characteristic stress, τ_0 , and thus the activation volume, V (see equation 4.10) can be derived. From the offset of the curves at various temperatures the time constant, A_0 , and the activation energy, ΔH , are determined. Since at a sufficiently high pressure ductile deformation behaviour is observed even in polystyrene, the pressure coefficient, μ , was determined up-front in a uniaxial tensile test under superimposed pressure at the IRC in Leeds and proved to be equal to 0.14. The solid lines in figure 4.2a are fits with the parameters for PS N5000 given in table 4.1. For the elastic parameters E and ν literature values are taken [36].

The strain hardening modulus is determined from the slope of the stress-strain curve at large strains. The last two parameters, the softening limit, D_∞ , and the softening slope, h , are obtained by a visual fit on the true stress-strain curve of a uniaxial compression

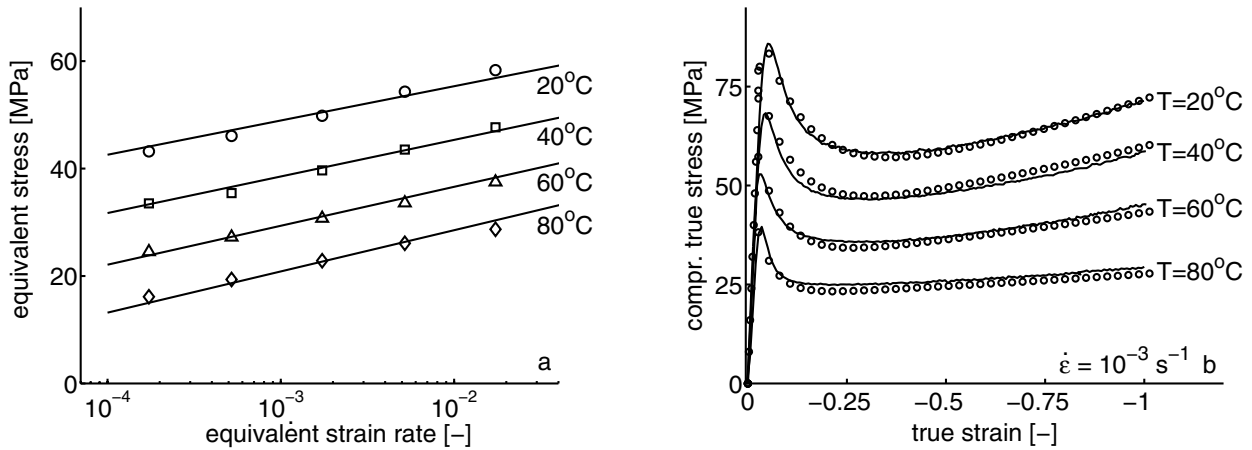


Figure 4.2: Equivalent yield stresses of PS as function of equivalent strain rate and temperature (a) and the compressive behaviour of PS at various temperatures (b), markers represent the experiments, solid lines the simulations using the parameters given in table 4.1.

	PS N5000	PC Lexan 101 ^R / Makrolon CD2000	
E	3300	2400	[MPa]
ν	0.37	0.4	[-]
V	$9.52 \cdot 10^{-4}$	$3.4 \cdot 10^{-3}$	[m ³ mol ⁻¹]
ΔH	$1.70 \cdot 10^5$	$2.90 \cdot 10^5$	[J mol ⁻¹]
A_0	$1.11 \cdot 10^{-20}$	$3.6 \cdot 10^{-25}$	[s]
G_R	11	29	[MPa]
D_∞	9	26	[-]
h	60	200	[-]
μ	0.14	0.07	[-]

Table 4.1: Material parameters of PS N5000 and Makrolon CD2000/Lexan 101^R [24].

test at 20°C and 10^{-3} s^{-1} , see figure 4.2b. The parameters derived under these testing conditions are the reference values and will be referred to with the subscript 0. The material parameters used in the simulations are given in table 4.1.

Since the temperature not only influences the yield stress, but also has a significant influence on modulus, softening limit and strain hardening, a temperature dependence of these properties for polystyrene is incorporated in the simulations. The temperature dependence of the modulus is derived from dynamical mechanical thermal analysis [6] and reads:

$$E(T) = E_0(-0.0264 T + 1.79) \quad (4.18)$$

Although for visco-elastic materials a more complex relation would be appropriate, for the isothermal simulations this simple relation is adequate. From this temperature dependent modulus and the Poisson ratio the bulk modulus, κ , and shear modulus, G are derived which are used as input in the numerical model. The temperature depen-

dence of the strain hardening modulus and the softening limit are derived from uniaxial compression tests at various temperatures, see figure 4.2b, and yields:

$$D_{\infty}(T) = D_{\infty,0}(-0.012 T + 4.516) \quad G_R(T) = G_{R,0}(4.91 - 0.0133 T) \quad (4.19)$$

In these empirical relations T [K] is the absolute temperature. Since the value of the strain softening parameter D evolves in time according to equation 4.12, the assumed temperature dependence can only be used in stationary temperature fields. The slight rate dependence of the strain softening [31] is not incorporated in the numerical model. Apart from the difference in tensile strength and a slight difference in strain hardening modulus [42], the difference in molecular weight (distribution) for the polycarbonate grades has no influence on the intrinsic properties, and hence the same parameter set is used for Lexan 101^R and Makrolon CD2000, adopted from [24].

The solid lines in figure 4.1 and 4.2b represent the numerical simulations using the parameter sets from table 4.1 and demonstrate the ability of the compressible Leonov to give a quantitative description of the intrinsic deformation behaviour of glassy polymers.

FEM model

The geometry used in the finite element simulations is an axisymmetric model of a tensile bar with a small imperfection, situated at the surface in the middle of the tensile bar. The cylindrical tensile bar has a dimensionless parallel length of 1 and a radius of 0.2. The circular imperfection has a radius of 0.02 and a maximum depth of 0.003 (1.5% of the radius of the bar). Govaert *et al.* [24] showed that the size and shape of the imperfection are only of minor influence on the deformation of the tensile bar. Only the draw ratio during stable neck growth is slightly influenced. The finite element model consists of 537 8-noded second-order elements, represented in figure 4.3. During the tensile test the bar is deformed at a constant linear strain rate of 10^{-3} s^{-1} . For the simulation in which a rubber layer is incorporated, a thin layer (10% of the radius of the bar) of elements is glued on the surface to the tensile bar. For the rubber a neo-Hookean model is chosen with a shear modulus of 150 MPa.

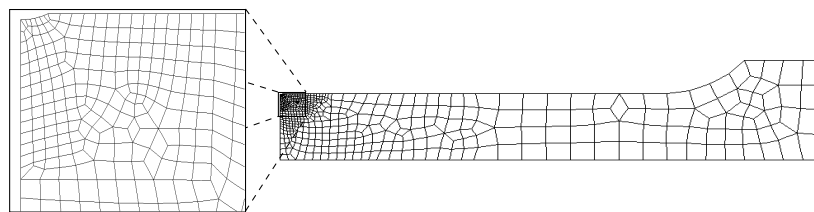


Figure 4.3: Finite element mesh of the tensile bar with imperfection (zoomed area).

4.4 Results

Deformation and localisation processes in polycarbonate

Results of finite element simulations

Figure 4.4 presents a numerical simulation of a tensile test on polycarbonate. During the initial elastic stage, stresses rise throughout the specimen and, until the yield point is

reached, the stress is approximately equal in all marked positions. Yield and subsequent plastic deformation occurs first underneath the imperfection (bullet) and, immediately after yielding, the material deforms, localising the strain in this zone, accompanied by a local drop in stress because of strain softening. Both events cause the stress to drop in the elastically deformed regions and the other three markers descend along the elastic curve, see figure 4.4a.

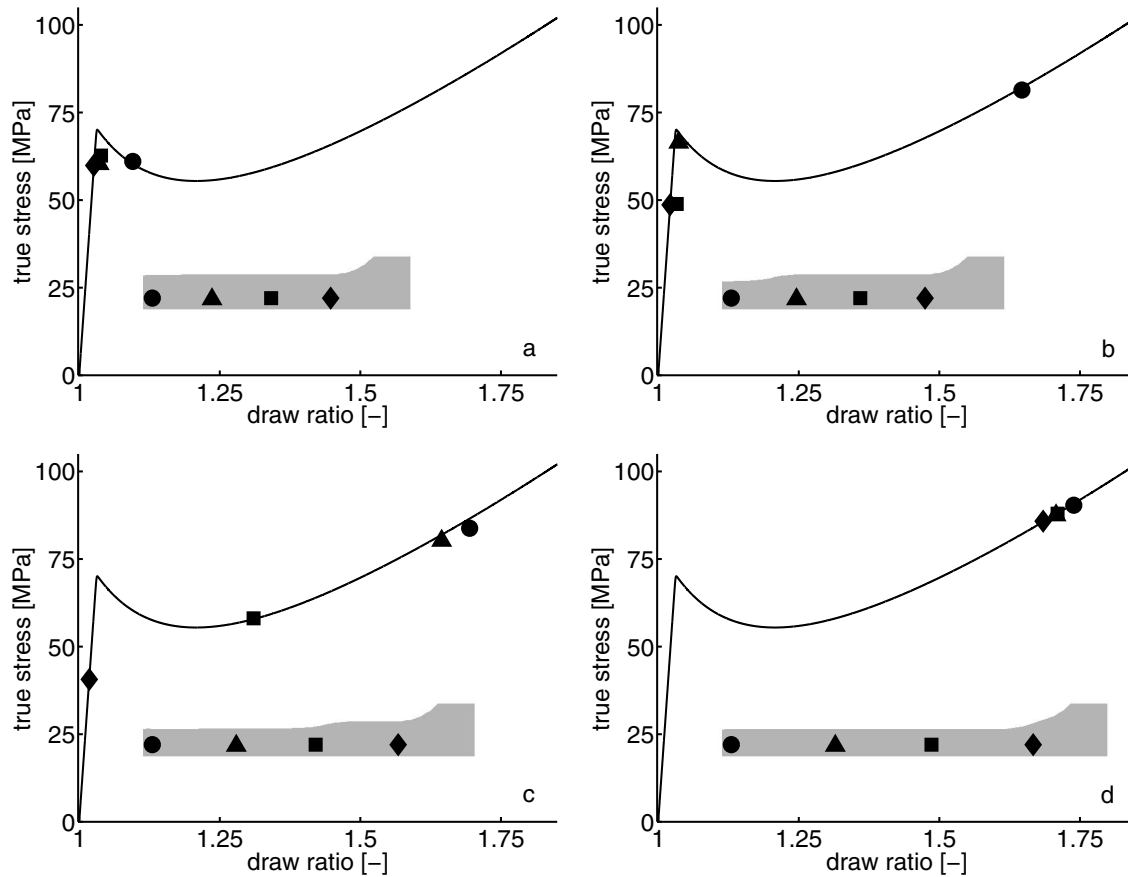


Figure 4.4: Numerical simulation of a tensile test on PC: stable neck growth.

With ongoing deformation, the material in the deformed region experiences strain hardening. As a result the force required to deform this material exceeds the force required to induce yielding in the adjacent material (shoulder). Figure 4.4b represents the stage in which the material in the neck (bullet) is stabilised and the shoulder (triangle) of the neck reaches the yield point. Next yielding occurs in the shoulder, while the material already present in the neck is not strained further. This continuing process of yielding, localisation and stabilisation results in formation of a stable neck which proceeds along the tensile bar (see figure 4.4c) until the neck reaches the tabs of the tensile bar (diamond). Then again the stress is quite homogeneously distributed throughout the tensile bar, which can be witnessed from the fact that all markers are approximately at the same position in the intrinsic stress-strain curve, see figure 4.4d. With ongoing deformation, cold-drawing in the neck proceeds until the tensile strength in the neck is exceeded.

The process of stabilisation of the neck can be demonstrated by the evolving stress and draw ratio in the neck during deformation. In figure 4.5, the engineering stress versus

nominal draw ratio is plotted (solid line), which represents the macroscopic response in a tensile test. Stress rises until the yield stress is reached, followed by a sudden drop as the neck is formed. Throughout the process of necking, the engineering stress remains at a constant level. The dashed line in the graph represents the local draw ratio in the neck (underneath the imperfection), as function of the nominal draw ratio. Immediately after yielding, the draw ratio increases rapidly and levels off to a merely constant value, indicating that the deformation is stabilised in the neck. The exact value at which the neck is stabilised is of course dependent on the value of the yield stress, the strain softening, and strain hardening. Once the neck reaches the tabs of the tensile bar (figure 4.4d), stress and draw ratio increase again until failure occurs.

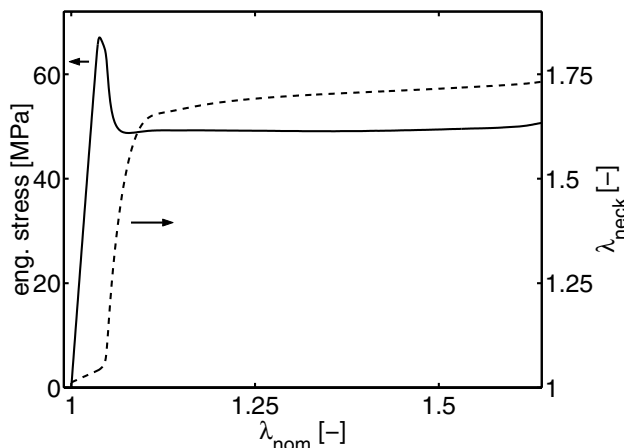


Figure 4.5: Numerical tensile test on PC: engineering stress (solid) and draw ratio in the neck (dashed) versus the nominal draw ratio.

The influence of thermal history

The intrinsic behaviour of glassy polymers is known to be dependent on the thermal history [17, 19] and figure 4.6 shows that annealing induces a slight increase in yield stress of, in this case, polycarbonate (Lexan 101^R). The change in strain softening (or yield drop) equals the increase in yield stress since the large strain behaviour (strain hardening), remains unaffected by annealing. The subtle changes in strain softening

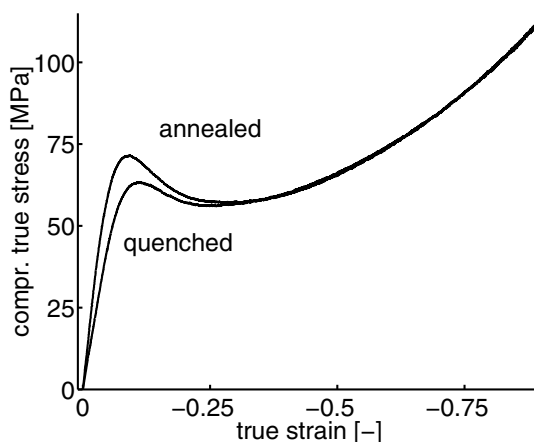


Figure 4.6: Compression experiments demonstrating the influence of aging on the intrinsic behaviour of PC: an increase in yield stress and strain softening.

can have major consequences for the macroscopic deformation behaviour. Figure 4.7

shows the stress-strain curves of uniaxial tensile tests on Makrolon CD2000, before and after thermal treatment. For the injection moulded tensile bar, a neck appears shortly after yielding (see figure 4.7a and 4.8a) and the process continues as described before.

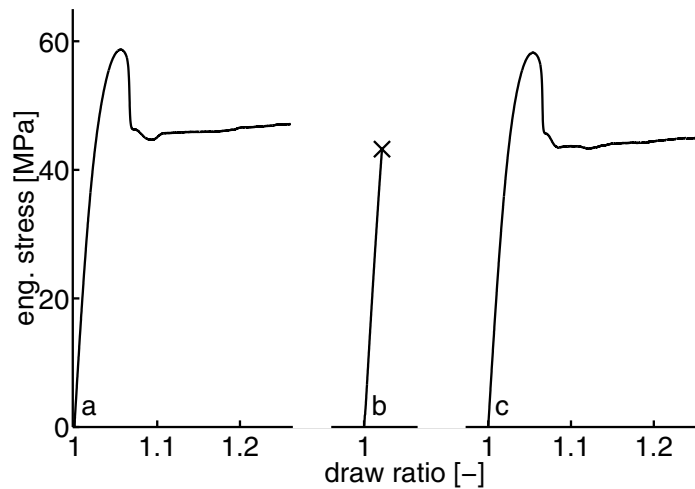


Figure 4.7: Effect of thermal treatments on the macroscopic deformation: necking in injection moulded PC (a), embrittlement after annealing (b), and renewed necking after heating above T_g and subsequent rapid cooling (c).

In the annealed material, brittle fracture is observed in the apparent elastic region, well below the macroscopic yield stress (see figure 4.7b and 4.8b). The enhanced intrinsic strain softening after annealing (see figure 4.6), induces a more severe localisation of strain during deformation, which, due to the limited tensile strength of this low molecular weight grade, can not be stabilised.

That this brittle fracture is indeed caused by changes in intrinsic properties and not by degradation can be witnessed from the fact that the phenomenon is reversible. By bringing the annealed material again above its glass transition temperature and subsequent rapid cooling, stable neck growth is observed again in a tensile test (see figure 4.7c), similar to the behaviour of the injection moulded material prior to the treatments.

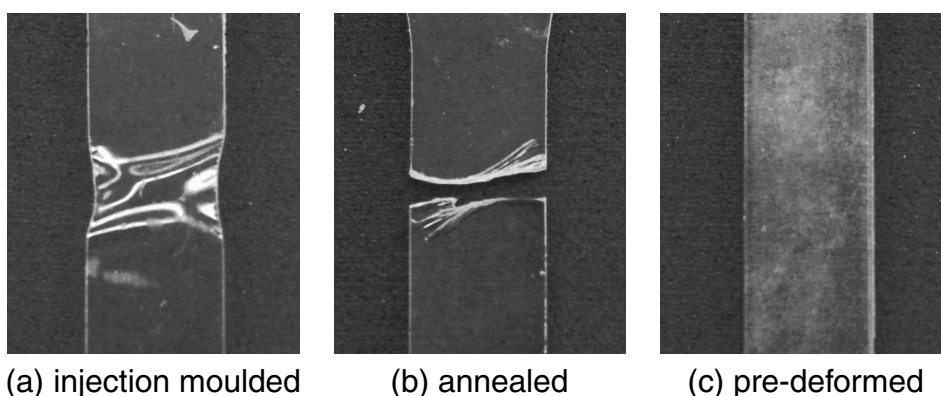


Figure 4.8: Influence of thermo-mechanical history on macroscopic deformation of Makrolon CD2000, from necking in the injection moulded material (a), to brittle fracture after annealing (b) and homogeneous deformation after rolling (c).

The influence of mechanical history

Mechanical rejuvenation, also referred to as mechanical pre-conditioning or pre-deformation, has proven to be an effective method for the reduction, or even elimination, of strain softening. Bauwens [23] showed that by alternating bending prior to a tensile test, homogeneous deformation behaviour can be achieved for PVC samples. Similar results were reported by Govaert *et al.* [24] and Tervoort and Govaert [5] who pre-conditioned cylindrical tensile bars of polycarbonate by torquing and studied macroscopic deformation behaviour before and after rejuvenation in tension. Uniaxial compression tests showed that the significant amount of strain softening (see figure 4.1) was eliminated while the large strain behaviour (strain hardening) remained unchanged. The elimination of strain softening prevented localisation of strain and neck-formation and hence the pre-conditioned samples exhibited uniform deformation behaviour. Figure 4.8c and 4.12 shows the homogeneous deformation of a rolled (thickness reduction of 15%) polycarbonate bar and illustrates this effect. It must be noted that strain softening restores in time; the yield stress and yield drop increase again, on a time scale of months, resulting in renewed neck formation in a uniaxial tensile test [37].

Results of a neck-stability analysis

The stability of macroscopic deformation in tension can be predicted if the intrinsic deformation behaviour, i.e. the yield stress, rejuvenated yield stress, and strain hardening modulus are known up-front.

The approach of Haward [38] will be followed, who considered a material with no strain softening (yield stress equal to the rejuvenated yield stress $\sigma_{y,r}$, see figure 4.12a) and neo-Hookean strain hardening (with modulus G_R). Under the influence of ageing, the yield stress is assumed to increase according to: $\sigma_y = \kappa_y \sigma_{y,r}$, where κ_y is an arbitrary multiplier (larger than 1) that can be determined experimentally. This simple approach is not quite as accurate as the equations in the numerical model, but enables a straight-forward neck-stability analysis.

A stable neck is formed if the load transferred by the neck equals the load required to induce yielding in the undeformed zone. Neglecting the small strain in the elastically deformed zones (i.e. $\lambda = 1$), the expression for equilibrium is given by:

$$\kappa_y \sigma_{y,r} A_0 = \left[\sigma_{y,r} + G_R \left(\lambda_n^2 - \frac{1}{\lambda_n} \right) \right] \frac{A_0}{\lambda_n} \quad (4.20)$$

where A_0 is the initial cross-section of the bar and λ_n the draw ratio in the neck. Equation 4.20 can be rearranged into:

$$\frac{\sigma_{y,r}}{G_R} = \frac{\lambda_n^2 - \frac{1}{\lambda_n}}{\kappa_y \lambda_n - 1} \quad (4.21)$$

In figure 4.9a, equation 4.21 is graphically represented. The solid line represents the lines of equilibrium for rejuvenated ($\kappa_y = 1$). In the original analysis, without strain softening [38], it was already shown for a ratio of yield stress and strain hardening modulus smaller than 3 homogenous deformation must be observed and a ratio above this value stable neck growth is encountered in a uniaxial tensile test. Figure 4.9 shows that polycarbonate, which has a rejuvenated yield stress, $\sigma_{y,r}$ of 45 MPa and a strain hardening modulus, G_R of 29 MPa (and thus a ratio $\frac{\sigma_{y,r}}{G_R}$, of 1.55, indicated by the dashed

line), is situated well below the equilibrium line of $\kappa_{y} = 1$. Therefore homogeneous deformation is predicted for rejuvenated polycarbonate in uniaxial tension, which is consistent with the observations of rolled polycarbonate samples that exhibit homogeneous deformation without necking (see figure 4.8c).

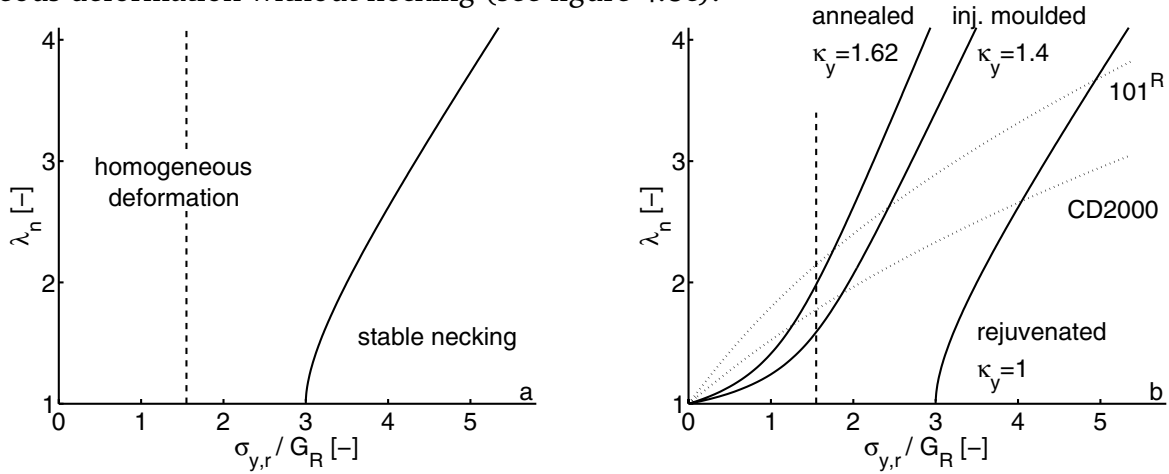


Figure 4.9: Stability analysis, analogous to [38]: homogeneous deformation below a ratio $\frac{\sigma_{y,r}}{G_R}$ of 3 and above stable neck growth (a). Prediction of the deformation mode for two PC grades (b). Solid lines represent the equilibrium lines of stable neck growth at distinct $\kappa_{y,s}$ (see equation 4.20), the dashed line indicates a ratio $\frac{\sigma_{y,r}}{G_R}$ of 1.55 (characteristic for PC), and the dotted lines represent the tensile strength limits, depending on molecular weight (see equation 4.22).

Once a polymer exhibits strain softening ($\kappa_{y} > 1$), the eq. line drops initially to zero, which, from a mechanical point of view, means that strain localisation is inevitable. The additional solid lines in figure 4.9 represent injection moulded polycarbonate, with a yield stress of approximately 63 MPa ($\kappa_{y} = 1.4$) and annealed polycarbonate, where the yield stress rises to 73 MPa ($\kappa_{y} = 1.62$), respectively. The dashed line and the equilibrium line intersect at a λ_n of around 1.7, approximately the draw ratio observed during neck growth. (see figure 4.5). Upon annealing the equilibrium line drops further and is crossed by the dashed line at a draw ratio of 2. This illustrates that after annealing a higher load has to be transferred by the polymer network, accompanied by a higher λ_n , to stabilise the deformation.

As proposed by Flory [39] and shown for polystyrene by Merz *et al.* [40] and McCormick *et al.* [41], the tensile strength of polymers increases with the number-averaged molecular weight. The maximum stress that can be transferred by the polymer network is dependent on the molecular weight of the grade and is assumed to be equal to $\kappa_t \sigma_{y,r}$, where κ_t is a multiplier which can be determined experimentally. The tensile stress at the moment of failure equals the rejuvenated yield stress plus the stress transferred by the polymer network, which can be rearranged according to:

$$\kappa_t \sigma_{y,r} = \sigma_{y,r} + G_R \left(\lambda_n^2 - \frac{1}{\lambda_n} \right) \quad \rightarrow \quad \frac{\sigma_{y,r}}{G_R} = \frac{\lambda_n^2 - \frac{1}{\lambda_n}}{\kappa_t - 1} \quad (4.22)$$

This equation is represented by the dotted lines in figure 4.9 for Makrolon CD2000 ($\sigma_t = 120$ MPa, $\kappa_t = 2.67$) and Lexan 101^R ($\sigma_t = 165$ MPa, $\kappa_t = 3.67$) [42].

For the Lexan 101^R, with a relative high molecular weight, the tensile strength at failure is sufficiently high. However, for the Makrolon CD2000, the dotted line of tensile maximum strength is crossed by the dashed line, in case of annealing, before the equilibrium

line is reached. This means that fracture occurs before the neck is stabilised (see figure 4.8b). This analysis illustrates that the embrittlement of polymers like polycarbonate in uniaxial tension, is strongly dependent in this example on the molecular weight (via κ_t) and annealing time (via κ_y).

Deformation and localisation processes in polystyrene

Results of FEM simulations

Now we investigate the influence of intrinsic properties on localisation in polystyrene (ignoring mechanisms like crazing, which will occur as a result of severe strain localisations, see for these aspects [30–32]). Figure 4.10 shows the simulation of a tensile test on polystyrene. Initially the deformation is similar to polycarbonate, as shown in figure 4.4, homogeneous, elastic deformation until yielding occurs at the imperfection (see figure 4.10a). The pronounced strain softening exhibited by polystyrene, induces a much more severe localisation of strain, the stress drops drastically after yielding and hardly rises again at large strains due to insufficient strain hardening. The differences in draw ratio illustrates this the more, varying from 1 to 4 for polystyrene in figure 4.10, whereas for polycarbonate this range was only 1 to 1.8, see figure 4.4. The deformation

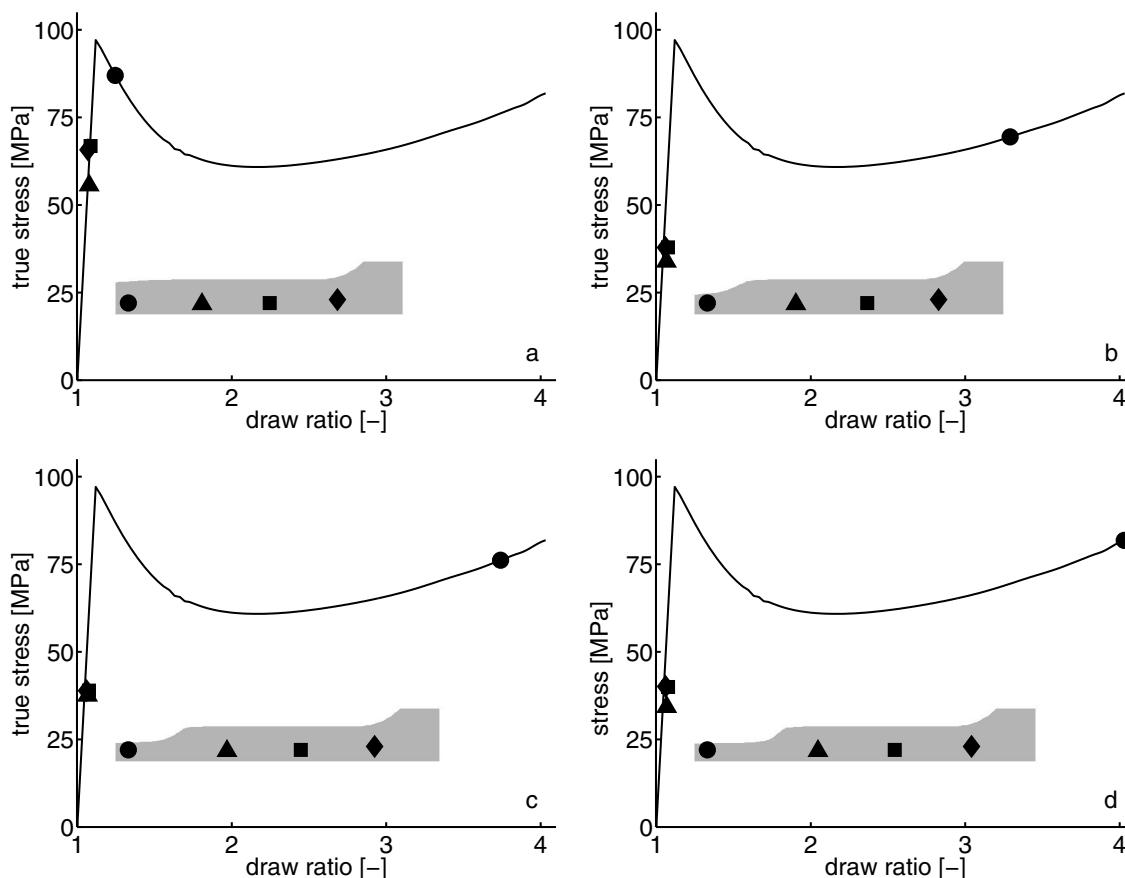


Figure 4.10: Numerical simulation of a tensile test on PS: unstable growth.

keeps on localising, as shown in figures 4.10b-d, without stabilisation. Ultimately, the tensile strength in the deformed region will be exceeded. At a local draw ratio of 4, close to the theoretical maximum draw ratio [1, 2] the simulation is stopped. Hence,

the intrinsic behaviour of polystyrene does not allow stable deformation behaviour. Its large amount of strain softening and weak strain hardening result in extreme localisation of strain which can never be stabilised. This clearly demonstrates why injection moulded polystyrene at room temperature can not exhibit ductile or tough deformation behaviour.

The influence of mechanical history

Mechanical rejuvenation can also be applied to polystyrene. However, due to its craze-sensitivity this can not be achieved by torquing and but has to be performed by rolling. This procedure, reported by Broutman for various amorphous polymers, excluding polystyrene, [16, 43], was applied by Govaert *et al.* [25] to polystyrene (N5000). They showed that a thickness reduction of 30% was sufficient to remove any strain softening in a polystyrene sample. In a subsequent tensile test the macroscopic response of the rejuvenated material was determined where injection moulded material suffered from crazing and brittle fracture at macroscopic strain of 2% (see figure 4.11a). The rejuvenated material deformed homogeneously up to strains exceeding 30%. As demonstrated

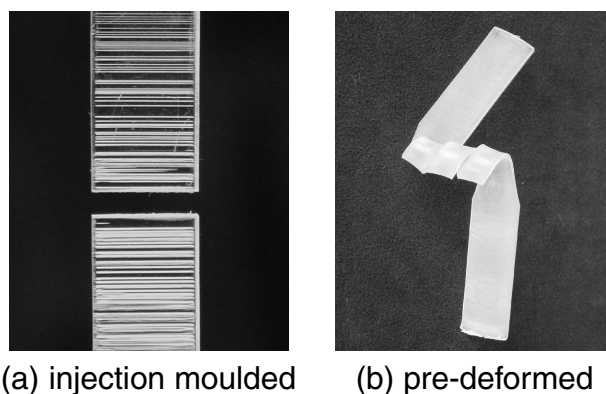


Figure 4.11: Macroscopic deformation behaviour of PS, before (a) and after rolling (b).

in figure 4.11b, pre-deformed polystyrene can be curled without the initiation of any crazing process. In figure 4.12a the stress-strain curves of polystyrene and polycarbonate tensile bars are presented, tested immediately after rolling. The yield stress has decreased dramatically and strain softening is virtually eliminated. As a consequence, homogeneous deformation is observed in these tensile tests. As mentioned before, the yield stress recovers again with ongoing time. Since the large strain behaviour remains unaffected by mechanical rejuvenation and ageing, strain softening recovers in pace with the yield stress. The yield stress as function of time after rolling (ageing time) is given in figure 4.12b.

Although some molecular orientation occurs during rolling, this can not be held responsible for the enhanced ductility for two reasons. Broutman *et al.* [16, 43] demonstrated that the Izod impact strength on rolled polycarbonate is only slightly influenced by the test angle relative to the roll-direction. Moreover, the enhanced ductility and the reduction in strain softening are, similar to polycarbonate, only of temporary nature, whereas molecular orientation does not relax on this time-scale. In time, yield stress and strain softening increase, resulting in renewed localised deformation, crazing and brittle fracture on a time-scale of hours to days [44].

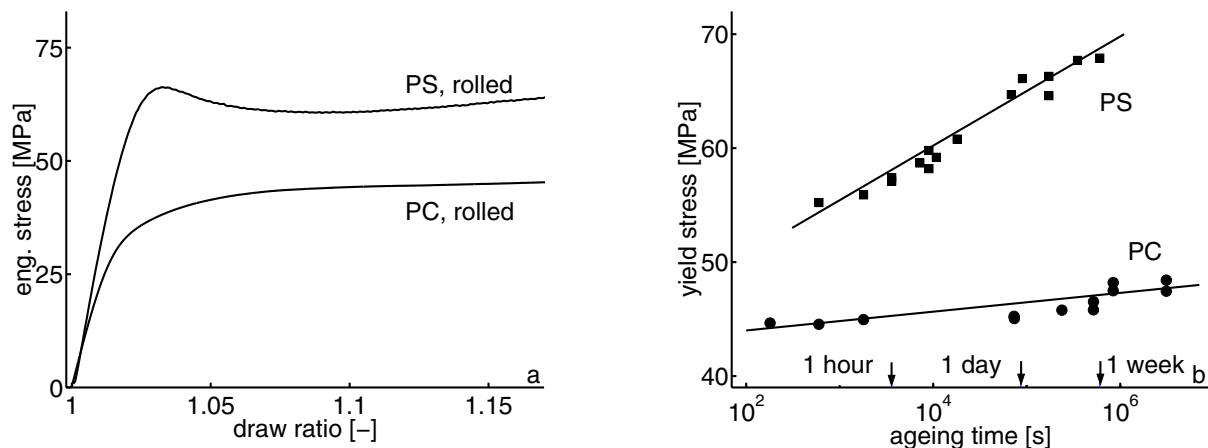


Figure 4.12: Deformation behaviour (a) and ageing kinetics (b) of PS and PC after rolling. The lines in graph b are drawn as a guide to the eye.

This graph clearly demonstrates that the recovery of yield stress in polystyrene occurs much faster than that for polycarbonate. This also explains why renewed brittle fracture returns on a much faster time-scale in polystyrene than necking in polycarbonate.

The influence of testing temperature

It is well known that at a temperature of 80-90°C, a brittle-to-ductile transition is achieved in a tensile test on polystyrene [45, 46]. This phenomenon originates from changes in intrinsic behaviour at this temperature, as similar to the yield stress, strain softening displays a dependence on temperature. In figure 4.2b it was already shown that for polystyrene, tested in uniaxial compression at a strain rate of 10^{-3} s^{-1} , both yield stress and strain softening decrease with increasing temperature. The amount of strain softening at 80°C is only approximately 30% of the amount of strain softening at 20°C.

Since a reduction in strain softening can have major consequences for the macroscopic deformation behaviour, a finite element simulation of a uniaxial tensile test on polystyrene is performed at an elevated temperature of 90°C. Figure 4.13 shows the results of this simulation. Despite the fact that the geometry of the model is identical to the geometry used in the previous simulations of figure 4.4 and 4.10, the slight imperfection does not induce inhomogeneous deformation at the onset of yielding (figure 4.13a) and as a result, nearly homogeneous deformation is observed during deformation, see figure 4.13b. Only the diamond marker, positioned close to the tab of the tensile bar, lays back slightly as the local cross-section reduces slower and the strain is lower in this position (figure 4.13c and 4.13d).

This simulation is consistent with experimental observations. Tensile tests performed at temperatures ranging from 20 to 100°C (around T_g), demonstrate that localisation of strain is indeed greatly reduced or even absent (figure 4.14a). From a testing temperature of approximately 90°C (depending on the thermodynamical state of the material), similar to the numerical simulations, homogeneous deformation is observed in these tensile tests. Figure 4.14b summarises this temperature induced brittle-to-ductile transition for polystyrene. The exact temperature at which this transition occurs is of course also dependent of the thermo-mechanical history of the material.

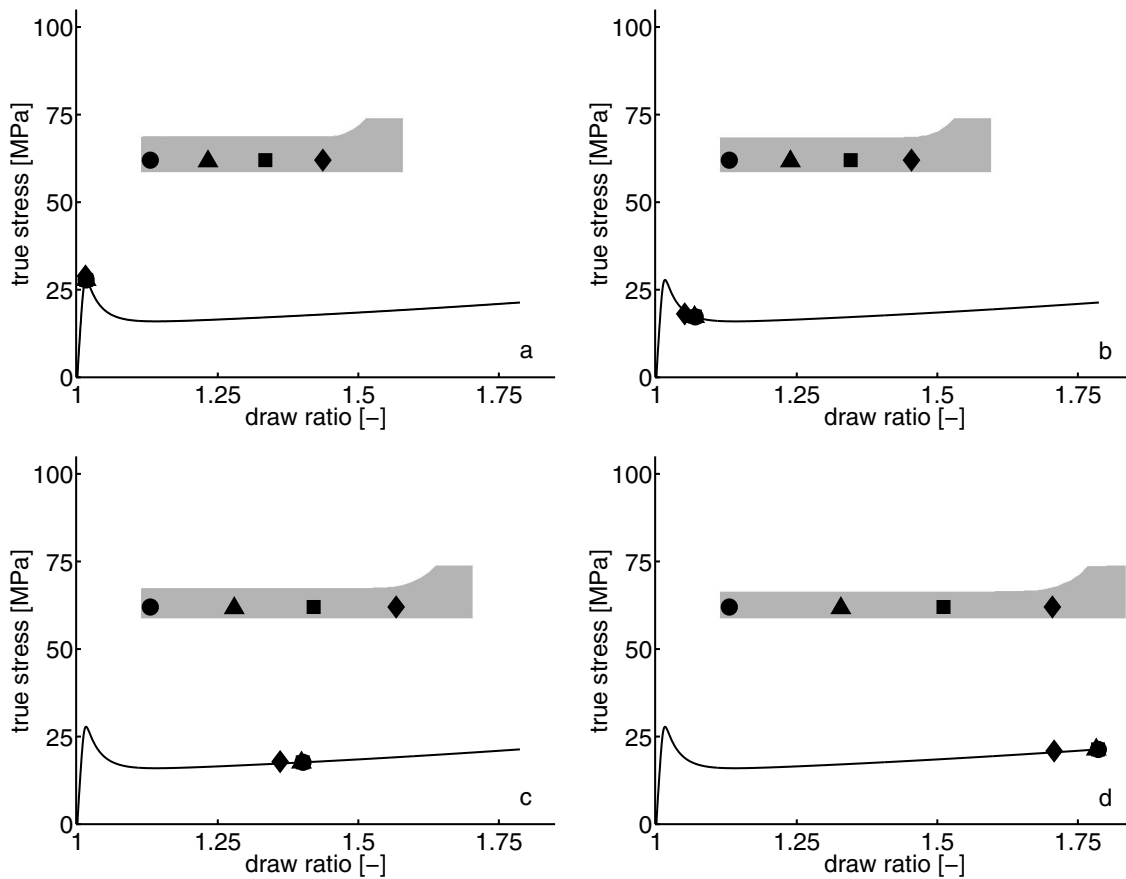


Figure 4.13: Numerical simulation of a tensile test on PS at 90°C: homogeneous deformation.

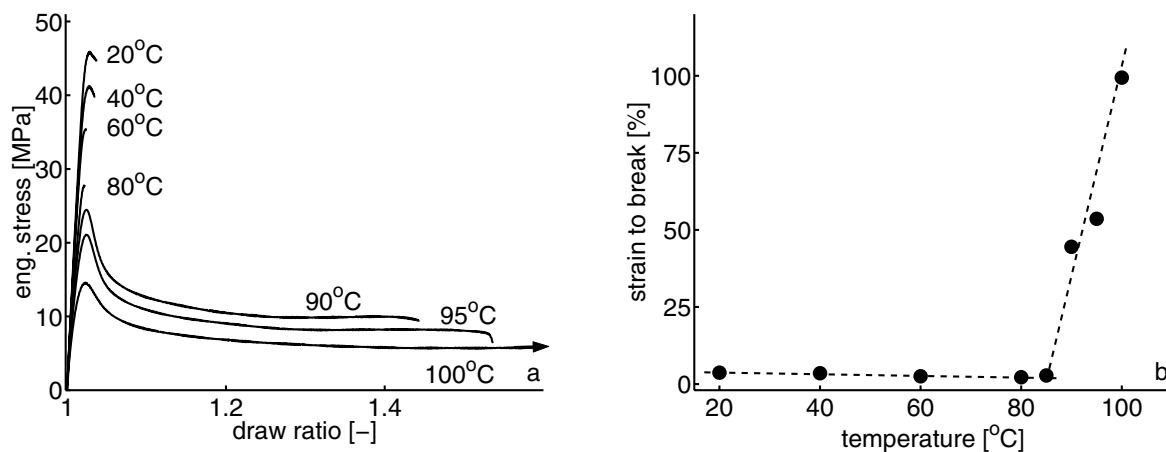


Figure 4.14: Experimental tensile tests on PS at elevated temperatures (a), resulting in a brittle-to-ductile transition (b).

The stabilising influence of rubber inclusions

By increasing the strain hardening contribution of the polymer network, a more stable deformation behaviour can be achieved, e.g. by cross-linking of polystyrene [7] or by blending with polyphenylene oxide (PPO) [6, 9–13]. Apart from changing the intrinsic network density of polystyrene, local strain hardening of deforming ligaments can be induced by the addition of rubber particles. Heterogeneous systems are necessary any-

way to relieve local triaxial stress states in all polymer systems to circumvent defect and notch sensitivity [47–49], but this is out of the scope of the present paper. Here we only demonstrate how the ultimate impact modifier, which is a (small), core-shell rubber particle with a pre-cavitated core and a rather stiff rubbery shell [49,50] stabilises local deformation zones in polystyrene. The tensile bar now is modelled covered by a rubber layer, the thin extra layer at the surface, in figure 4.15.

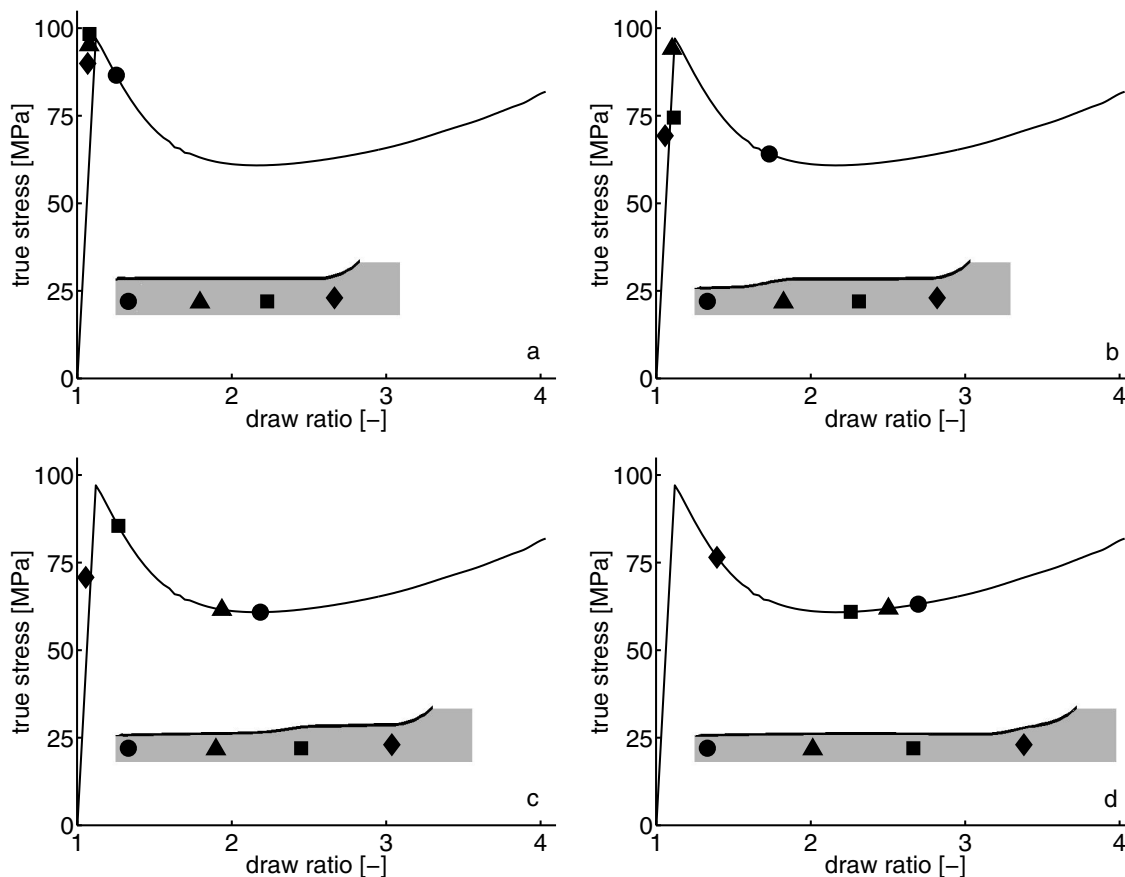


Figure 4.15: Numerical simulation illustrates the stabilising effect of a rubber shell on the deformation of a PS tensile bar.

Similar to the simulations of figure 4.4, inhomogeneous deformation is induced by the imperfection at the onset of yielding (figure 4.15a). As can be seen in figure 4.15b the force transferred by the tensile bar itself is not sufficient to induce yielding in the adjacent material. However, the load bearing capacity of the rubber shell supports the deformation in the tensile bar, stabilises the neck and transfers the deformation to shoulder of the neck (figure 4.15c). Therefore, stable neck growth is observed and the entire tensile bar is plastically deformed already at a macroscopic draw ratio of approximately 2 (figure 4.15d, compare with figure 4.10b-d). A thin shell with a rather high modulus (150 MPa) was chosen here to illustrate the stabilising effect over the entire length of the tensile bar, but already for a rubber modulus of 30 MPa (of course dependent on the thickness of the layer) stabilisation is achieved. However, simulations up to very large strains would be required to visualise this stable deformation behaviour.

4.5 Conclusions

The macroscopic deformation behaviour of glassy polymers is dominated by the intrinsic post-yield behaviour. The subtle interplay of strain softening and strain hardening is demonstrated by finite element simulations of inhomogeneous deformation of polycarbonate in tension. Changes in strain softening due to annealing or mechanical pre-conditioning, have major consequences for the macroscopic deformation behaviour, ranging from homogeneous deformation after mechanical rejuvenation of brittle polymers to brittle fracture after annealing of ductile polymers.

A neck-stability analysis demonstrated that the macroscopic response in tension can be predicted if the intrinsic properties are known up-front. This analysis emphasises the sensitivity of the macroscopic deformation behaviour on the thermo-mechanical history and the influence of the molecular weight.

Finite element simulations of polystyrene in tension showed the extreme localisation of strain which occurs due to the pronounced strain softening and weak strain hardening. In the simulations here failure mechanism like crazing were not considered, they are a topic of a forthcoming paper [32].

Mechanical pre-deformation of polystyrene results in ductile deformation behaviour in tension [25]. However, this enhanced ductility is of transient nature [44]. The recovery of yield stress and strain softening results in renewed severe localisation of strain and brittle fracture. Applying a similar rolling procedure to polystyrene and polycarbonate reveals that the time-scale on which yield stress and strain softening recover are very much different. The origin of this difference in transient behaviour is most probably related to the physical origin of strain softening and a discussion on this topic can be found in [44]. Finally it is investigated how a local support of a deforming fibril by a rubber shell, part of a rubber modified material, indeed can induce delocalisation in polystyrene.

Acknowledgments

The authors wish to acknowledge the financial support provided by the Dutch Technology Foundation (STW) (Grant EWT.3766).

References

- [1] Donald, A.M. and Kramer, E.J., *Polymer*, **23**, 451 (1982)
- [2] Donald, A.M. and Kramer, E.J., *J. Pol. Sci., Pol Phys. Ed.*, **20**, 1129 (1982)
- [3] Meijer H.E.H., Govaert L.E., Smit R.J.M., A Multi-Level Finite Element Method for Modelling Rubber-Toughened Amorphous Polymers, In: *Toughening of Plastics*, Ed. R. Pearson, American Chemical Society, Boston, 50-70 (1999)
- [4] Haward, R.N. and Young, R.J., *The Physics of Glassy Polymers*, 2nd ed., Chapman & Hall, London (1997)
- [5] Tervoort, T.A. and Govaert, L.E., *J. Rheol.*, **44**, 1263 (2000)
- [6] van Melick, H.G.H., Govaert, L.E., Meijer, H.E.H., Influence of network density on the strain hardening behaviour of glassy polymers, *Polymer*, submitted
- [7] Henkee, C.S. and Kramer, E.J., *J. Pol. Sci., Pol. Phys. Ed.*, **22**, 721 (1984)

- [8] Prest jr., W.M. and Porter, R.S., *Pol. Sci. Eng., Part A2*, **10**, 1639 (1972)
- [9] Donald, A.M., and Kramer, E.J., *J. Mat. Sci.*, **17**, 1871 (1982)
- [10] Yee, A.F., *Pol. Preprints.*, **17**, 145 (1976)
- [11] Serrano, A.M., Welsch, G.E., Gibala, R., *Pol. Eng. Sci.*, **22**, 946 (1982)
- [12] Feng, H., Feng, Z., Ruan, H., Shen, L., *Macromol. Chem.*, **4**, 104 (1993)
- [13] Creton, C.; Halary, J.-L.; Monnerie, L., *Polymer*, **40**, 199 (1998)
- [14] Hutchinson, J.M., *Prog. Pol. Sci.*, **20**, 703 (1995)
- [15] Struik, L.C.E., *Physical aging in amorphous polymers and other materials*, Elsevier, Amsterdam (1978)
- [16] Broutman, L.J. and Patil, R.S., *Pol. Eng. Sci.*, **11**, 165 (1971)
- [17] Hasan, O.A. and Boyce, M.C., *Polymer*, **34**, 5085 (1993)
- [18] Xie, L., Gidley, D.W., Hristov, A., Yee, A.F., *Pol. Sci., Part B: Pol. Phys.*, **33**, 77 (1995)
- [19] Cross, A. and Haward, R.N., Mills, N.J., *Polymer*, **20**, 288 (1979)
- [20] Haward, R.N., *Colloid & Polymer Sci.*, **258**, 643 (1980)
- [21] Aboulfaray M., G'Sell C., Mangelinck D., McKenna G.B., *J. Non-Cryst. Solids* **172-174**, 615 (1994)
- [22] G'Sell C., Plastic deformation of glassy polymers: constitutive equations and macromolecular mechanisms. In: H.J. Queens *et al.*, Eds., *Strength of metals and alloys*, Pergamon Press, Oxford, 1943-1982 (1986)
- [23] Bauwens, J.C., *J. Mat Sci.*, **13**, 1143 (1978)
- [24] Govaert, L.E., Timmermans, P.H.M., Brekelmans, W.A.M., *J. Eng. Mat. Tech.* **122**, 177 (2000)
- [25] Govaert, L.E.; Melick, H.G.H. van; Meijer, H.E.H., *Polymer*, **42**, 1271 (2001)
- [26] G'Sell, C.; Hiver, J.M.; Dahouin, A.; Souahi, A., *J. Mat. Sci.*, **27**, 5031 (1992)
- [27] Spitzig, W.A. and Richmond, O., *Pol. Eng. Sci.*, **19**, 1129 (1979)
- [28] Arruda, E.M., Boyce, M.C., Jayachandran, R., *Pol. Eng. Sci.* **34**, 716 (1994)
- [29] Zaroulis, J.S. and Boyce, M.C., *Polymer*, **38**, 1303 (1997)
- [30] Kramer, E.J., In: Kausch, H.H., Ed., *Adv. Pol. Sci.*, Springer, Berlin, **52/53**, 1-56 (1983)
- [31] van Melick, H.G.H., Bressers, O.E.J.T., den Toonder, J.M.J., Govaert, L.E., Meijer, H.E.H., Craze-initiation in glassy polymers: influence of strain rate, thermal history and network density, *Polymer*, submitted
- [32] van Melick, H.G.H., Govaert, L.E., Meijer, H.E.H., Prediction of brittle-to-ductile transitions in polystyrene, *Polymer*, submitted
- [33] Tervoort, T.A.; Smit, R.J.M.; Brekelmans, W.A.M.; Govaert, L.E., *Mech. Time-Dep. Mat.*, **1**, 269 (1998)
- [34] Eyring, H., *J. Chem. Phys.*, **4**, 283 (1936)
- [35] Hasan, O.A., Boyce, M.C., Li, X.S., Berko, S., *J. Pol. Sci., Pol. Phys.*, **31**, 185 (1993)
- [36] van Krevelen, W., *Properties of polymers*, Elsevier, Amsterdam (1972)
- [37] Klompen, E.T.J., *Deformation behaviour of glassy polymers : consequences of thermorheological complex behaviour*, Institute for Continuing Education, Eindhoven University of Technology (1996)
- [38] Haward, R.N., *Polymer*, **28**, 1485 (1987)
- [39] Flory, P.J., *J. Am. Chem. Soc.* **67**, 2048 (1945)
- [40] Merz, E.H., Nielsen, L.E., Buchdahl, R., *Ind. Eng. Chem.* **43**, 1396 (1951)

- [41] McCormick, H.W., Brower, F.M., Kin, L., *J. Pol. Sci.*, **39**, 87 (1959)
- [42] Govaert, L.E., van Aert, C.A.C., Boekholt, J., In: Proc. 10th International conference on deformation, yield and fracture of polymers, The Institute of Materials, Cambridge, United Kingdom, 423-426 (1997)
- [43] Broutman, L.J. and Krishnakumar, S.M., *Pol. Eng. Sci.*, **14**, 249 (1971)
- [44] van Melick, H.G.H., Raas, B., Nauta, W.J., Govaert, L.E., Meijer, H.E.H., Kinetics of ageing and re-embrittlement of rejuvenated polystyrene, *Polymer*, submitted
- [45] Vincent, P.I., *Polymer*, **1**, 425 (1960)
- [46] Matsushige, K., Radcliffe, S.V., Baer, E., *J. Appl. Pol. Sci.*, **20**, 1853 (1976)
- [47] Smit, R.J.M., Brekelmans, W.A.M., Meijer, H.E.H., *J. Mat. Sci.*, **35**, 2855 (2000)
- [48] Smit, R.J.M., Brekelmans, W.A.M., Meijer, H.E.H., *J. Mat. Sci.*, **35**, 2869 (2000)
- [49] Smit, R.J.M., Brekelmans, W.A.M., Meijer, H.E.H., *J. Mat. Sci.*, **35**, 2881 (2000)
- [50] Jansen, B.J.P., Rastogi, S., Meijer, H.E.H., Lemstra, P.J., *Macromol.*, **34**, 3998 (2001)

Chapter 5

Craze-initiation in glassy polymers: influence of strain rate, thermal history, and network density

Initiation of a localised plastic zone is numerically simulated using a constitutive model that incorporates an accurate description of the post-yield behaviour with the important phenomena of strain softening and strain hardening. Subsequent nucleation of voids in the deformation zone is detected using a hydrostatic stress criterion. This criterion is identified and validated. A micro-indenter with a sapphire sphere is used to produce indents that are later examined with an optical microscope. These observations lead to a critical force at which crazes are initiated in polystyrene. Combining these experiments with a numerical study shows that the loading part of indentation can be accurately predicted. A critical hydrostatic stress of 40 MPa is extracted from the numerical model by monitoring of the local stress field at the moment that the indentation force reaches the experimentally determined force level at which crazes were found to initiate. This criterion is validated by indentations on samples with different thermal histories, and at various loading rates. Finally, the influence of network density on the value of the hydrostatic stress criterion is investigated by indentation of blends of polystyrene and poly(2,6-dimethyl-1,4-phenylene-oxide). It is shown that the critical hydrostatic stress increases with network density.

Reproduced from:

Craze-initiation in glassy polymers: influence of strain rate, thermal history and network density
H.G.H. van Melick, O.F.J.T. Bressers, J.M.J. den Toonder, L.E. Govaert, H.E.H. Meijer, submitted to **Polymer**.

5.1 Introduction

Macroscopic brittle fracture of glassy polymers is generally preceded by formation of crazes, small crack-like defects, of which the opposite faces are bridged by super-drawn fibrils. Crazes have, due to these fibrils, unlike real cracks, some load-bearing capacity and when viewed on a microscopic level, they display large plastic deformations. For this reason, crazes are the most important source of fracture toughness in brittle glassy polymers, even though the material volume involved in the deformation is generally small. It is, therefore, not surprising that a vast amount of research has been performed in the past on all aspects of crazing: craze nucleation, growth and failure, the micro-structure of crazes, the influence of molecular parameters, etc., and a number of excellent reviews are available [1–4].

Figure 5.1 depicts some of the microscopic events that are likely to be involved in craze nucleation [2]. First, plastic deformation starts at a local stress concentration. The non-linear nature of the yield process and the strain softening character of polymer glasses result in localisation of deformation as plastic strain increases. Since the material at some distance of the local deformation zone is relatively undeformed, the differences in volumetric strain induce a build-up of triaxial stresses. At this stage two possibilities exist. Typically for (unnotched) polycarbonate, the strain-hardening response of the material can stabilise the strain-localisation process and the micro-shear band spreads out. It has been shown [5] that the hydrostatic stress required to plastically expand a micro-porous region is greatly reduced if the material is in a state of flow. The initiation of the dilatation process is enhanced by the more severe localisation, as found in (unnotched) polystyrene (and also in notched polycarbonate), since the dilatative stresses become so large that void nucleation occurs and, finally, crazes develop in the deformation zone.

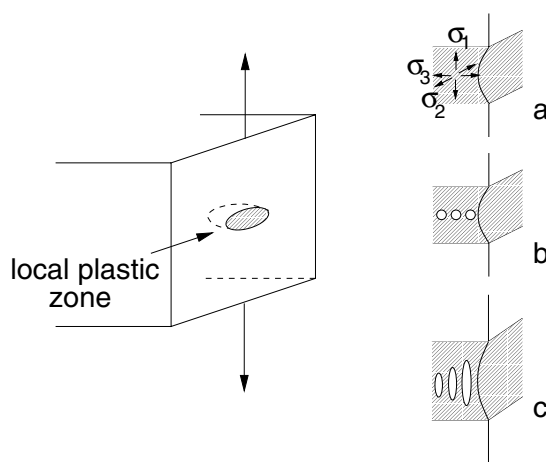


Figure 5.1: Schematic drawing of microscopic events involved in craze nucleation: a) formation of a localised surface plastic zone and build-up of lateral stresses, b) nucleation of voids in the plastic zone and c) deformation of the polymer ligaments between voids and coalescence of individual voids to form a void network (after [2]).

From this sequence of events, it is clear that the macroscopic failure behaviour of glassy polymers is determined by two factors: 1) the intrinsic post-yield behaviour of the material, and 2) its resistance against void-nucleation.

The post-yield behaviour of glassy polymers is characterised by strain softening and strain hardening [6] and, although the exact molecular origin of strain softening is still largely unknown, it is well documented that strain softening exhibits a pronounced dependence on the thermal and mechanical history [6–13]. Slow-cooling rates tend to increase strain softening, whereas quenching leads to moderate or, in case of polyvinylchloride (PVC), even negligible softening [7]. The phenomenon appears to be related to the erasure of physical ageing effects by plastic deformation: mechanical rejuvenation. The origin of strain hardening is well established: a contribution of the entanglement network as a result of stress-induced segmental mobility [6, 12, 14].

The extent to which polymers are susceptible to strain localisation is determined by a subtle interplay between strain hardening and strain softening [15]. The initiation of localised deformation zones is governed by strain softening, which allows the zone to grow with decreasing stress, elastically unloading its surrounding. The amount of strain hardening determines whether or not the deformation zone is stabilised [15–17]. Strain softening, however, appears to be the key factor in this localisation phenomenon. Upon removal, or strong reduction, of strain softening through thermal (quenching) or mechanical (plastic pre-deformation) methods, the occurrence of strain localisation is inhibited. Prime examples are homogeneous deformation of quenched PVC [7] and remarkable transition from crazing to macroscopic plastic flow in polystyrene after a mechanical treatment consisting of a thickness reduction of 30% by means of rolling [13]. These effects are, however, of a temporary nature, as strain softening tends to return in time as a result of physical ageing [13, 15].

In the past 15 years, considerable effort was directed towards the numerical simulation of strain localisation phenomena. The development of 3D constitutive models that were able to capture the post-yield behaviour of glassy polymers started off with the work of Boyce and co-workers at MIT [18–21]. This work was later followed by studies of the group of van der Giessen [22, 23] and our group [11, 12, 24–30]. As a result of these activities the numerical simulation of plastic localisation in various loading geometries is now well established.

Also substantial research effort has been conducted in the identification of craze initiation criteria for amorphous polymers. Narisawa and co-workers investigated a range of amorphous polymers, mostly in notched tensile and bending tests, and determined values for critical dilative stresses [31–33]. However, considering the defect sensitivity and, consequently, initiation of crazes at the surface, such a test is inappropriate for polystyrene. This was recognised by Camwell and Hull [34], who compressed a polystyrene sheet between flat dies, during which both shear bands and crazes were generated in the same specimen. Narisawa *et al.* [32] slightly modified this experiment into a plane-strain indentation between parallel plates using a flat-punch. Using Hill's slip-field line theory, they derived a critical hydrostatic stress of around 25 MPa for polystyrene, although the validity of their approach was questioned by Kells and Mills [35] in a similar approach. The adequate description of the small and large strain deformation behaviour of glassy polymers by using the compressible Leonov model, enabled us, in a combined experimental and numerical study, to monitor the stress/strain fields in this plane-strain indentation test, that indeed included large local plastic deformation [36]. Despite the elegance of the indentation technique to generate a craze in the bulk (rather than at the surface) of the material in a reproducible way, two major drawbacks were encountered. First, the size of the specimens (60x20x6 mm³) resulted in

some uncertainty about the exact thermodynamical state of the material and makes a clear distinction between quenched and annealed material virtually impossible. Hence the exact intrinsic properties which are required in the finite element analysis can not be determined. Second, a clear influence of friction and lubrication between the supporting plates, providing the plane strain conditions, was observed at the high indentation loads (≈ 9 kN). The stress fields in the experiments most probably will not be equal to these corresponding to the true plane strain conditions in the simulations. Most striking in this respect is the inability to capture the force-displacement curve in a quantitative way, for which the numerical model had already proven its capability in compression, tension and, in a more complex geometry, spherical indentation tests [11, 12, 37]. In an axisymmetric setup the friction problems could be solved but, due to the larger sample size, more problems would arise concerning the thermodynamical state of the material.

In conclusion an experiment is required that circumvents the defect-sensitivity of polystyrene, that allows for thin samples with a well-defined thermal and mechanical history and that can be described accurately by finite element simulations. As a spin-off from a previous project [37], indentation with spherical indenters on flat polymeric surfaces has proven to be an accurate experiment to generate crazes in a well-controlled and reproducible way. At a certain load during indentation, pile-up of material occurs next to the contact area between indenter and polymer. Besides plastic deformation, positive hydrostatic stresses evolve in this pile-up which results in small crazes just below the surface of the polymer. To identify the local stress distribution within the pile-up, finite element simulations of the indentation experiment can be performed. As a material model, the compressible Leonov-model [11, 24, 25] is used, which captures the complex yield behaviour of glassy polymers quite well. The capability of this model to describe the indentation of amorphous polymers was already shown [37]. The hydrostatic stress criterion is obtained by a combination of numerical simulations and experimental observations. From the experiments the force is recorded at which crazes are initiated. Using a numerical simulation the critical hydrostatic stress is identified as the maximum hydrostatic stress in the pile-up zone at this specific indentation force.

The applicability of the criterion obtained is subsequently investigated by comparing numerical predictions of craze initiation with experimental observations at various loading rates (i.e. indentation force rates) and on samples with different thermal histories (quenched and annealed PS). Using the same approach the influence of network density on the critical hydrostatic stress is studied by indentation of blends of polystyrene and poly(2,6-dimethyl-1,4-phenylene-oxide) (PPO).

5.2 Materials and experimental methods

Materials

The base materials used were commercial polystyrene (Styron 634, Dow Chemical) and two blends of polystyrene (PS) and poly(2,6-dimethyl-1,4-phenylene-oxide) (PPO 803, General Electric Plastic), that contained respectively 20% and 40% PPO. The granular material was compression moulded into plates of $100 \times 100 \times 3$ mm³ in a stepwise manner. In the middle of the mould a thin glass-plate was placed to obtain a smooth surface, suitable for indentation.

The material was pre-heated in the mould at 90°C above its glass-transition temperature (T_g) for 15 minutes and then compressed in 5 minutes, at the same temperature, in 5 steps of increasing force (up to 300 kN). In between these steps, pressure was released to allow for degassing. The mould was then placed into a cold press and cooled to room temperature at a moderate force (100 kN).

From the centre of these plates small square platelets were cut (20x20 mm²). In order to eliminate residual stresses and thermal history effects the platelets were heat-treated for 30 minutes at 15°C above T_g . Subsequently, the platelets were given a thermal treatment, either annealing or quenching. During annealing the samples were held at 20°C below T_g for three days and, subsequently, slowly cooled in one day in an oven to room temperature. During quenching the samples were cooled rapidly in ice-water from 15°C above T_g .

Experimental setup

Indentations were performed on a micro-indenter; a custom-designed apparatus at Philips Research Laboratories in Eindhoven. The forces which can be measured, range from 20 mN up to 20 N with an accuracy of 2 mN; the accuracy of the displacement is 20 nm. Forces and displacements were measured by means of coils at the bottom of the indenter column. The indenter used was a sapphire sphere, with a radius of 150 μm , glued onto a brass holder. The compliance of the apparatus was determined by a reference measurement on silica glass. The elastic indentation depth-force curve was predicted by Hertz' theory. From the deviation between the theoretical and experimental curve, the compliance was determined to be $6 \cdot 10^{-2} \mu\text{mN}^{-1}$, and the corresponding stiffness of the measuring system is $1.67 \cdot 10^7 \text{ Nm}^{-1}$.

A typical indentation procedure starts with a position-controlled movement of the indenter towards the sample until the surface is contacted, with a pre-load of 5 mN. Next the platelet is loaded, in force control, up to a predefined maximum force at force rates ranging from 10 mNs⁻¹ up to 1 Ns⁻¹. When a predefined maximum force is reached, the indenter is retracted in position control. The retraction velocity is adjusted to the loading rate to keep the time of loading and unloading identical. During indentation both the load and the displacement are recorded. The experiments are performed in a sequence of increasing force steps. At each step of 0.5 N, the indentations are repeated at least 10 times. After the experiments, the indents are examined using an optical microscope (Leica DM/RM) to check whether crazes were formed by the force applied. This microscope uses polarised light for the interference contrast to visualise the crazes. To obtain the material parameters, required for the numerical simulations, uniaxial compression tests were performed on a servo hydraulic MTS Elastomer Testing System 810. Cylindrical specimens ($\varnothing 6 \text{ mm} \times 6 \text{ mm}$) were compressed at room temperature and a constant logarithmic strain rate between two parallel, flat steel plates. The friction between the sample and the steel plates was reduced using PTFE tape (3M 5480, PTFE skived film tape) on the sample and a soap-water mixture on the surface between the steel and the tape. No bulging or buckling of the sample was observed, indicating that the friction was sufficiently reduced. A constant true logarithmic strain rate varying from 10^{-4} up to 10^{-2} s^{-1} was achieved in strain control.

5.3 Numerical methods

To obtain a quantitative criterion for craze nucleation, numerical simulations of the indentation experiment were carried out. Information that could not be extracted from the experiments, such as stresses and strains in the indented material, were derived from the model. By comparing the computed forces and displacements with the experimental results, the numerical model was validated. From the experiments a critical force for craze initiation was determined and from the accompanying simulations a quantitative craze-nucleation criterion was derived.

Material model

Numerical simulations are only useful if the intrinsic deformation behaviour is covered well. In previous work, an elasto-viscoplastic constitutive equation for polymer glasses was introduced, the so-called compressible Leonov-model, of which the relevant equations are briefly summarised in the appendix. The nomenclature and meaning of the material parameters used in this study can be found in [11, 24, 25].

FEM model

Two deformable bodies are considered: the indenter and the material examined. The contact between indenter and sample is assumed to be frictionless (the influence was examined by varying the friction in the model and was found to be negligible). In the axisymmetric model, the polystyrene sample chosen is large enough to prevent the edges influencing the stress-distribution, and the sapphire indenter is modelled as a half-sphere (see figure 5.2a). The z-axis is the axis of rotational symmetry.

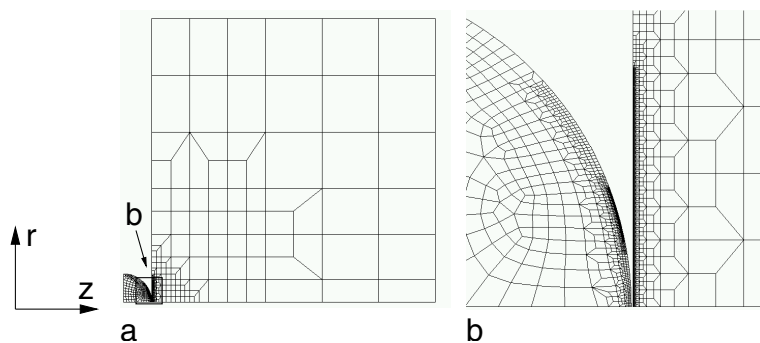


Figure 5.2: *Finite element mesh used in simulations: (a) indenter (left) and sample, (b) zoomed region with mesh-refinement.*

Axisymmetric conditions require the nodes positioned on the z-axis to be fixed in radial direction. Furthermore, rigid-body movement of the sample is prevented by fixation on the right-hand side. The deformable indenter, which can only be moved in x-direction, is loaded on the left-hand side and pressed into the sample at a constant, pre-defined loading rate.

The materials used in the numerical simulations were sapphire (indenter) and polystyrene. The sapphire was assumed to be linear elastic and properties were taken from literature ($E=304$ GPa and $\nu=0.234$ [38]), whereas the parameters of the polystyrene were extracted from uniaxial compression tests, represented below.

To exclude any mesh-dependence a stepwise element refinement was performed until

the solution converged to a steady, mesh independent, result. In order to prevent excessive computation times the mesh refinement was restricted to areas of interest (see figure 5.2b).

5.4 Results

Materials characterisation

Bulk properties

Material parameters required for the numerical simulations are extracted from uniaxial compression tests at room temperature. In this loading geometry localisation of deformation is inhibited and the true stress/true strain behaviour can be obtained up to large (compressive) strains. Figure 5.3 shows the rate dependence of PS at strain rates ranging from $3 \cdot 10^{-4}$ up to $3 \cdot 10^{-3} \text{ s}^{-1}$, representative for the strain rates occurring during indentation.

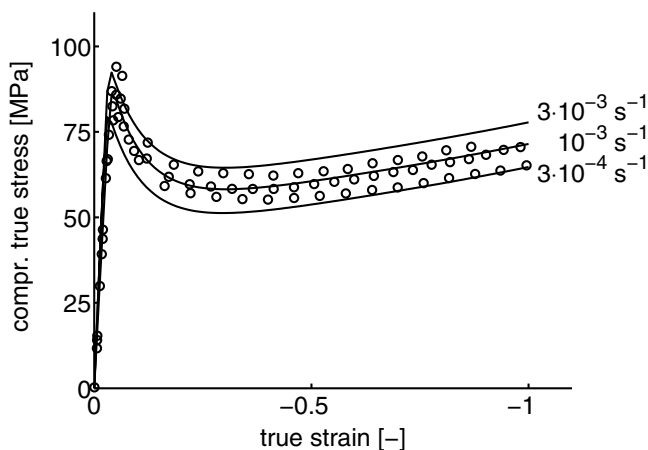


Figure 5.3: Rate-dependent compressive behaviour of polystyrene, experiments (circles) and simulations (solid lines).

The strain rate predominantly influences the level of the yield stress and has a less pronounced influence on the post-yield behaviour: strain softening and strain hardening. The solid lines in figure 5.3 are predictions using the compressible Leonov-model with the parameters indicated in table 5.1. From the yield stresses, obtained at various strain rates, the model parameters A and τ_0 can be determined. The softening parameters D_∞ and h are fitted on the compression curve at $1 \cdot 10^{-3} \text{ s}^{-1}$, whereas the strain hardening modulus is defined as the slope of the curve at large strains of the true-stress versus $\lambda^2 - \lambda^{-1}$ (neo-Hookean behaviour). For the modulus E and the Poisson ratio ν , literature values are taken [39].

The one-mode model used here assumes linear elastic behaviour up to the yield point, and as a result the strain at yield is slightly under-predicted. Since, in reality, the pre-yield behaviour is (non-linear) visco-elastic, the model can be expected to be less satisfactory in predicting the behaviour in the unloading part of the indentation. A multi-mode version of the model performs much better, see e.g. [25], but requires too much computational time for the problem under consideration. Moreover, an accurate description of the loading curve proves to be more relevant for this investigation than that of the unloading curve. The rate dependence of the yield point is captured quite well

by a single Eyring process, although the strain softening is slightly under-predicted for large strain rates and slightly over-predicted for low strain rates.

Thermal history

It is well known that physical ageing influences the yield behaviour of glassy polymers. This was first observed by Horsley [40] in 1958 for PVC, and later this was reported for PC [6] and PS [8,41]. Figure 5.4 presents the experimental results of compression tests on two PS samples, differing in thermal history .

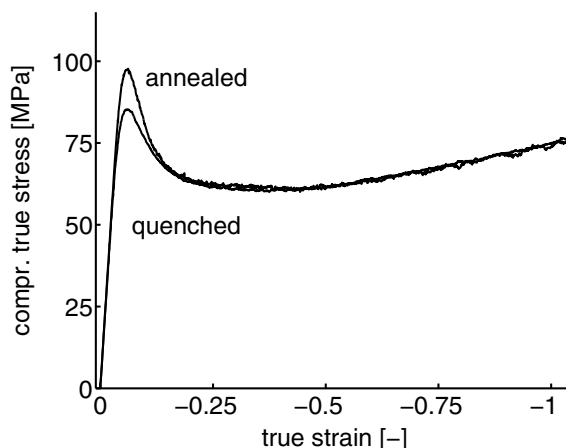


Figure 5.4: Influence of thermal history on intrinsic behaviour in compression experiments: annealing results in an increased yield stress and strain softening.

The yield stress and the amount of strain softening are higher for annealed than for quenched polystyrene, whereas the large strain behaviour remains unchanged. From a true strain of approximately -0.2 the initial difference has vanished and the thermal history does not influence the deformation behaviour anymore. The material is in a so called rejuvenated state [8]. Since the thermal history influences the yield stress and strain softening, the time constant of the viscosity A , the softening slope h and softening limit D_∞ are adapted. In table 5.1 the material parameters for all materials used are given.

Network density

To investigate the influence of network density on crazing behaviour, various PS/PPO samples (0, 20 and 40% PPO) are subjected to indentation experiments. The network density of PS/PPO, a compatible mixture in all ratios, increases with increasing fraction PPO, which enhances the strain hardening contribution at large strains (see figure 5.5) Along with the ability of the compressible Leonov model to capture the deformation behaviour of the PS/PPO blends (solid lines), figure 5.5 shows that the yield stress is largely unaffected and the strain softening decreases with increasing PPO fraction. The latter is attributed to the fact that stabilising influence of the strain hardening has a noticeable effect at small strains. In table 5.1 the material parameters for PS/PPO blends are also given.

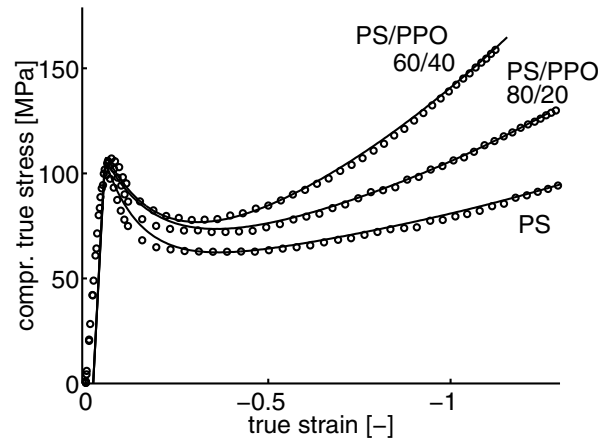


Figure 5.5: Compressive behaviour of PS/PPO blends: increased network density results in an enhanced strain hardening contribution.

material	E [MPa]	A [s]	τ_0 [MPa]	h [-]	D_∞ [-]	G_R [MPa]
PS, quenched	3300	$2.6 \cdot 10^8$	2.56	40	7	11
PS, annealed	3300	$1.0 \cdot 10^{12}$	2.56	75	11	11
PS/PPO 80/20	3000	$1.0 \cdot 10^{11}$	2.63	65	13	25
PS/PPO 60/40	2700	$1.4 \cdot 10^{10}$	2.63	68	20	50

Table 5.1: Material parameters for all materials, derived from uniaxial compression tests, used as input for the simulations.

The Poisson ratio ($\nu=0.37$) is not incorporated in the table as it is assumed to be identical for all materials.

Indentation experiments

Reference sample

To investigate the reproducibility and accuracy of indentations, a reference sample of annealed polystyrene is indented in a sequence of one hundred indentations. Figure 5.6 presents a series of representative indentation curves, differing in maximum load level. The coinciding experimental curves (markers) at distinct maximum load levels illustrate the reproducibility and accuracy of the experiments. The numerical simulation of the indentation process (solid line), gives a good agreement in the relevant portion. Only a slight adjustment had to be made to the time-constant A to account for the difference in yield stress, due to thermal history effect, of the indentation and uniaxial compression samples. In the parameter set for annealed polystyrene of table 5.1, this was already accounted for.

The force-displacement curves are characteristic for polymer indentation: a monotonic rise of the loading curve and, after a force maximum, an unloading curve with a gradually decaying slope. The area between the loading and the unloading curve represents, besides the work required to deform the material plastically, a time-dependent component. Upon unloading the deformed material will experience relaxation which, dependent on the time-scale of the experiment, will continue after unloading. This

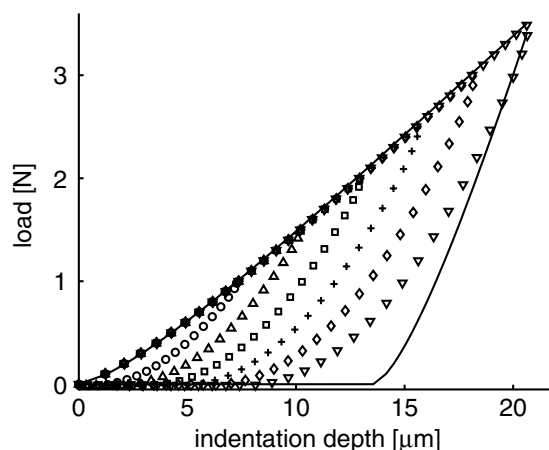


Figure 5.6: Experimental force-displacement curves of indentations on PS at various load levels (different markers); the solid line represents the numerical simulation.

time-dependent relaxation behaviour is also responsible for the smooth transition from loading to unloading at the load maximum, and the gradual decay of the slope of the unloading curve at low forces.

Loading rate and thermal history

That indentation experiments are sensitive enough to discriminate strain rate and thermal history effects, can be seen in the results shown in figure 5.7. Since the loading curve is predominantly determined by the yield stress and elastic modulus, an increasing strain rate raises the resistance to indentation and results in a steeper loading curve.

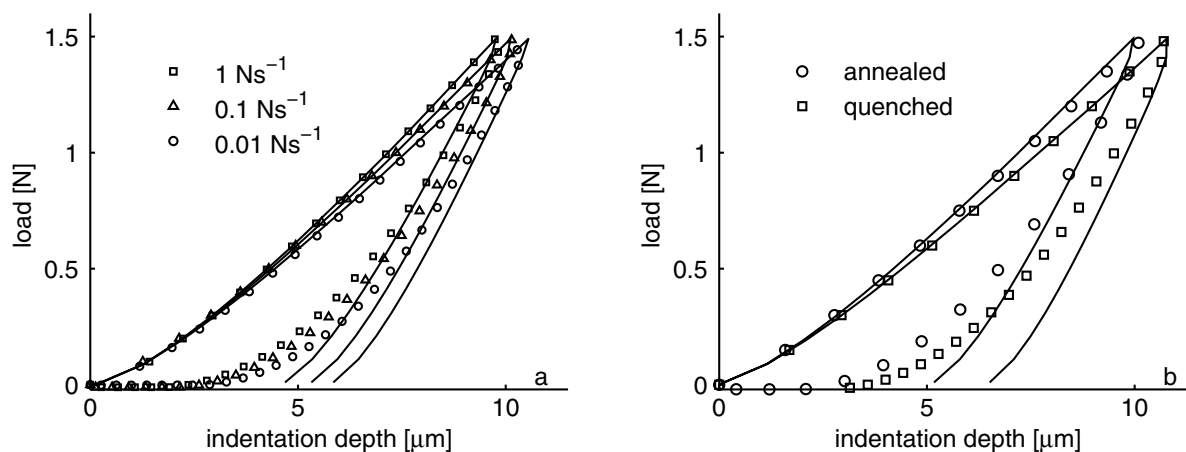


Figure 5.7: Influence of strain rate (a) and thermal treatments (b) on the experimental indentation curves (markers) of PS, solid lines represent numerical simulations.

Annealing induces a subtle increase in yield stress relative to a quenched sample (see figure 5.4). Since it is known that thermal history has only a slight influence on the elastic modulus [42], the increased resistance to indentation after annealing can be fully attributed to the increased yield stress after annealing.

Network density

The indentations performed on PS/PPO demonstrate the difficulty in discriminating between the contribution of modulus and yield stress on the loading curve. Figure 5.5

and the values in table 5.1 show that with increasing PPO fraction, the modulus slightly decreases while the yield stress slightly increases. The influence of these counteracting effects is shown in figure 5.8: for PS/PPO with 20% PPO (squares) the resistance to indentation increased relative to pure PS (circles) while for 40% PPO (triangles) and pure PS the loading curves coincide. The remaining plastic indent indicates that there is indeed a difference between PS and PS/PPO with 40% PPO.

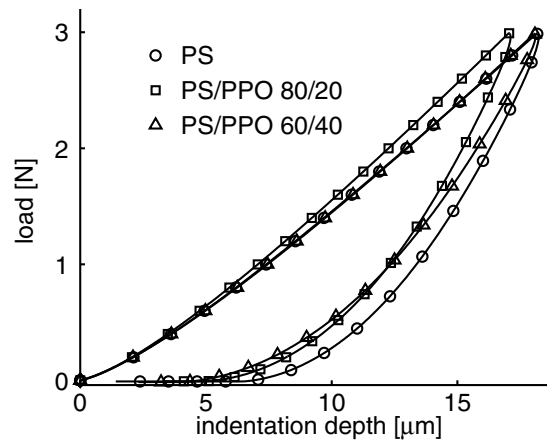


Figure 5.8: Experimental force-displacement curves for PS (circles), PS/PPO 80/20 (squares) and PS/PPO 60/40 (triangles), the solid lines to guide the eye.

Identification of a craze-nucleation criterion

Reference sample

At high indentation loads crazes are formed, departing from the edge of the contact, between indenter and sample, in radial direction, see figure 5.9b. In-situ monitoring of the indentation process showed that these crazes are initiated in the loading stage of the experiment. A sequence of indentation experiments, with a load rate of 0.1 N s^{-1} , increasing in force (at least 10 indentation at each force step) are performed on the reference sample (annealed PS). At each force step, the number of crazes were counted. Figure 5.9a shows the number of crazes observed after indentation, at various load levels, as function of the applied load. The markers (circles=annealed PS) represent the average number of crazes observed at a single force step. The solid line through these average values indicates a linear increase of the number of crazes with increasing load. Enveloping the solid lines a probability corridor (dashed lines) is drawn which accounts for the distribution (95% confidence interval) on the number of crazes observed.

Extrapolation of the line to the x-axis, marks the onset of craze-initiation. It is concluded that an average force of 1.35 N is required to initiate crazing during indentation of annealed PS. Considering the distribution in the observations, a craze-initiation force-interval of 1.05 to 1.65 N is assumed.

Since the crazes are initiated during the loading part and the loading part was adequately described (see figure 5.6 and 5.7), finite element simulations are used to investigate the stress distribution around the indenter at the initiation of crazes. These simulations show that during indentation the material adjacent to the indenter is pushed outwards in radial direction, and hence induce positive stresses in circumferential direction. In figure 5.10, the hydrostatic stress is plotted in the region of interest, near

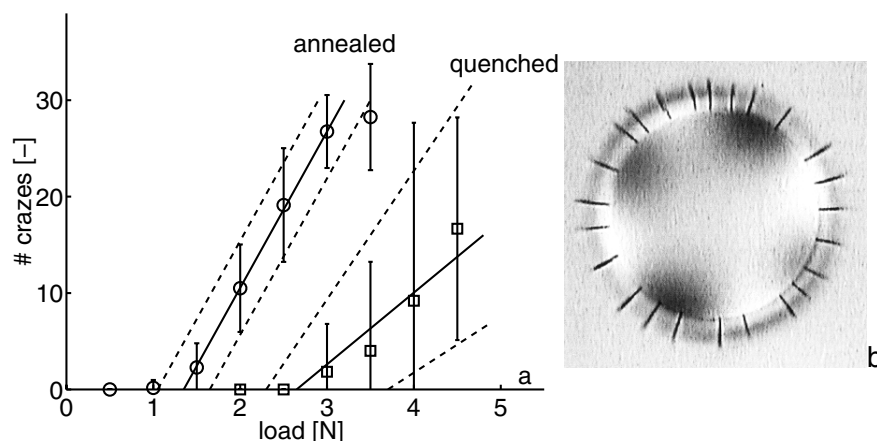


Figure 5.9: Number of crazes formed during indentation (a), solid lines indicate the average values, the dashed lines the 95% confidence interval, for annealed PS (circles) and quenched PS (squares), and a microscopic picture of a plastic indent with crazes (b).

the contact of indenter and sample, where the crazes are observed experimentally. A maximum in hydrostatic stress is found in this region, near the surface of the sample. The requirement that crazing is preceded by plastic deformation is met, as the softening variable D is larger than 0 in this region, this implies that the material is plastically deformed.

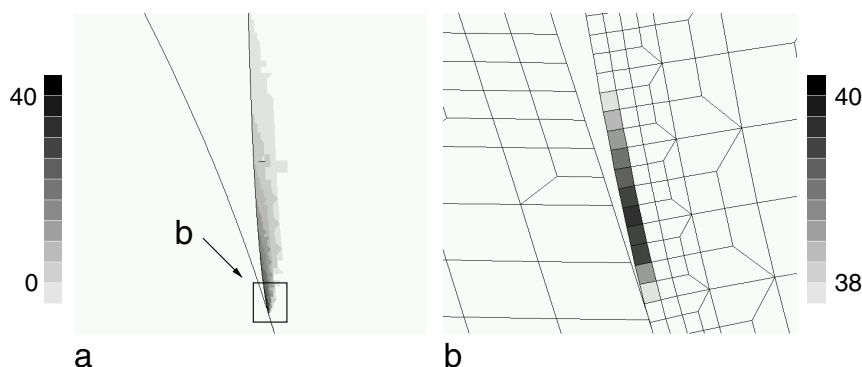


Figure 5.10: Numerical prediction of the build-up of hydrostatic stress in the region where crazes are observed experimentally (a), zoomed in on the area of interest (b).

Figure 5.11 shows the maximum hydrostatic stress as function of load. While the load is raised with a load rate identical to the experiments, from 0 to 4 N, the hydrostatic stress level increases. The position at which this maximum occurs shifts as the contact circle of indenter and sample moves in radial direction with increasing load. This results in a staggered path of maximum hydrostatic stress, shown in figure 5.11.

From the average force required for craze initiation, as derived from figure 5.9 and considering the experimental error on craze-observation, the critical hydrostatic stress for craze nucleation is $40 [\pm 2]$ MPa.

Thermal history

To validate the conclusion that a craze initiation criterion, composed of the requirement of a localised plastic zone and a critical hydrostatic stress, required for void nucleation,

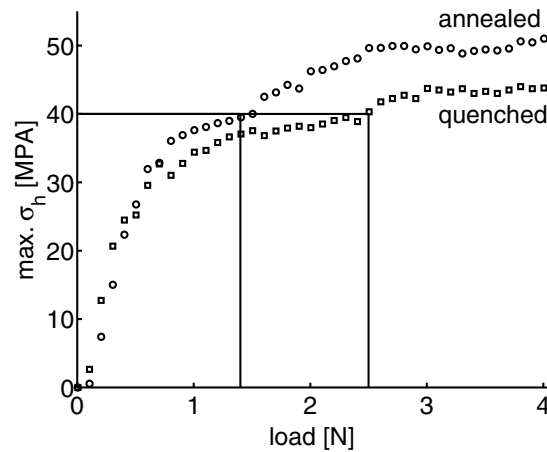


Figure 5.11: Maximum hydrostatic stresses in simulation; average critical force and corresponding critical hydrostatic stress for annealed PS (circles) and quenched PS (squares).

is appropriate to describe void nucleation, the influence of thermal history is investigated. The previous results for annealed PS are therefore compared to craze-initiation in a quenched PS sample. The material parameters for the quenched PS are also presented in table 5.1. In figures 5.4 and 5.7b it was already shown that the yield stress and the resistance to indentation for quenched PS are lower compared to annealed PS. Microscopic observations reveal that the crazes formed in quenched PS are not only much smaller and thinner compared to annealed PS, they are often very difficult to detect and can only be visualised using polarised light. Besides the force required to initiate crazes (2.6 N), the distribution in values of the number of crazes observed in quenched PS is much larger (ranging from 2.3 to 3.7 N), see figure 5.9.

The maximum hydrostatic stress as function of the applied load is also shown for the quenched sample (squares) in figure 5.11. The slope of the maximum hydrostatic stress versus load are comparable for the annealed and the quenched sample up to 0.7 N. At a hydrostatic stress approximately 30 MPa, the paths begin to diverge as the hydrostatic stress in the quenched sample evolves slower. The critical hydrostatic stress of 40 MPa, determined for annealed PS, corresponds to a critical force of craze formation in the quenched material of 2.5 N. Considering the experimentally observed 2.6 N (within a range of 2.3 to 3.7 N), it is reasonable to assume that the hydrostatic stress required for void-nucleation both annealed and quenched polystyrene equals 40 MPa.

Loading rate

Further validation of this craze-initiation criterion is done by investigating the influence of the loading rate during indentation. The stress-strain behaviour and the indentation curves of PS are dependent on the loading rate, as was shown in figures 5.3 and 5.7a. Again the reference sample of annealed PS and its material parameters (see table 5.1) are used in these experiments and simulations. For indentations 5 loading rates are taken, ranging from 0.01 to 1 Ns⁻¹.

With increasing loading rate, the resistance to indentation rises, as was shown in figure 5.7a. Besides the increase in yield stress at increasing loading rate, visco-elastic effects can also play a role as the time scale of the experiments shortens.

Figure 5.12 shows the force-interval at which crazes in the experiment are observed for all different loading rates applied. The procedure to determine these intervals was identical to the procedure used for the annealed and quenched PS (see figure 5.9). The force-intervals at which crazing is observed experimentally prove to be nearly independent of the loading rate within the range measured.

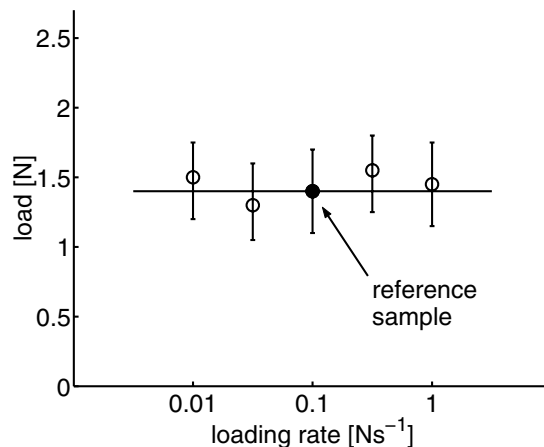


Figure 5.12: The critical load at which crazes are first observed in PS is not influenced by the loading rate.

Numerical simulations were performed at the same loading rates and the results are presented in figure 5.13. The slight differences seen in the indentation curves (figure 5.7a) have virtually no influence on the development of the maximum hydrostatic stress. Since the force interval at which crazes are observed is similar at all loading rates, it can be concluded that the critical hydrostatic stress at which crazes are initiated is independent of the loading rate. This is consistent with the findings of recent work by Govaert *et al.* [43].

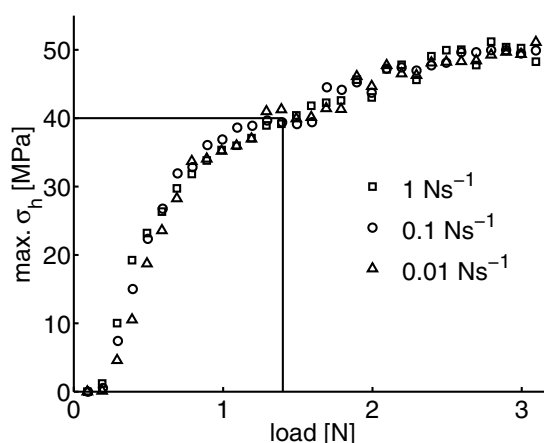


Figure 5.13: Building up of hydrostatic stress during loading at various loading rates for annealed PS: no rate dependence.

Network density

In the previous sections a void-nucleation criterion was identified for polystyrene, based on the assumption that void-nucleation is preceded by localised plastic deformation and incipient void nucleation by dilative stresses. This critical hydrostatic stress of 40 MPa

proved to be independent of the thermal history and strain rate. Among others, Kramer and co-workers [3, 44] and Wu [45] suggested that the network density influences the crazing behaviour and critical craze-nucleation stress. Therefore, the procedure followed to determine a critical craze-nucleation stress for polystyrene is repeated for PS/PPO blends. The network density of polystyrene increases when blended with PPO. The material parameters used in the simulations are given in table 5.1. In the figures 5.5 and 5.8 it was shown that for an increasing PPO fraction the yield stress slightly increases, the modulus decreases but above all, the strain hardening contribution is strongly enhanced.

Figure 5.14 shows the number of crazes formed during indentation at various load levels. The force required to initiate crazes increases with PPO fraction and thus with the network density. For the blend with 20% PPO (squares) the force is 3 N (± 0.2 N), for 40% PPO (triangles) this is 5 N (± 0.2 N).

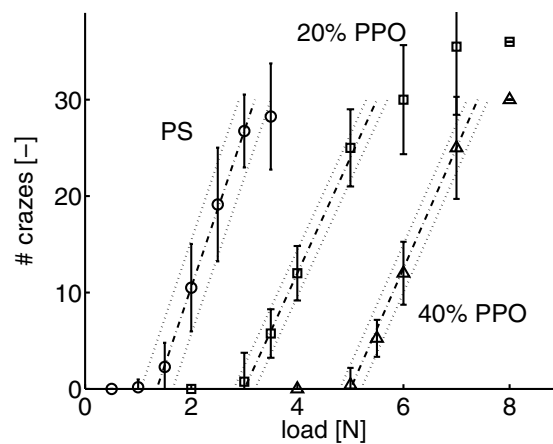


Figure 5.14: Number of crazes formed by indentation for annealed PS (circles), PS/PPO 80/20 (squares) and PS/PPO 60/40 (triangles). the dashed lines represent the 95% confidence interval.

Simulations of these indentation experiments, in which the maximum hydrostatic stress is again monitored, show that despite the differences in the indentation curves (see figure 5.8), the development of the maximum hydrostatic stress in the sample is barely influenced, see figure 5.15.

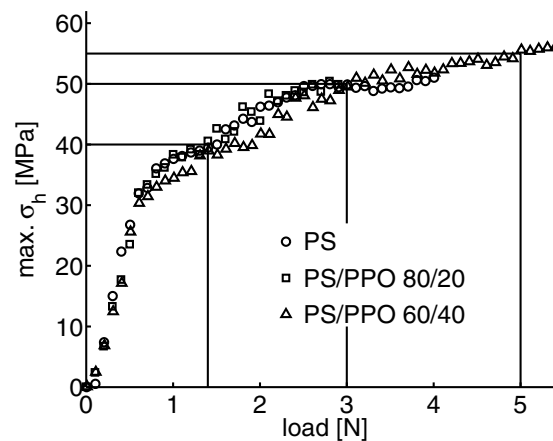


Figure 5.15: Development of σ_h as function of load for annealed PS (circles), PS/PPO 80/20 (squares) and PS/PPO 60/40 (triangles).

All curves have a positive slope with an increasing indentation force. The critical force for pure PS is reached at 1.35 N (as shown before), which corresponds to a critical hydrostatic stress of approximately 40 MPa. According to the experiments crazing is observed at a force of 3.0 N for PS/PPO with 20% PPO, corresponding to a hydrostatic stress of 50 MPa (dotted lines in figure 5.16) and for a fraction of 40% PPO the critical indentation force is 5.1 N, corresponding to a hydrostatic stress of approximately 55 MPa. The uncertainty intervals around the critical forces and hydrostatic stress are similar for all materials. The network density for PS and PS/PPO blends, is obtained by DMTA [14, 46]. For PS a network density of $3.0 \cdot 10^{25}$ chains/m³ is found. With increasing PPO fraction the network density rises to $4.9 \cdot 10^{25}$ chains/m³ (20% PPO) and $7.9 \cdot 10^{25}$ chains/m³ (40% PPO). In figure 5.16 the critical hydrostatic stress is given as function of network density.

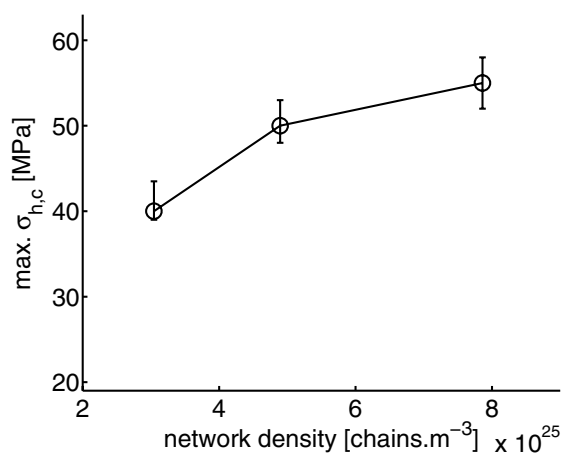


Figure 5.16: Critical hydrostatic stress as a function of the network density.

It can be concluded that the resistance to craze-nucleation of glassy polymers, like PS and PS/PPO, increases with increasing network density, which is in full agreement with the findings of Sauer [47]. The extrapolation of the trend in figure 5.16 to higher network densities, e.g. polycarbonate, gives a good approximation of the critical craze nucleation stress reported by Narisawa and co-workers ($\nu_e = 3.0 \cdot 10^{26}$ chains.m⁻³ [45], $\sigma_{h,c} = 90$ MPa [31]).

5.5 Conclusions

A combination of a numerical analysis using a proper constitutive model that can cover the rate dependent intrinsic yield behaviour, and a local, rate independent, craze-nucleation criterion can be used effectively to predict craze initiation in glassy polymers.

Micro-indentation of polystyrene at a sufficiently high load leads to crazing. Using the numerical model, the hypothesis of Kramer is confirmed that crazing of polymers is preceded by localised plastic deformation. Due to the nonlinear nature of yielding, strain softening results in localisation of deformation as the plastic strain increases, accompanied by a build-up of hydrostatic stress. The hydrostatic stress is the only parameter that initiates void-nucleation after the material shows local deformation and softening.

During the loading stage of indentation crazes are formed, beginning near the contact circle between indenter and specimen in radial direction. Visualisations, by means of microscopy, enable determination of the number of crazes and the critical force at which they are formed.

From the numerical simulations the critical hydrostatic stress for void nucleation is determined to be 40 MPa for annealed PS, and this event occurs just outside the contact zone between polystyrene and indenter. The criterion is validated by varying thermal history and loading rate during indentation. Quenched PS shows very tiny crazes at a higher force, the trend depicted by the numerical simulation is good and the prediction by the craze-nucleation criterion agrees with the observations. The exact value of the crazing force for the quenched sample is difficult to predict. Varying the loading rate does not influence the crazing force and both the numerical model and experiments resulted in the same force. The post yield behaviour is changed by adding PPO to PS, increasing the network density. An increase of the network density results in a higher value of the critical craze-nucleation stress, 50 MPa for the blend with 20% PPO and 55 MPa for the blend with 40% PPO.

Acknowledgements

The authors wish to acknowledge the financial support provided by the Dutch Technology Foundation (STW) (Grant EWT.3766).

References

- [1] Kambour, R.P., *J. Pol. Sci.: Macromol. Rev.*, **7**, 1 (1973)
- [2] Kramer, E.J., In: H.H. Kausch, Ed., *Adv. Pol. Sci.*, Springer Verlag, Berlin, **52/53**, 1-56 (1983)
- [3] Kramer, E.J. and Berger, L.L., In: H.H. Kausch, Ed., *Adv. Pol. Sci.*, Springer Verlag, Berlin, **91/92**, 1-68 (1990)
- [4] Kinloch, A.J. and Young, R.J., *Fracture behaviour of polymers*, 2nd ed., Elsevier's Appl. Sci. Publ. Ltd, London and New York (1985)
- [5] Argon, A.S. and Hannoosch J.G., *Phil. Mag.*, **36**, 1195 (1975)
- [6] Adam, G.A., Cross, A., Haward, R.N., *J. Mat. Sci.*, **10**, 1582 (1975)
- [7] Cross, A., Haward, R.N. Mills, N.J., *Polymer*, **20**, 288 (1979)
- [8] Hasan, O.A. and Boyce, M.C., *Polymer*, **34**, 5085 (1993)
- [9] Bauwens, J.C., *J. Mat. Sci.*, **13**, 1443, (1978)
- [10] G'Sell, C. In: Queen HJ, ed., *Strength of metals and alloys*, Oxford, Pergamon Press, 1943-1982 (1986)
- [11] Govaert, L.E., Timmermans, P.H.M., Brekelmans, W.A.M., *J. Eng. Mat. Tech.*, **122**, 177 (2000)
- [12] Tervoort, T.A. and Govaert, L.E., *J. Rheol.*, **4**, 1263 (2000)
- [13] Govaert, L.E., van Melick, H.G.H., Meijer, H.E.H., *Polymer*, **42**, 1271 (2001)
- [14] van Melick, H.G.H., Govaert, L.E., Meijer, H.E.H., Influence of network density on the strain hardening behaviour of glassy polymers, *Polymer*, submitted.

- [15] van Melick, H.G.H., Govaert, L.E., Meijer, H.E.H., Localisation phenomena in glassy polymers: influence of thermal and mechanical history, Polymer, submitted.
- [16] Ender, D.H. and Andrews, R.D., Pol. Lett., **36**, 3057 (1965)
- [17] Henkee, C.S. and Kramer, E.J., J. Pol. Sci., Pol. Phys. Ed., **22**, 721 (1984)
- [18] Boyce, M.C., Parks, D.M., Argon, A.S., Mech. Mat., **7**, 15 (1988)
- [19] Hasan, O.A., Boyce, M.C., Li, X.S., Berko, S., J. Pol. Sci., Part B: Pol. Phys., **31**, 185 (1993)
- [20] Arruda, E.M. and Boyce, M.C., Int. J. Plast., **9**, 697 (1993)
- [21] Boyce, M.C., Arruda, E.M., Jayachandran, R., Pol. Eng. Sci., **34**, 716 (1994)
- [22] Wu, P.D. and van der Giessen, E., J. Mech. Phys. Solids, **41**, 427 (1993)
- [23] Wu, P.D. and van der Giessen, E., Int. J. Plast., **11**, 211 (1995)
- [24] Tervoort, T.A., Smit, R.J.M., Brekelmans, W.A.M., Govaert, L.E., Mech. Time-depend. Mat., **1**, 269 (1998)
- [25] Tervoort, T.A., Klompen, E.T.J., Govaert, L.E., J. Rheol., **40**, 779 (1996)
- [26] Smit, R.J.M., Brekelmans, W.A.M., Meijer, H.E.H., Comp. Meth. Appl. Mech. Eng., **155**, 181 (1998)
- [27] Smit, R.J.M., Brekelmans, W.A.M., Meijer, H.E.H., J. Mech. Phys. Sol., **47**, 201 (1999)
- [28] Smit, R.J.M., Brekelmans, W.A.M., Meijer, H.E.H., J. Mat. Sci., **35**, 2855 (2000)
- [29] Smit, R.J.M., Brekelmans, W.A.M., Meijer, H.E.H., J. Mat. Sci., **35**, 2869 (2000)
- [30] Smit, R.J.M., Brekelmans, W.A.M., Meijer, H.E.H., J. Mat. Sci., **35**, 2881 (2000)
- [31] Ishikawa, M., Narisawa, I., Ogawa, H., Pol. Sci. Phys., **15**, 1791 (1977)
- [32] Narisawa, I., Ishikawa, M., Ogawa, H., Phil. Mag. A, **41**, 331 (1980)
- [33] Ishikawa, M., Ogawa, H., J. Macromol. Sci.-Phys., **B19**, 421 (1982)
- [34] Camwell, L. and Hull, D., Phil. Mag., **27**, 1135 (1973)
- [35] Kells, D. and Mills, N.J., Phil. Mag., **44**, 1149 (1981)
- [36] van Melick, H.G.H., Internal report, Materials Technology, Eindhoven University of Technology (2001)
- [37] van Melick, H.G.H., van Dijken, A.R., den Toonder, J.M.J., Govaert, L.E., Meijer, H.E.H., Phil. Mag. A, 2002, accepted.
- [38] Simons, G. and Wang, H., *Single Crystal Elastic Constants and Calculated Aggregate Properties: A Handbook*, 2nd ed., (1971)
- [39] van Krevelen, W., *Properties of polymers*, Elsevier, Amsterdam (1972)
- [40] Horsley, R.A., *Plastic progress*, Iliffe and Sons, London and New York, 77 (1958)
- [41] Marshall, A.S., Petrie, S.E.B., J. Appl. Phys., **46**, 4223 (1975)
- [42] Hutchinson, J.M., Prog. Pol. Sci., **20**, 703 (1995)
- [43] Govaert, L.E., Tervoort, T.A., Meijer, H.E.H., Polymer, submitted.
- [44] Donald, A.M., and Kramer, E.J., J. Mat. Sci., **17**, 1871 (1982)
- [45] Wu, S., Pol. Eng. Sci., **30**, 753 (1990)
- [46] Prest jr., W.M. and Porter, R.S., Pol. Sci. Eng., Part A2, **10**, 1639 (1972)
- [47] Sauer, J.A. and Hara, M., In: H.H. Kausch, Ed., Adv. Pol. Sci, **91/92**, 82-118 (1990)

Appendix

In this appendix the relevant equations of the compressible Leonov model are summarised. A elaborate description of this elasto-visco plastic model can be found in Govaert *et al.* [11] and Tervoort *et al.* [24, 25].

$$\boldsymbol{\sigma} = \boldsymbol{s} + \boldsymbol{r} \quad (5.1)$$

$$\boldsymbol{s}^d = G\tilde{\boldsymbol{B}}_e^d \quad \text{and} \quad \boldsymbol{s}^h = \kappa(J - 1)\boldsymbol{I} \quad (5.2)$$

$$\dot{J} = J\text{tr}(\boldsymbol{D}) \quad (5.3)$$

$$\overset{\circ}{\tilde{\boldsymbol{B}}}_e = (\boldsymbol{D}^d - \boldsymbol{D}_p) \cdot \tilde{\boldsymbol{B}}_e + \tilde{\boldsymbol{B}}_e \cdot (\boldsymbol{D}^d - \boldsymbol{D}_p) \quad (5.4)$$

$$\boldsymbol{r} = G_R \tilde{\boldsymbol{B}}^d \quad (5.5)$$

$$\boldsymbol{D}_p = \frac{\boldsymbol{s}^d}{2\eta(\tau_{eq}, D, p)} \quad (5.6)$$

$$\eta(\tau_{eq}, D, p) = A(D, p) \tau_0 \frac{\frac{\tau_{eq}}{\tau_0}}{\sinh\left(\frac{\tau_{eq}}{\tau_0}\right)} \quad (5.7)$$

$$\tau_{eq} = \sqrt{\frac{1}{2}\text{tr}(\boldsymbol{s}^d \cdot \boldsymbol{s}^d)} \quad (5.8)$$

$$\dot{D} = \left(1 - \frac{D}{D_\infty}\right) \dot{\gamma}_p \quad (5.9)$$

$$\dot{\gamma}_p = \sqrt{2\text{tr}(\boldsymbol{D}_p \cdot \boldsymbol{D}_p)} \quad (5.10)$$

Chapter 6

Near-surface mechanical properties of glassy polymers

Polymeric material near a free surface can have properties which deviate considerably from the bulk properties. A reduced glass transition temperature in thin polymeric films was reported and was attributed to an enhanced segmental mobility near a free surface. It was also reported that sufficiently thin polymeric structures show a higher ductility than the bulk material. In this paper, the hypothesis that the near-surface mechanical properties of amorphous polymers differ from the bulk properties due to the presence of an absolute length-scale will be investigated. Micro- and nano-indentations are performed on polystyrene, using a range of indenter sizes and indentation loads. In addition, numerical simulations are carried out with an advanced material model for polystyrene. A comparison between experimental and numerical results indeed indicates that a length-scale effect is present near the surface. Simulations performed at an elevated temperature indicate that the results presented are consistent with the observations of a reduced T_g .

6.1 Introduction

Recent research in different fields of polymer science has shown that properties of small polymeric structures and polymeric material near a free surface can deviate considerably from the bulk properties. The most well known examples come from the field of polymer physics. Keddie *et al.* [1, 2] showed by ellipsometry that the glass transition temperature (T_g) of thin polystyrene (PS) films (<40 nm) on hydrogen-passivated silicon substrates is lower than the bulk glass transition temperature. Subsequent studies

Reproduced in part from:

Near-surface mechanical properties of amorphous polymers

H.G.H. van Melick, A.R. van Dijken, J.M.J. den Toonder, L.E. Govaert, H.E.H. Meijer, **Philosophical Magazine A**, accepted for publication.

on polymethylmethacrylate (PMMA) showed a large influence of the substrate on this effect. A decreased T_g was found for thin PMMA films on gold while an increased T_g was observed for a substrate of silicon with a native oxide layer [3, 4]. The influence of a substrate was eliminated in the Brillouin Light Scattering experiments on thin free-standing PS films by Forrest *et al.* [5] and Forrest and Mattson [6]. These experiments revealed that the T_g decreases strongly for films thinner than 70 nm (see figure 6.1a). For films smaller than 30 nm the measured T_g reduced even to the ambient temperature. An extensive review of the studies on the T_g measurements of thin polymeric films can be found in [7].

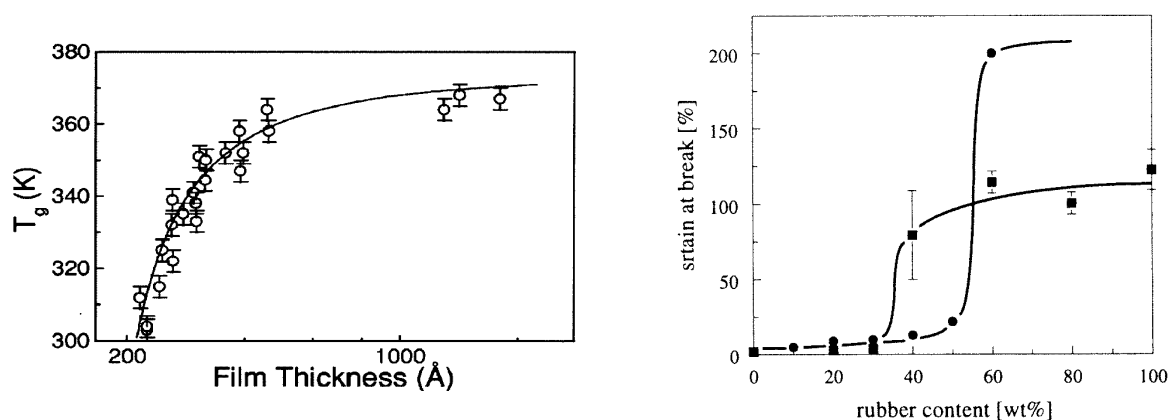


Figure 6.1: Two examples of length-scale effects in polymers. (a) Reduced T_g in thin free-standing polystyrene films (reproduced in part with permission from [6]) and (b) enhanced toughness by incorporation of nano-sized rubber particles of size 200 nm (■) and 80 nm (●) (reproduced with permission from [16]).

Generally the phenomenon of a reduced T_g in thin polymer films is assigned to an enhanced segmental mobility near the free surfaces of the polymer. Direct observation of a faster relaxation near a free surface was recently done by Wallace [8]. By near-edge X-ray absorption fine structure spectroscopy, they measured the relaxation rate of polystyrene molecules of a uniaxially deformed sample simultaneously near a free surface and in the bulk. Relaxation of the chains near the free surface were proven to be significantly faster than the bulk chains. However, the length-scale of this relaxation is much smaller than the length-scale observed in the previously mentioned T_g measurements.

The effect of an absolute length-scale has also been observed in the field of polymer engineering. In daily practice of liquid crystal displays, a rubbing technique is used to orient the surface layer of, mostly, vinyl-polymers [9, 10]. Toney *et al.* [11] showed by X-ray experiments on thin polyimide films that the top layer (5 nm) was oriented after rubbing with a cloth, which indicated that the yield stress near this surface was significantly lower than the bulk yield stress. Another example of an intrinsic length-scale is the toughness enhancement of thin polymeric films and ligaments. In very thin multi-layered tapes [12] and non-adhering rubber-filled polymeric matrices [13–16], in which the layer or ligament thickness is smaller than a critical value, a strong increase in macroscopic strain to break is observed, indicating that locally the mechanical properties deviate considerably from the bulk properties. This toughness enhancement for rubber-filled polystyrene is represented in figure 6.1b.

The observations mentioned above are consistent since the mechanical properties of polymers are directly related to the segmental mobility and hence are strongly correlated to T_g . It is therefore to be expected that mechanical properties, such as yield stress and strain softening, are different in thin films or near a free surface compared to those in the bulk.

The aim of this paper is to probe this effect of a length-scale on the mechanical properties of amorphous polymers near a free surface by micro- and nano-indentation. This technique was chosen since, in contrast to conventional techniques, it is able to cover various length-scales (mm to nm) and it can measure mechanical properties on the very small scale that is required here. The indentations were done with spherical indenters of various sizes on polystyrene sheet material. The force-displacement curves were recorded and compared with, length-scale independent, finite element simulations. The bulk properties, used as input for the elasto-viscoplastic model, were obtained from uniaxial compression tests on identical material.

6.2 Numerical model

The response of bulk polystyrene to a uniaxial compression test is shown in figure 6.2a. The experimental curve (circles) illustrates the typical mechanical behaviour that is representative for a range of amorphous polymers: a small-strain (visco-) elastic response, followed by yield, intrinsic strain softening and subsequent strain hardening.

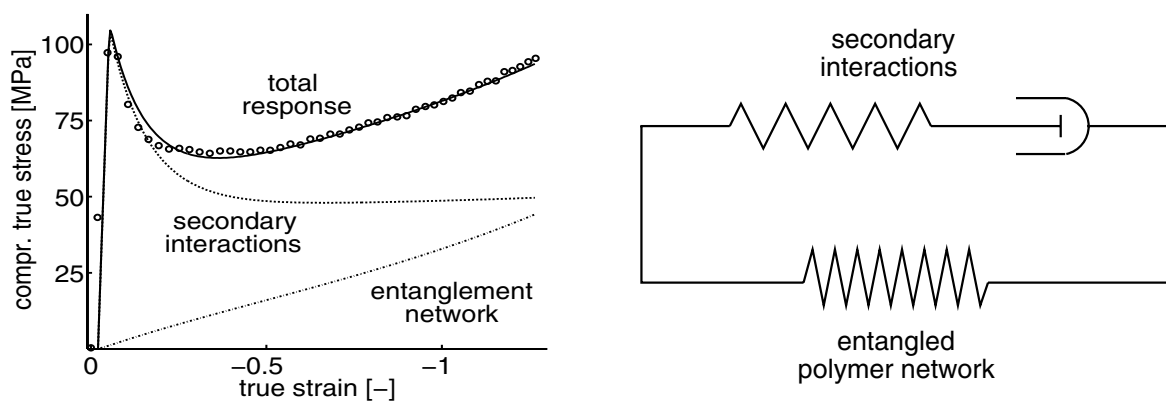


Figure 6.2: (a) Stress-strain response of bulk polystyrene in a uniaxial compression test, experiment (circles) and simulation (solid line). The dashed and dash-dotted lines represent the two contributions present in the model, as described in this paragraph. (b) 1-D representation of the generalised compressible Leonov model.

In the stress response two contributions can be distinguished. First there is a contribution of the secondary interactions (e.g. Van der Waals bonds) between the polymer chains, which determine the (visco-) elastic properties at small deformations and the yield behaviour (represented by the dashed line). The second contribution originates from the entangled polymer network. This contribution determines the behaviour at large strains and is governed by the strong covalent bonds within the polymer chain (represented by the dash-dotted line). In the model used here, the so-called generalised compressible Leonov model [17–19], this distinction is also made. In the 1-D

mechanical analogon (see figure 6.2b), the secondary interactions comprise a compressible elastic spring and a non-linear dashpot and the entangled polymer network a neo-Hookean spring. The total Cauchy stress ($\boldsymbol{\sigma}$) of the model (represented by the solid line in figure 6.2a), can accordingly be decomposed in a driving stress (\boldsymbol{s}) and a hardening stress (\boldsymbol{r}):

$$\boldsymbol{\sigma} = \boldsymbol{s} + \boldsymbol{r} \quad (6.1)$$

The driving stress can be split into a deviatoric and hydrostatic part. The expressions for the stresses in these parts yield:

$$\boldsymbol{s}^d = G\tilde{\boldsymbol{B}}_e^d \quad \text{and} \quad \boldsymbol{s}^h = \kappa(J - 1)\boldsymbol{I} \quad (6.2)$$

where G is the shear modulus, $\tilde{\boldsymbol{B}}_e$ the isochoric elastic left Cauchy-Green deformation tensor, κ the bulk modulus, J the volume change factor and \boldsymbol{I} the unity tensor. The relative volume change J and the isochoric elastic left Cauchy Green deformation tensor $\tilde{\boldsymbol{B}}_e$ are implicitly given by [17]:

$$\dot{J} = J\text{tr}(\boldsymbol{D}) \quad (6.3)$$

$$\overset{\circ}{\tilde{\boldsymbol{B}}_e} = (\boldsymbol{D}^d - \boldsymbol{D}_p) \cdot \tilde{\boldsymbol{B}}_e + \tilde{\boldsymbol{B}}_e \cdot (\boldsymbol{D}^d - \boldsymbol{D}_p) \quad (6.4)$$

The left-hand side of this equation represents the (objective) Jaumann derivative of the isochoric elastic left Cauchy Green tensor. The tensor \boldsymbol{D} denotes the deformation rate tensor, \boldsymbol{D}_p the plastic deformation rate tensor.

The hardening behaviour of the material is described with a neo-Hookean relation for the hardening stress tensor \boldsymbol{r} :

$$\boldsymbol{r} = G_R \tilde{\boldsymbol{B}}^d \quad (6.5)$$

where G_R is the strain hardening modulus (assumed temperature independent). The neo-Hookean approach shown in equation 6.5 proved to be very successful in describing the strain hardening behaviour of polycarbonate in uniaxial compression, uniaxial extension and shear (torsion) [19].

As proposed by [17] a Newtonian flow rule with a stress dependent Eyring viscosity is used to relate the plastic deformation rate to the deviatoric driving stress:

$$\boldsymbol{D}_p = \frac{\boldsymbol{s}^d}{2\eta} \quad (6.6)$$

As described by [18], the model has been extended by adding pressure dependence (p) and intrinsic strain softening (D) to the viscosity function. The evolution of the softening equation was originally proposed by [20]. The viscosity function is described by an Eyring relationship:

$$\eta(\tau_{eq}, D, p) = A(D, p)\tau_0 \frac{\frac{\tau_{eq}}{\tau_0}}{\sinh\left(\frac{\tau_{eq}}{\tau_0}\right)} \quad (6.7)$$

and:

$$\tau_{eq} = \sqrt{\frac{1}{2}\text{tr}(\mathbf{s}^d \cdot \mathbf{s}^d)} \quad , \quad A = A_0 \exp\left(\frac{\Delta H}{RT}\right) \exp\left(\frac{\mu p}{V} - D\right) \quad \text{and} \quad \tau_0 = \frac{RT}{V} \quad (6.8)$$

where A_0 is a constant pre-exponential factor, ΔH the activation energy, R is the gas constant, and V the activation volume. In the evolution of the softening (given in equation 6.9), the softening parameter D is initially set to zero. In time, this parameter evolves to the softening limit D_∞ .

$$\dot{D} = \left(1 - \frac{D}{D_\infty}\right) \dot{\gamma}_p \quad (6.9)$$

where:

$$\dot{\gamma}_p = \sqrt{2\text{tr}(\mathbf{D}_p \cdot \mathbf{D}_p)} \quad (6.10)$$

A detailed description of the model can be found in [17] and [18].

The material model was incorporated into the commercial Finite Element package MARC [21] and validated under various loading conditions [18]. An example of the FE mesh used for the simulations of the indentations is depicted in figure 6.3a. The mesh becomes more and more refined towards the region of contact (see figure 6.3b), to be able to account for the large stress gradients that may occur in this region. Axisymmetric quadrilateral linear elements were used. The total domain shown in the left of figure 3 has dimensions $1000 \times 1000 \mu\text{m}^2$, and consists of 773 nodes and 706 elements.

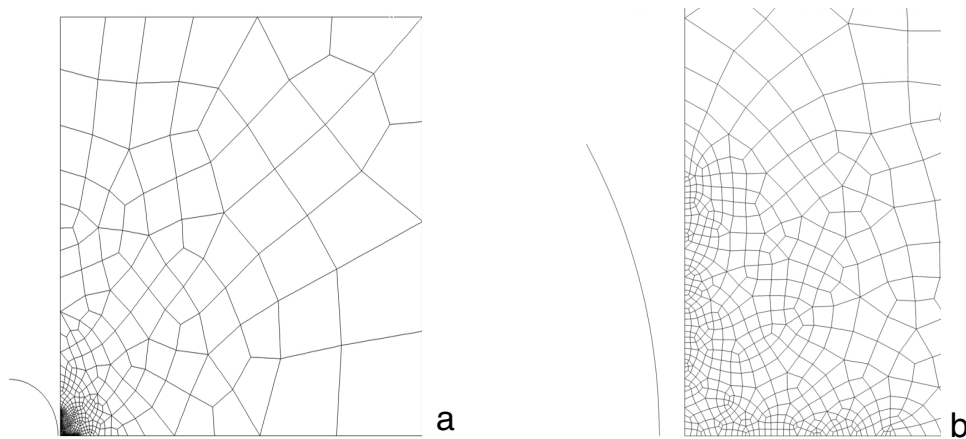


Figure 6.3: Complete FE mesh (a) and a magnified area with mesh-refinement in the contact region (b).

The indenter was modelled as a rigid sphere, and the contact was assumed to be frictionless. Loading proceeded from initial contact in a stepwise manner, in 500 to 1000 steps depending on the specific case. Mesh refinement, use of second order elements and step refinement proved to be of no influence on the solution. The solution of the previously described simulations is therefore considered to be converged.

6.3 Materials and methods

The material used is a commercially available polystyrene, Styron 634 (Dow Chemical). The granular material was compression moulded in a square mould ($160 \times 160 \times 7 \text{ mm}^3$). In the middle of the mould a thin glass plate of $100 \times 100 \times 3 \text{ mm}^3$ was placed. This glass plate ensured that the polymer surface is smooth and clean, and therefore no further machining or polishing was required. Furthermore the properties were not influenced by cooling effects at the mould surface since the surface to be indented came from the middle part of the material. The mould with granular PS was heated for approximately 10 minutes at 190°C . Next the material was compressed stepwise with increasing force (up to 300 kN). In between the steps, the force was released to allow for degassing and avoid formation of air bubbles. Afterwards the mould was placed in the cooling press in which the temperature was reduced to ambient temperature within 5 minutes. The specimens, used for indentation, were cut out of the middle of the moulded plate. A second plate without glass plate was moulded under identical conditions. From this plate cylindrical specimens were machined which were used in the uniaxial compressions tests. From the uniaxial compression tests, at various strain rates and temperatures, the material parameters required for the generalised compressible Leonov model were determined (given in the table of figure 6.4). The parameter for the pressure dependence was determined by tensile tests under superimposed pressure at the IRC in Leeds. As can be seen in figure 6.4, the numerical model correctly describes the deformation of PS in a uniaxial compression test.

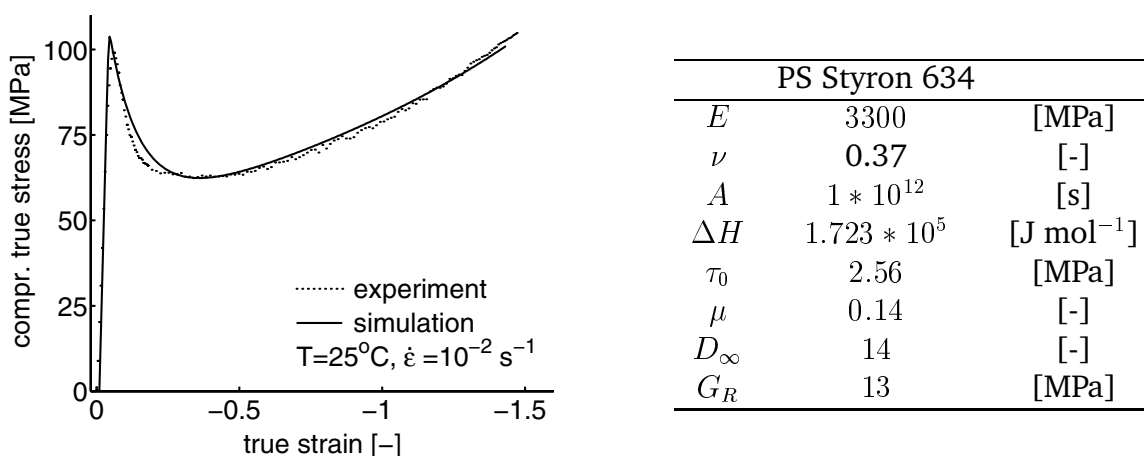


Figure 6.4: Comparison of experiment and simulation for a uniaxial compression test and the parameters for the generalised compressible Leonov model, as determined from the uniaxial compression tests.

The indentations were carried out on two different apparatus, namely a micro-indenter that was designed and constructed at Philips Research, and a commercial nano-indenter, i.e. the NanoTest 600 of Micro Materials. The micro-indenter was used for larger indentation peak loads, i.e. larger than 50 mN, and the nano-indenter was used for smaller indentation loads, down to $200 \mu\text{N}$. Considering both instrumental and environmental measurement noise, the accuracy of the measured loads and displacements were 2 mN and 20 nm for the micro-indenter, and $10 \mu\text{N}$ and 0.5 nm for the nano-indenter. The compliance of both systems was determined by carrying out indentations on fused silica with a spherical indenter of radius $150 \mu\text{m}$. The data were fitted to the Hertzian

elastic equation, with use of the known elastic parameters of fused silica ($E=72$ GPa, $\nu=0.17$), and compliances of 0.1 nm/mN for the micro-indenter and 0.7 nm/mN for the nano-indenter were measured.

The indentations on polystyrene were performed with spherical indenters with a range of sizes. The radii of the indenters used were 250 , 150 , 25 , and 2.2 μm . The former two are sapphire spheres, and the latter two are diamond cones with rounded tips, supplied by Synton (Switzerland). The radii of the two smallest tips were measured directly with an AFM and their geometry proved to be well-described. Comparison of indentation with these spheres on fused silica and the Hertzian solution, showed that 25 and 2.2 μm are good approximations of the indenter radii.

The experiments were performed in such a way that the indentations with the various indenters were geometrically identical, i.e. a scaled experiment with the radius of the indenter as a scaling parameter. Also the loading rate was chosen in such a way that each scaled experiment was performed in the same time. Each experiment consisted of one full loading-unloading cycle. A range of scaled peak indentation loads was used, from 200 μN to 400 mN. The measurements were done at a temperature between 21 and 25°C , and a relative humidity of 50% .

6.4 Results and discussion

In this section, some key results of the experiments and the simulations will be shown. From the experiments, it was found that the results obtained with the micro-indenter and those obtained with the nano-indenter are identical in the overlapping load-range of the instruments. Also, the reproducibility of the experiments was good. To illustrate this the experimental data of each indentation consisting of five successive indentations on various regions of the material are given in figures 6.5 and 6.6. Both these results underline the accuracy of the experiments. In figure 6.5, both the experimental curves and the simulated curve are given for the 150 μm sphere.

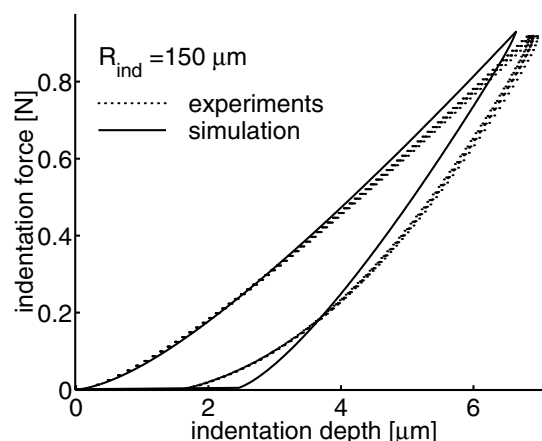


Figure 6.5: Results of experiments (dotted lines) and simulation (solid line) of the indentation with the 150 μm sphere.

In the simulations the bulk material parameters for polystyrene, obtained from the uniaxial compression test were used. There is excellent agreement between the simula-

tion and the experiment during the loading part of the curve. During unloading, the agreement still is reasonable, but the (visco-)elastic recovery of the material is underestimated by the simulations. The probable reason for this is that only one Leonov mode is present in the material model and thus the relaxation behaviour is poorly described. Tervoort *et al.* [19] showed that by incorporation of 18 Leonov modes the relaxation behaviour of these types of polymers can be accurately described. However, incorporation of more modes is computationally expensive and, since the focus is on the loading behaviour, simulations with one Leonov mode are sufficiently adequate.

The experiments are also performed with indenters of 250 and 25 μm . Figure 6.6 shows the force-displacement curves are similar to those in figure 6.5. Except for the unloading behaviour the experiments are well predicted by the simulations.

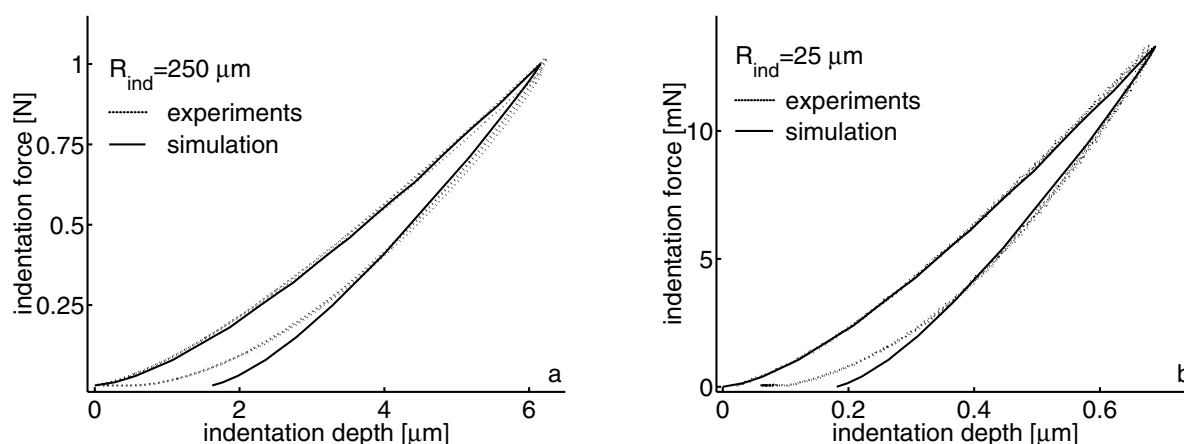


Figure 6.6: Results of experiments (dotted lines) and simulations (solid lines): (a) the indentation with the 250 μm sphere and (b) the indentation with the 25 μm sphere.

For the larger indenters (radii of 250, 150 and 25 μm), experiments and simulations with the bulk properties of polystyrene agree well. This indicates that no effect of an absolute length-scale is present in these experiments.

However, for the indentations with the smallest sphere (2.2 μm) and smallest indentation loads, a significant discrepancy appears between the experimental result and the simulation, as shown in figure 6.7. The indentation depth is underpredicted by the simulation, indicating that the material has less resistance to deformation. Also the shape of the indentation curve is significantly different from the large-scale indentations. Was the visco-elastic recovery underpredicted in the simulations with the largest indenters, the measured recovery after indentation with the smallest sphere is much less than in the indentations with the larger indenters.

Since it could be argued that the discrepancy between experiments and simulation originates from a deviating indenter geometry, comparative simulations are required. The experimental results, in this respect, could only be explained by an indenter with a smaller radius and hence simulations were performed with an indenter with a 10% smaller radius. This 10% 'error', which is rather much in the AFM measurements and calibration analysis, does result in a slightly larger indentation depth (approximately 3 nm), but can not account for the large difference between experiments and simulation and can certainly not be responsible for the drastically change in shape of the indentation curves.

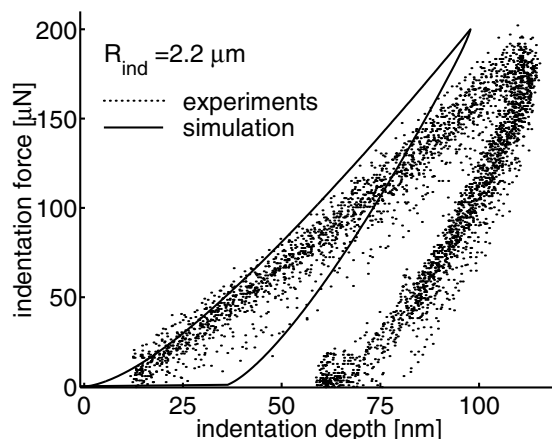


Figure 6.7: Results of experiments (dotted lines) and simulation (solid line) of the indentation with the $2.2 \mu\text{m}$ sphere.

The simulations were performed with bulk material properties as input. The discrepancy between the numerical and experimental results from figure 6.7, suggest that the mechanical properties, and the yield stress in particular, are lower in the near-surface region of the actual experiment. In these last experiments the indentation depths which are reached are in the order of 100 nm. Although the zone that is participating in the deformation is larger than the indentation depth, near-surface effects will play a role. The reported effects of reduced T_g , as described in the introduction, have a length-scale similar to the scale of indentation. Hence, the hypothesised length scale effect seems to be observed in the indentation with the $2.2 \mu\text{m}$ indenter.

As discussed in the introduction, an enhanced segmental mobility near a free surface could have an effect on both the T_g and mechanical properties. The segmental mobility is not a measure for the absolute level of T_g but for the difference between the testing temperature and T_g . A reduced T_g can therefore be 'simulated' by an increased testing temperature. To illustrate this the experiments are compared to a simulation which is performed 'closer' to T_g , i.e. at an elevated temperature (approximately 60°C). Although

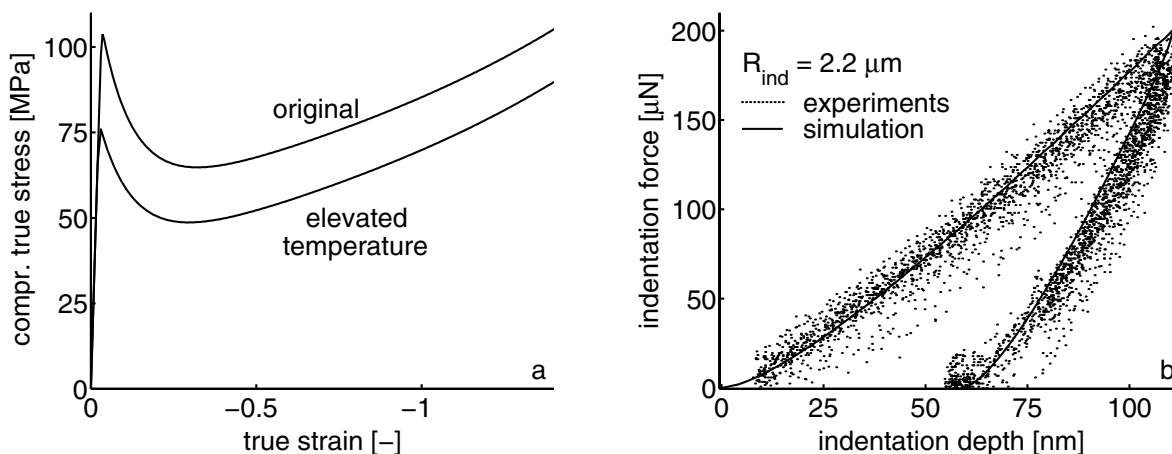


Figure 6.8: Simulation at an elevated temperature. (a) The intrinsic deformation behaviour is at ambient and elevated temperature and (b) comparison of indentation experiment and simulation.

certainly not correct, as we are changing the bulk properties and not the near-surface

properties, this simulation can give an indication whether the experimentally observed effect can be rationalised by a reduced T_g . As can be seen in figure 6.8a an increased temperature leads to a lower yield stress and less strain softening of the material. The large strain behaviour remains unchanged.

The result of the simulation with the altered parameters is shown in figure 6.8b, along with the experimental results from figure 6.7. The agreement between the loading curves is good, indicating that the near-surface layer might have reduced yield stress. From the fact that also the unloading curve is predicted well, no conclusions can be drawn. It must be emphasised that the simulations at elevated temperature has no physical relation with the actual experiment, but it does support the hypothesis that the near-surface properties are significantly different from the bulk properties.

6.5 Conclusions

Experiments and simulations of spherical indentations in polystyrene were performed, using a range of indenter sizes and indentation loads. The experimental results for the large-size, large-load indentations are described well by simulations with polystyrene bulk properties. For the smallest indenter, the experimental and simulated curves deviate considerably, which indicates that a length-scale effect is present. Simulations with altered properties, mimicking a material with a lower glass transition temperature (T_g), do agree quite well with the small-size, small-load experiments. It must be emphasised that this simulation is physically not completely correct, but the trend is well predicted. This supports the hypothesis that the near surface properties of polystyrene differ from those in the bulk, and that the length-scale effect observed is consistent with the observations of a lower T_g being lower near the surface.

Acknowledgements

The authors wish to acknowledge the financial support provided by the Dutch Technology Foundation (STW) (Grant EWT.3766).

References

- [1] Keddie, J.L., Jones, R.A.L., and Cory, R.A., *Europhys. Lett.*, **27**, 59 (1994)
- [2] Keddie, J.L., and Jones, R.A.L., *Israel J. Chem.*, **35**, 21 (1995)
- [3] Keddie, J.L., and Jones, R.A.L., *Dynamics in Small Confining Systems II*, In: J.M. Drake, J.M., J. Klafter, R. Kopelman, Eds., *Mat. Res. Soc. Symp. Proc.*, Materials Research Society, Pittsburgh, Pennsylvania, **366**, 183-188 (1995)
- [4] van Zanten, J.H., Wallace, W.E., and Wu, W-L., *Phys. Rev. E.*, **53**, R2053 (1996)
- [5] Forrest, J.A., Dalnoki-Veress, K., Dutcher, J.R., Rowat, A.C., and Stevens, J.R., *Disordered Materials and Interfaces*, In: H.Z. Cummins, H.Z., D.J. Durian, D.I. Johnson, Eds., *Mat. Res. Soc. Symp. Proc.*, Materials Research Society, Pittsburgh, Pennsylvania, **407**, 131-136 (1996)
- [6] Forrest, J.A., and Mattsson, J., *Phys. Rev. E.*, **61**, R53 (2000)
- [7] Forrest, J.A., and Jones, R.A.L., In: A. Karim and S. Kumar, *Polymer Surfaces, Interfaces, and Thin Films*, World Scientific Publishing, Singapore, 251-294 (2000)

-
- [8] Wallace, W.E., Fischer, D.A., Efimenko, K., Wu, W-L., and Genzer, J., *Macromol.*, **34**, 5081 (2001)
- [9] van Aerle, N.A.J.M., Barmentio, M., and Hollering, R.W.J., *J. Appl. Phys.*, **74**, 3111 (1993)
- [10] van Aerle, N.A.J.M., and Tol, A.J.W., *Macromol.*, **27**, 6520 (1994)
- [11] Toney, Michael F, Russell, Thomas P, Logan, J. Anthony, Kikuchi, Hirotsugu, Sands, James M., Kumar, and Sanat, K., *Nature*, **374**, 709 (1995)
- [12] van der Sanden, M.C.M., Meijer, H.E.H., Lemstra, P.J., *Polymer*, **34**, 2148 (1994)
- [13] Wu, S., *J. Appl. Pol. Sci.*, **35**, 549 (1988)
- [14] van der Sanden, M.C.M., de Kok, J.M.M., and Meijer, H.E.H., *Polymer*, **35**, 2995 (1994)
- [15] Magalhaes, A.M.L., and Borggreve, R.J.M., 1995, *Macromol.*, **28**, 5841 (1995)
- [16] Jansen, B.J.P, Rastogi, S., Meijer, H.E.H., and Lemstra, P.J., *Macromol.*, **34**, 3998 (2001)
- [17] Tervoort, T.A., R.J.M. Smit, W.A.M. Brekelmans, and L.E. Govaert, *Mech. Time-depend. Mat.*, **1**, 269 (1998)
- [18] Govaert, L.E., Timmermans, P.H.M., and Brekelmans, W.A.M., *J. Eng. Mat. Tech.*, **122**, 177 (2000)
- [19] Tervoort, T.A. and Govaert, L.E., *J. Rheo.*, **44**, 1263 (2000)
- [20] Hasan, O.A., Boyce, M.C., Li, X.S., and Berko, S., *J. Pol. Sci. Part B: Pol. Phys.*, **31**, 185 (1993)
- [21] van der Aa, M.A.H., Schreurs, P.J.G., Baaijens, F.P.T., *Mech. of Mat.*, **33**, 555 (2001)
- [22] Tervoort, T.A., Klompen, E.T.J., and Govaert, L.E., *J. Rheo.*, **40**, 779 (1996)

Chapter 7

Prediction of brittle-to-ductile transitions in polystyrene

In this study it is attempted to predict brittle-to-ductile transitions (BDTs) in polystyrene blends, induced either by an increase in temperature or by a decrease in interparticle distance. A representative, two-dimensional volume element (RVE) of a polystyrene matrix with 20% circular voids, is deformed in tension. During deformation a hydrostatic-stress based craze-nucleation criterion [1] is evaluated. The simulations demonstrate that crazes initiate at low temperatures while a transition from crazing to shear yielding (BDT) is found around 75°C. The numerical results correlate well with tensile tests on a similar heterogeneous polystyrene. The presence of an absolute length, as experimentally found, is more difficult to explain. Near a free surface a T_g -depression is measured for polystyrene and also the resistance to indentation in polystyrene is lower than expected from bulk properties. Both observations are rationalised by an enhanced segmental mobility of chains near a free surface. As a consequence of these findings, an absolute length-scale could be incorporated in the numerical simulations. For simplicity, the length-scale is modelled by taking a temperature gradient over a thin layer near the internal free surfaces of the RVE. Deformation of the RVE with different absolute length-scales shows that indeed also the experimentally found brittle-to-ductile transition can be predicted if the ligament thickness between the inclusions ('voids') in polystyrene is below a critical value of ca. 15 nm.

Reproduced from:

Prediction of brittle-to-ductile transitions in polystyrene

H.G.H. van Melick, L.E. Govaert, H.E.H. Meijer, submitted to **Polymer**.

7.1 Introduction

Numerical prediction of strain localisation phenomena in glassy polymers has received substantial attention during the last decades. Following the work of Haward and Thackray [2], Boyce and co-workers [3–6] developed a model that was able to capture the post-yield behaviour of glassy polymers. Studies of the group of van der Giessen [7, 8] and our group [9–17] lead to the conclusion that the numerical simulation of plastic localisation in various loading geometries is now well established. However, failure, an important issue in the deformation behaviour, could not yet be predicted.

The importance of failure prediction can be envisaged by taking the macroscopic deformation behaviour of polystyrene as an example. Already in the apparent elastic region crack-like defects, so-called *crazes* appear at the surface of a tensile bar under loading. The faces of these crazes are bridged by fibrillar material which provides the crazes some load bearing capacity. From the highly stretched fibrils [18, 19] it can be witnessed that on a local scale polystyrene is extremely ductile, but, due to its pronounced strain softening and weak strain hardening, the strain tends to localise in these small local zones which can not be stabilised [20].

Kramer [21] recognised that the extreme localisation is even to be considered as a prerequisite event for the initiation of the crazes. His main conclusion was that the formation of a small, localised plastic deformation zone, within a relatively undeformed matrix first leads to a build-up of triaxial stresses. Subsequently, this deformation can either be stabilised provided that the polymer network is able to transfer sufficient load, or cannot be stabilised causing the localisation to evolve to extremes meanwhile building-up dilative stresses until, at a sufficiently high dilative stress, (successive) nucleation of voids occurs. With ongoing deformation the voids coalesce into a void network and form a craze.

Resistance to void nucleation is dependent on the network density of polymers [22–24]. This partly explains the craze- and defect-sensitivity of polystyrene, that forms -due to its high chain stiffness- a low entangled network. Recently it was shown, by means of a combined experimental and numerical indentation study, that void nucleation, indeed preceded by plastic deformation, in polystyrene occurs at a critical hydrostatic stress of 40 MPa [1]. With increasing network density this critical hydrostatic stress level was found to increase.

The build-up of high dilative stresses, which ultimately leads to crazing, can be only circumvented by introducing heterogeneity into the material. For polystyrene, the incorporation of rubber particles resulted in a mechanism which is identified as *multiple crazing* [25–27]. Although this engineering method increased the material volume participating in the deformation process and, thus increased toughness, it did not lead to a transition from crazing to shear yielding and can, consequently, be considered to be only a partial solution to the problem. The ultimate toughness improvement should induce such a crazing to shear yielding transition. This can be achieved by only two routes. Either the overall stress level has to be lowered such that a critical stress level is not reached, or the thickness of the polymer ligaments in between the inclusions has to be reduced such that crazing cannot occur [28–31]. The first route proves to be not very practical, but indeed can be realised, e.g. by increasing the test temperature, by (mechanical) rejuvenating of the material, or by adding plasticisers. The latter route introduces the concept of a critical interparticle thickness [31, 32] and relies on

the explanation that an absolute length-scale in the material is met. Recently, evidence is reported concerning the existence of this absolute length-scale. A reduced glass-transition temperature, T_g , was found for thin polystyrene films [33–35], rationalised by an enhanced mobility of chains near a free surface, and nano-indentation experiments showed a decreased resistance to indentation at shallow indentation depth (100 nm) near the free surface of bulk polystyrene [36].

In the present study the deformation of heterogeneous polystyrene systems is investigated by means of finite elements simulations, employing the compressible Leonov model [9, 10]. A system of polystyrene with 20% voids is modelled as a representative volume element (RVE) [17]. During deformation, the stress and strain distribution are monitored and the critical hydrostatic stress criterion (40 MPa) for craze nucleation [1] is continuously evaluated. Since increasing the testing temperature results in an overall lowering of the stress level, the simulations are performed at various temperatures to identify a transition from crazing to shear yielding. The results of the predicted brittle-to-ductile transition are compared to the results of uniaxial tensile tests on polystyrene filled with 20% non-adhering core-shell rubbers.

Next the influence of an absolute length-scale is investigated in the simulations. The enhanced segmental mobility, held responsible for the T_g -decrease in thin polystyrene films, is modelled with a temperature gradient over a thin layer near free surfaces of the RVE. By varying the width of this gradient, the deformation of RVE with different length-scales is investigated, finally leading to an absolute length-scale dependent brittle-to-ductile transition that was earlier found in experiments.

7.2 Numerical modelling

The constitutive model, successfully used for glassy polymers, is the compressible Leonov model, extensively described in [9–11]. Validation of the model for polystyrene can be found in [20]. Finite element simulations of a representative volume element (RVE) are used here to study the effect of the intrinsic properties on the macroscopic deformation behaviour and to, locally, evaluate stresses and strains in order to obtain a failure criterion. The RVE, a 2-D representation of the micro-structure on the lowest level considered in multi-level FEM [13], is composed of a polymer matrix containing different volume fractions of randomly packed inclusions, in the simplest case consisting of spherical holes. The procedure to create such an RVE, starts with the random filling of a unit box with the desired volume percentage (20% in this case) of mono-sized spheres with diameter equal to 5% of the dimension of the unit box. Next an arbitrary cross-section through this box is meshed with plain strain 8-node quadrilateral elements (reduced integration) using MENTAT (MSC Software). The use of these quadrilateral elements proved to be necessary in the combination of the material model used with the excessive deformation inside the heterogeneous structure. At least 5 elements spanning the width of every ligament were required to obtain a fair description of the (large) deformations within the ligaments. This large number of elements required within the ligaments limited the maximum size of the RVE, thereby obstructing the representative character of the RVE (to be completely independent of the initial -random- choice of the RVE, roughly 300 inclusions should have been modelled, see [14]). The finite element mesh is composed of 7256 plane-strain 8-node quadrilateral reduced integration elements, shown in figure 7.1. To prevent rigid body movement the lower-left node is

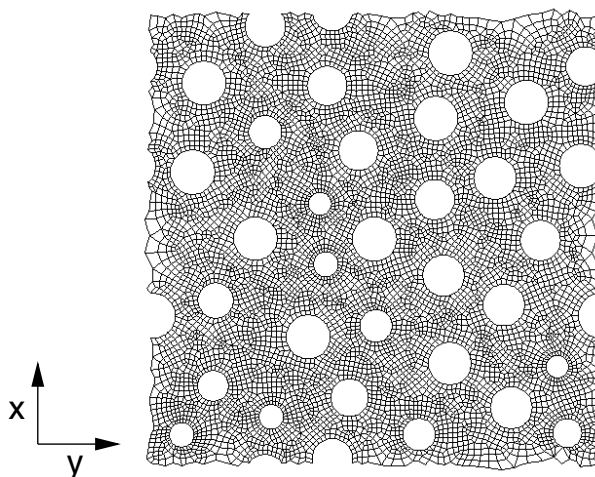


Figure 7.1: FEM mesh of an RVE for finite element simulations.

fixed in x- and y-direction, whereas the top-left node is only fixed in x-direction. Furthermore periodic boundary conditions are assumed on the edges of the RVE. These ensure that the right-hand side and top always fit to respectively the left-hand side and bottom and the RVE can be regarded as a representative part of a whole structure. Since the compressible Leonov finite element formulation [37] is available for two dimensional simulations only, plane strain conditions are assumed. In all simulations, a linear macroscopic strain-rate of 10^{-3} s^{-1} is applied in x-direction to deform the RVE. The RVE is loaded up to a macroscopic strain of 20%, since beyond this strain local re-meshing proved to be required to obtain an adequate description of the deformation of the excessively deformed ligaments.

Numerical strategy

Craze nucleation

During the simulations, the RVE is deformed at a constant linear strain rate of 10^{-3} s^{-1} , and the local stresses and strains are monitored meanwhile a hydrostatic stress-based craze-nucleation criterion is evaluated. This criterion identifies a critical hydrostatic stress of 40 MPa to be the onset of craze nucleation, provided that plastic deformation occurred in this zone [1]. For this purpose the softening parameter, D ($D > 0$ indicates plastic deformation), and the hydrostatic stress, σ_h , are monitored. When a critical level of 40 MPa is exceeded, it is assumed that a void is nucleated and that the RVE suffered from macroscopic brittle fracture. Thus the actual details of craze formation, the craze-growth process and the final local failure are not incorporated, since they all are considered to be of secondary importance only.

Incorporation of an absolute length-scale

Since the T_g -depression reported for thin, free-standing polystyrene films ($< 100 \text{ nm}$) are rationalised by an enhanced segmental mobility of the chains near a free surface [34, 35], a similar approach is used in our simulations. But instead of bringing the T_g of the material closer to ambient temperature, a temperature gradient, involving an increased temperature, in a thin layer near a free surface is introduced. The

thermally enhanced mobility, by which this is accompanied, results in a lower modulus, yield stress and strain hardening and a reduced strain softening. One could argue that the nature of the enhanced mobility in thin films is not necessarily equal to (isotropic) thermally induced segmental mobility and that its influence on modulus, yield stress and strain hardening might differ. But we will remain to the experimentally determined values at the surface of isotropic bulk polystyrene [20].

To incorporate length-scale effects, a temperature profile is generated in the RVE, prescribing a temperature equal to the glass-transition temperature (105°C) is prescribed at internal free-surfaces, i.e. void edges. In a time-dependent computation a natural temperature profile is generated. Since for thin free-standing films of less than 100 nm effects of T_g -depressions are reported [34,35], the distance over which the temperature profile is allowed to evolve is taken equal to 50 nm. This measure determines the absolute size of the RVE and the dimensions of the inclusions. From the diameter of the spheres and their volume fraction, a typical inter-particle distance can be derived which allows comparison of simulations and experiments.

The temperature profile obtained is used as thermal boundary condition in the subsequent simulations of the deformation. The evaluation of the craze-nucleation criterion is identical to that used in the isothermal simulations.

7.3 Results

BDT induced by temperature

Figure 7.2 shows the equivalent strain, ε_{eq}^* , at four different stages (macroscopic strains of 5, 10, 15 and 20%) during deformation of the RVE at 20°C (top) and 80°C (bottom). The heterogeneity of the structure first induces plastic deformation in the ligaments in between the voids which display yielding and strain softening (figure 7.2, 20°C, 5%). The pronounced strain softening at 20°C, see e.g. [20], results in a substantial load drop in the ligaments after yielding and, since the strain hardening of polystyrene is very weak, with ongoing deformation the ligaments are not able to transfer load to the surrounding material. The top row of figures illustrates the extreme localisation of strain in neighbouring ligaments (the dark colours in figure 7.2 represent the regions with the highest strain), which interconnect and form a localisation path. The excessively deformed ligaments surrounded by a hardly deformed matrix indicate that only a limited material volume participates in the deformation. Brittle fracture will occur either due to the early craze-initiation in between the voids, or by exceeding the maximum tensile strength within a ligament.

With increasing temperature, the yield stress and strain softening decrease significantly [20]. Although the force required to induce yielding in a ligament is, consequently, lower, the reduced drop in load after yielding is also low compared to the drop at 20°C, and can more easily be stabilised. The bottom row of figure 7.2, which shows the deformation at 80°C, illustrates this. At 5% of macroscopic strain the deformation is similar to that at 20°C and 5% strain. However, the strain in the ligaments is more easily stabilised and induces sequential yielding throughout the RVE. As a result a larger

*The equivalent strain is defined as the scalar norm of the logarithmic strain tensor \mathbf{E} , according to:

$$\varepsilon_{eq} = \sqrt{\frac{2}{3} \mathbf{E}^d : \mathbf{E}^d}.$$

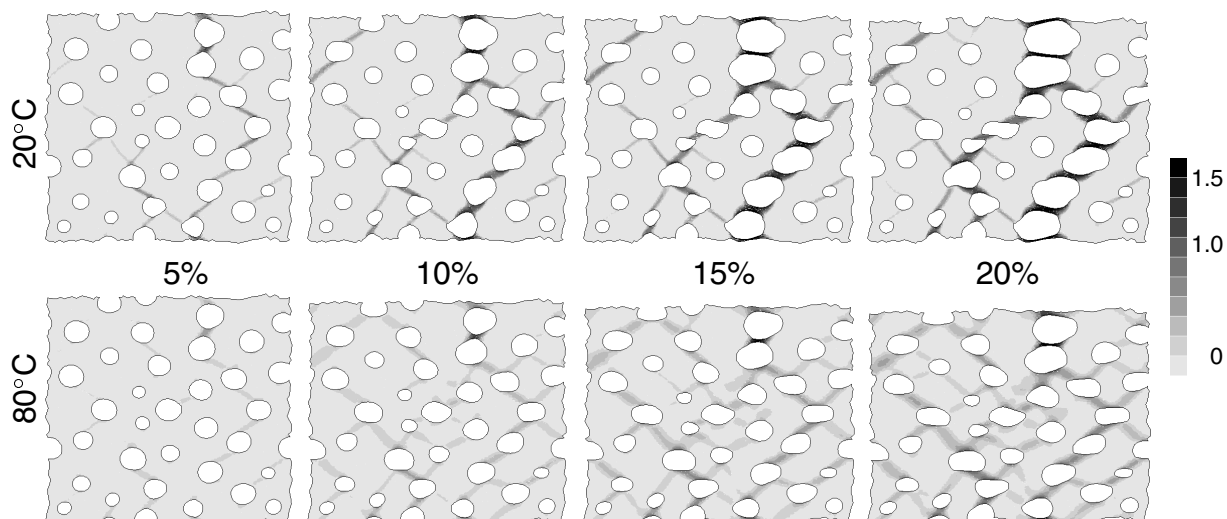


Figure 7.2: Equivalent strain, ε_{eq} , in the RVE in tension at 20 (top) and 80°C (bottom).

material volume participates in the deformation.

Figure 7.3 shows the engineering stress versus the macroscopic draw ratio of the RVE. The apparent yield stress of the RVE is of course lower than for the homogeneous material due to the incorporation of voids. Similar to the homogeneous material, both yield stress and strain softening are significantly reduced by increasing the testing temperature.

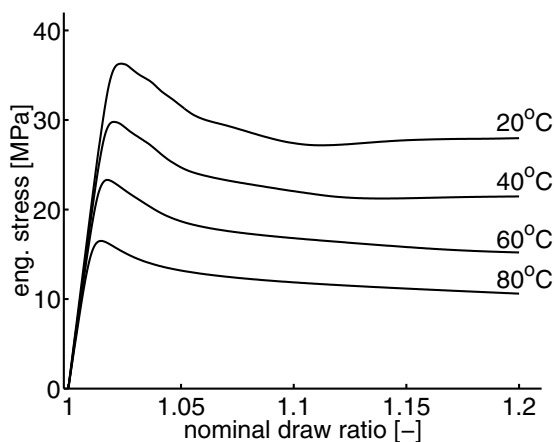


Figure 7.3: Engineering stress versus nominal draw ratio of the RVE at various temperatures.

Although localisation of strain and crazing are strongly related, this does not imply that crazing is inhibited if the strain is delocalised and that a transition from crazing to shear yielding is achieved at high temperatures. To evaluate the craze-nucleation criterion, the maximum hydrostatic stress is monitored in the plastically deformed regions. The simulations show that around the macroscopic yield point of the RVE, the hydrostatic stress reaches a maximum. Therefore in figure 7.4 the critical hydrostatic stress in the RVE is given at this stage (macroscopic strain of 2.5%). The black regions indicate the zones where a hydrostatic stress of 40 MPa is exceeded.

Until 60°C the hydrostatic stress of 40 MPa is exceeded at low strains, although the number and size of the regions where it is exceeded decreases drastically with tempera-

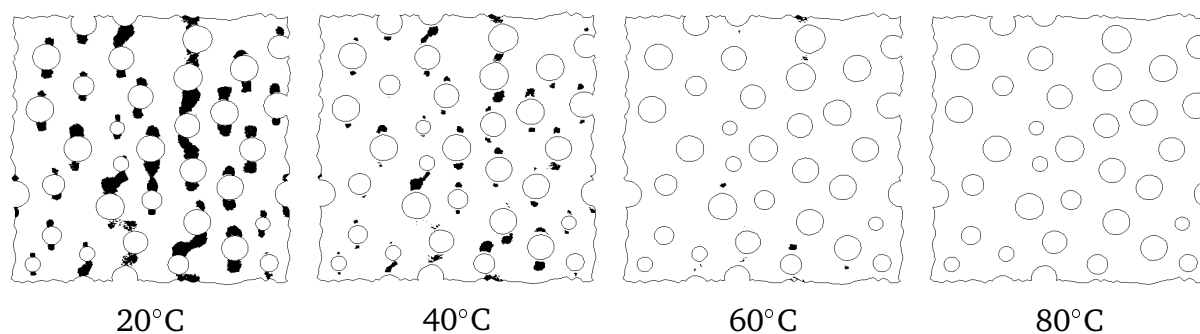


Figure 7.4: Hydrostatic stress in the RVE around the macroscopic yield point (2.5% macroscopic strain): black regions indicate the regions in which after plastic deformation a critical hydrostatic stress level of 40 MPa is exceeded.

ture. At all these temperatures the RVE is considered to suffer from macroscopic brittle fracture. For 80°C at this stage the criterion is not exceeded. To judge whether at 80°C a critical hydrostatic stress is never exceeded, the development of this stress during deformation is studied in more detail. Figure 7.5 shows the maximum hydrostatic stress as function of macroscopic draw ratio for various temperatures.

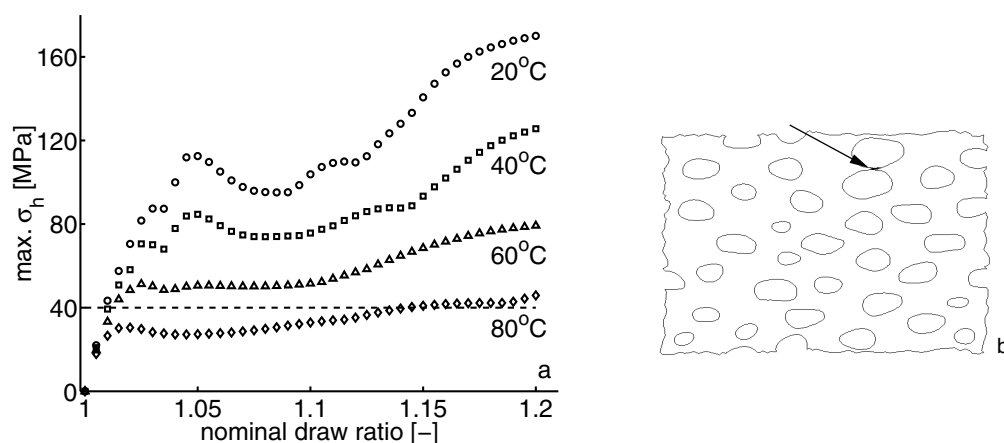


Figure 7.5: Developing hydrostatic stress in RVE at various temperatures (a), and hydrostatic stress exceeded at highly deformed ligament, indicated by the arrow, at 80°C.

The dotted line indicates the critical hydrostatic stress level of 40 MPa, the onset of voids nucleation. At 20°C, this level is already exceeded at 1% macroscopic strain. Although the maximum hydrostatic stress levels decrease when the temperature is increased, at 40 and 60°C the critical hydrostatic stress is still exceeded at a few percent of macroscopic strain. At 80°C the maximum in σ_h remains under the critical stress level until far beyond the macroscopic yield point of the RVE and at 15% macroscopic strain a critical level is reached in one ligament only (see figure 7.5b). This ligament is cold-drawn up to strains exceeding 150% and hence will not very likely exhibit crazing anymore, similar to pre-oriented polystyrene [38]. Therefore, the conclusion is justified that at 80°C no crazing is observed and hence ductile deformation behaviour is obtained in voided polystyrene with 20% voids.

To refine the temperature where the transition from crazing to shear yielding occurs, additional simulations were performed at 70 and 75°C: at 70°C the critical hydrostatic stress is reached at a few percent strain, whereas at 75°C this occurs only at 10% macro-

scopic strain, in a ligament where the local strain exceeds 100%. Similar to the simulation at 80°C, polystyrene will not likely craze anymore at 75°C. From these simulations it can be concluded that in between 70 and 75°C, crazing is inhibited during deformation and hence a temperature induced brittle-to-ductile transition is achieved for a heterogeneous polystyrene structure with 20% voids.

Since it was shown that yield stress and strain softening are key parameters in the developing level of hydrostatic stress, it is reasonable to assume that this BDT temperature is sensitive to the thermal history of the polymer and the strain rate of the test.

To validate the simulations, experiments were performed on polystyrene (PS N5000, Shell) filled with 20% core-shell rubbers (Kane Ace B511, 200 nm, Kaneka), which was mixed on a 25 mm Werner and Pfleiderer co-rotating twin-screw extruder, ZSK 25, at a temperature of 160°C and a rotation speed of 152 rpm. The material flux was optimised for the highest torque in order to achieve proper particle dispersion. Next the blend was injection moulded into tensile bars, according to ISO 527. Before compounding, the materials were dried in a vacuum-oven for 5 days. As was shown by TEM, in a study on a similar blends, compounded in a identical way, good dispersion of the core-shell rubbers is achieved under these processing conditions [28].

The injection moulded tensile bars were subjected to uniaxial tensile tests at conditions identical to those used in the simulations (temperatures ranging from 20-100°C and a strain rate of 10^{-3} s^{-1}). Figure 7.6a shows the engineering stress versus the nominal draw ratio during a tensile test at 80°C in both, experiments (circles) and simulations (solid line). They compare rather well. This suggest that the core-shell rubbers are non-adhering and that they hardly participate in the deformation process. Representing them as voids seems to be a valid assumption. The small discrepancies in yield stress can be rationalised by the difference in thermal history of the injection moulded tensile bars and compression moulded samples used for the characterisation of the material parameters of the model [20].

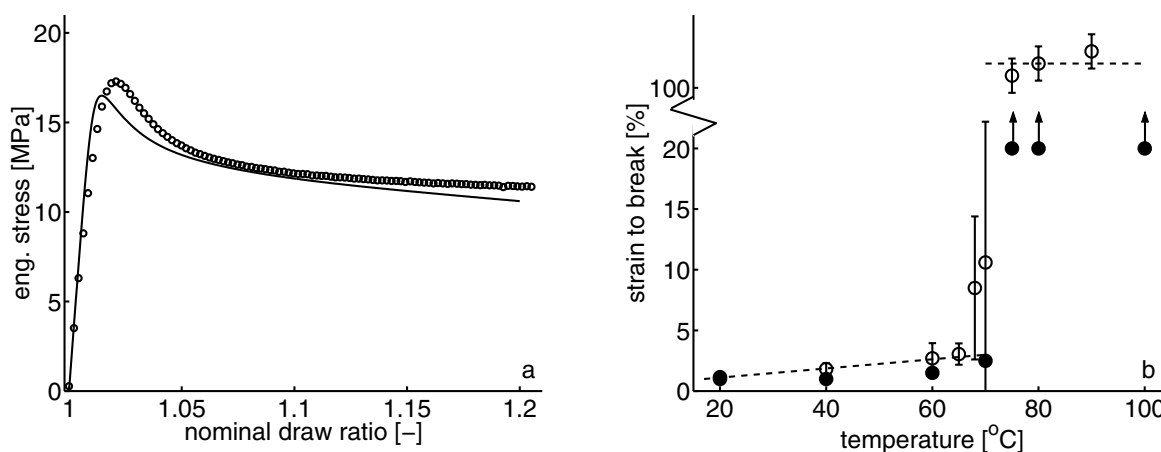


Figure 7.6: Stress/strain curves at 80°C (a), experiment (circles) and simulation (solid line), and temperature induced BDT (b), experiments (open circles) and simulations (filled circles). Arrows indicate that the simulations were stopped before failure was encountered.

Figure 7.6 shows that the experiments confirm the observations in the simulations: at a temperature of around 70-75°C a sharp transition from brittle-to-ductile is observed. The open circles with error-bars represent the macroscopic strains reached in the uni-

axial tensile tests, which were around 100%, whereas the simulations were stopped at 20% macroscopic strain because of the necessity of remeshing within the ligaments. The arrows indicate that by remeshing also in the simulations larger strains could have been reached. The small discrepancies in strain at break in the region of 60 to 70°C can be explained by the fact that in the simulations brittle fracture is assumed to occur at the first moment a critical hydrostatic stress of 40 MPa is exceeded, whereas experimentally failure at more sites is required for macroscopic failure. Hence the strain at break in brittle failure is always underestimated in the simulations. The macroscopic ductile fracture which occurs at high strains (above 70°C) in the experiments is the result of sequential failure of the polymer ligaments when their tensile strength is exceeded.

BDT induced by length-scale effects

The presence of an absolute length-scale in amorphous polymer is modelled by a temperature gradient over a thin layer near a free surface. In figure 7.7 the temperature profiles are given at various moments in time during the simulation. The grey value-bar on the right-hand side of the figure indicates that the temperature on the free surface (dark colour) is equal to the bulk glass-transition (T_g , 105°C), whereas in the bulk the temperature remains equal to the ambient temperature (T_a , 20°C).

In figure 7.7a the increase in temperature has evolved to approximately one third of the diameter of the sphere. Assuming that the influence of the free surfaces around the voids runs 50 nm deep, this RVE represents a polystyrene matrix with 20% inclusions of 150 nm diameter. Following this procedure, the size of the inclusions of figure 7.7b-d are estimated to be 80 nm, 40 nm, and 20 nm.

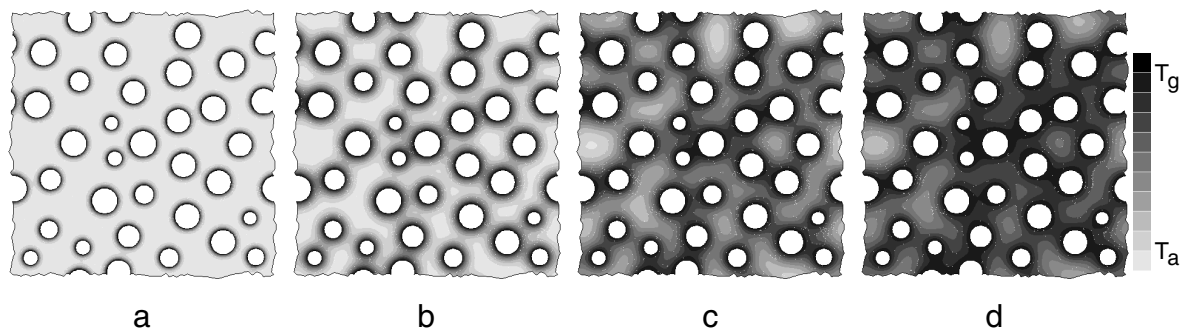


Figure 7.7: Temperature at various stages in the thermal simulation, representing voided polystyrene with voids of 150, 80, 40, and 20 nm respectively.

The in their developments interrupted, and fixed temperature distributions are used as boundary conditions for the coupled simulation, where the deformation is determined. In figure 7.8 the results are given for the deformation of an RVE in which the absolute length scale has no influence (diameter voids equals 1 μm , top) and one where it has (40 nm inclusions, bottom). For the large voids, the deformation equals that of the simulation as presented before at a temperature of 20°C, see figure 7.2: a strong localisation of strain in the thin ligaments in between the voids. For the 40 nm inclusions, figure 7.8 (bottom), the temperature gradient results in a reduction in yield stress and strain softening in a thin layer around the inclusions. This leads to a slightly less localised deformation although strain still tends to localised within a few ligaments.

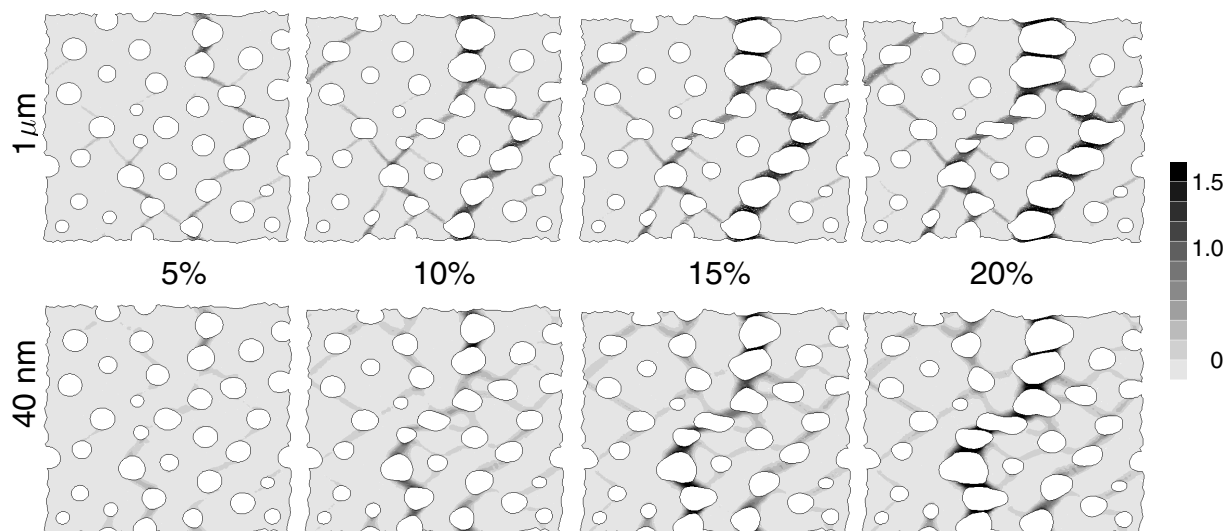


Figure 7.8: Equivalent strain, ε_{eq} , in the RVE in tension at for inclusions of $1 \mu\text{m}$ (top) and 40 nm (bottom)

The stress strain curves for the RVE with different sizes of inclusions, given in figure 7.9, show that, with decreasing inclusion size and hence decreasing ligament thickness in between the particles, the yield stress and the strain softening of the RVE strongly decrease.

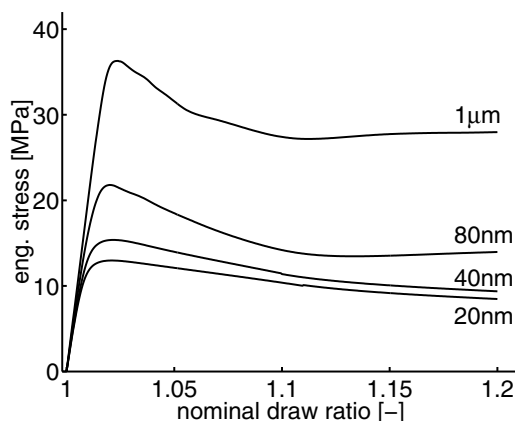


Figure 7.9: Engineering stress versus nominal draw ratio for voided PS (20% voids) and inclusion sizes of $1 \mu\text{m}$, 80 nm , 40 nm and 20 nm .

To evaluate whether these materials exhibit crazing, the hydrostatic stress has to be evaluated again during the simulations. In figure 7.10 the maximum hydrostatic stress is presented as function of the macroscopic draw ratio of the RVE for 4 different sizes of inclusions. For the larger spheres, $1 \mu\text{m}$ and 80 nm the critical hydrostatic stress is already exceeded at a macroscopic strain of 1-2%. For the 40 nm spheres, the hydrostatic stress remains under a critical value far beyond the macroscopic yield point of the RVE. At macroscopic strains of 10% a critical stress level is reached somewhere within a strongly deformed ligament. Since the local strain in this ligament exceeds 100%, is not likely to craze anymore and therefore it seems reasonable to assume that at these small inclusion-sizes crazing is inhibited and shear yielding occurs throughout the specimen. Again the macroscopic strain is limited to 20% for computational reasons.

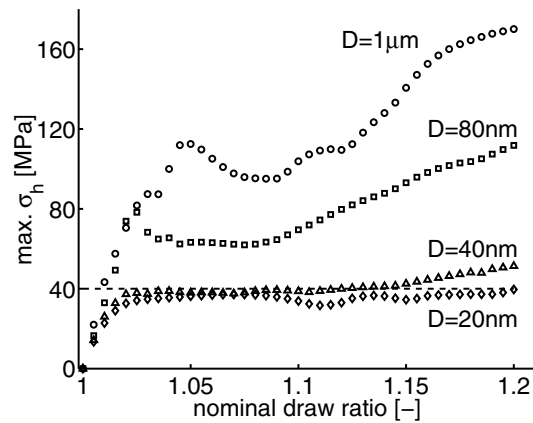


Figure 7.10: The developing maximum hydrostatic stress versus nominal draw ratio in the plastically deformed zones of the RVE for various void-sizes.

All simulations are summarised in figure 7.11 where the strain at break is represented as function of the interparticle distance (ID), which can be derived from the expression [31]:

$$ID = D \left[\left(\frac{\alpha \pi}{6V_f} \right)^{\frac{1}{3}} - 1 \right]$$

where D is the diameter and V_f the volume fraction of the inclusions. In this equation α accounts for the stacking of the rubber spheres within the matrix. Wu [31] showed that for nylon-rubber blends the packing resembles a simple cubic lattice for the lower volume fractions ($V_f < 40\%$), and α equals 1.

At larger void sizes and thus large ID s crazing is observed in the numerical simulations and only at a void diameter smaller than 40 nm crazing is inhibited. Since the volume fraction of the inclusions equals 20%, at a ID of approximately 15 nm, a sharp increase in strain to break is observed, indicating that a transition from crazing to shear yielding is achieved. The arrows once again indicate that the simulations were stopped for numerical reasons before failure occurred.

Experimental results provided by Van der Sanden [28] and Jansen [30], showed that a BDT occurs in non-adhering core-shell rubber filled polystyrene at 55 vol.% inclusions of 200 nm and 35 vol.% inclusions of 80 nm, respectively. In Jansen's example a critical inter-particle distance of 11.5 nm is found. Van der Sanden argued that high volume fractions of rubber particles result in a face-centered cubic stacking (FCC) and that α is equal to 2. The associated critical interparticle distance equals, therefore, 15 nm. These values compare well with the value found from the simulations.

The simulation which are presented here indicate the mobility of the polymer ligaments within the blends is strongly enhanced by increasing the amount of internal free surfaces.

7.4 Discussion and conclusions

In this paper numerical simulations of the deformation of voided polystyrene were performed to investigate the capability of finite element simulations, employing the compressible Leonov model, to predict brittle-to-ductile transitions in polystyrene.

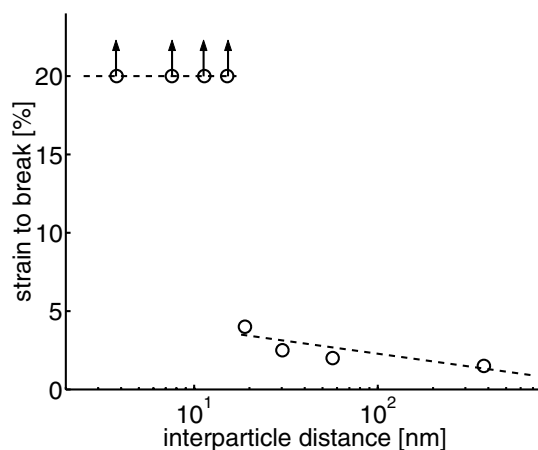


Figure 7.11: Brittle-to-ductile transition induced by an absolute length-scale: ductile deformation behaviour at $ID < 15$ nm, arrows indicate the simulations were stopped before failure occurred.

In previous studies [20, 39], it was shown that the post-yield behaviour plays a crucial role in the deformation of glassy polymers. Improvements must be focused on avoiding severe localisation of strain by eliminating strain softening and enhancing the strain hardening contribution of the polymer network. However, besides strain localisation, crazing will occur, which involves void nucleation in local plastically deformed zones under dilative stresses. Therefore, the control of build-up of hydrostatic stresses is important as well.

It is generally accepted that only by creating a heterogeneous structure, the hydrostatic stresses can be relieved and toughness improved. In rubber-modified polystyrene (HIPS) improved properties can be attributed to a deformation mechanism of multiple crazing and not to a transition from crazing to shear yielding. Consequently room for further improvement remains.

Finite element simulations of voided polystyrene were performed at a strain rate of 10^{-3} s^{-1} at various temperatures. During the simulations a craze-nucleation criterion (a critical hydrostatic stress of 40 MPa, preceded by plastic deformation) was evaluated to determine whether crazing would occur. It was demonstrated that a brittle-to-ductile transition can be achieved by increasing the testing temperature to around 75°C . At this temperature the critical hydrostatic stress is not exceeded. The results of the numerical simulations are in good agreement with the experimental results, using tensile tests on filled polystyrene (20% non-adhering core-shell rubber of 200 nm), which exhibited a brittle-to-ductile transition at a temperature around 70°C .

Reducing the ligament thickness in the voided structure is another, from application point of view far more interesting, route to achieve a brittle-to-ductile transition. The absolute length-scale encountered here is deduced from the measured T_g depression in thin, free standing polystyrene films, and attributed to an enhanced mobility of polymer chains near a free surface. The enhanced mobility was accounted for in the simulations by assuming a temperature gradient from the free surface into the bulk. The depth of this temperature gradient determines the absolute length-scale of the material. The simulations demonstrate that, by decreasing the absolute length-scale exceeding of the critical hydrostatic stress level can be avoided and a transition from crazing to shear yielding can be achieved. At 20% voids of 40 nm diameter, representing an interparticle

distance of approximately 15 nm, a brittle-to-ductile transition is observed, which correlates well with experimental observations of highly filled polystyrene/non-adhering rubber blends [28, 30]. The approach followed here implies that the critical interparticle distance is dependent on both temperature and strain rate.

The simulation which are presented in the last section indicate the mobility of the polymer ligaments within the blends is strongly enhanced by increasing the amount of internal free surfaces. As is shown in figure 7.9 this leads to a significant drop in modulus and yield stress and has a similar effect on the mechanical properties as the application plasticisers. For an engineering material, however, a less pronounced decrease in modulus and yield stress would be desirable.

Although at smaller inter-particle distances the maximum hydrostatic stress is sufficiently reduced to inhibit crazing, the localisation of strain within the ligaments is still quite severe, see figure 7.8 (bottom). The incorporation of *precavitated*, adhering core-shell rubbers, as proposed by [17, 30], could support these ligaments during deformation to transfer more load. As a result they would be able to induce sequential yielding throughout the RVE, increase the material volume participating in the deformation and hence further improve the toughness.

Acknowledgements

The authors wish to acknowledge Jules Kierkels for the experimental work and the financial support provided by the Dutch Technology Foundation (STW) (Grant EWT.3766).

References

- [1] van Melick, H.G.H., Bressers, O.F.T.J., den Toonder, J.M.J., Govaert, L.E., Meijer, H.E.H., Craze-initiation in glassy polymers: influence of strain rate, thermal history and network density, *Polymer*, submitted
- [2] Haward, R.N. and Thackray, G., *Proc. Roy. Soc. London A*, **302**, 453 (1967)
- [3] Boyce, M.C., Parks, D.M., Argon, A.S., *Mech. Mat.*, **7**, 15 (1988)
- [4] Hasan, O.A., Boyce, M.C., Li, X.S., Berko, S., *J. Pol. Sci., Part B: Pol. Phys.*, **31**, 185 (1993)
- [5] Arruda, E.M. and Boyce, M.C., *Int. J. Plast.*, **9**, 697 (1993)
- [6] Boyce, M.C., Arruda, E.M., Jayachandran, R., *Pol. Eng. Sci.*, **34**, 716 (1994)
- [7] Wu, P.D. and van der Giessen, E., *J. Mech. Phys. Solids*, **41**, 427 (1993)
- [8] Wu, P.D. and van der Giessen, E., *Int. J. Plast.*, **11**, 211 (1995)
- [9] Govaert, L.E., Timmermans, P.H.M., Brekelmans, W.A.M., *J. Eng. Mat. Tech.*, **122**, 177 (2000)
- [10] Tervoort, T.A., Smit, R.J.M., Brekelmans, W.A.M., Govaert, L.E., *Mech. Time-depend. Mat.*, **1**, 269 (1998)
- [11] Tervoort, T.A. and Govaert, L.E., *J. Rheol.*, **4**, 1263 (2000)
- [12] Tervoort, T.A., Klompen, E.T.J., Govaert, L.E., *J. Rheol.*, **40**, 779 (1996)
- [13] Smit, R.J.M., Brekelmans, W.A.M., Meijer, H.E.H., *Comp. Meth. Appl. Mech. Eng.*, **155**, 181 (1998)

- [14] Smit, R.J.M., Brekelmans, W.A.M., Meijer, H.E.H., *J. Mech. Phys. Sol.*, **47**, 201 (1999)
- [15] Smit, R.J.M., Brekelmans, W.A.M., Meijer, H.E.H., *J. Mat. Sci.*, **35**, 2855 (2000)
- [16] Smit, R.J.M., Brekelmans, W.A.M., Meijer, H.E.H., *J. Mat. Sci.*, **35**, 2869 (2000)
- [17] Smit, R.J.M., Brekelmans, W.A.M., Meijer, H.E.H., *J. Mat. Sci.*, **35**, 2881 (2000)
- [18] Donald, A.M.; Kramer, E.J., *Polymer*, **23**, 451 (1982)
- [19] Donald, A.M.; Kramer, E.J., *J. Pol. Sci., Pol. Phys. Ed.*, **20**, 1129 (1982)
- [20] van Melick, H.G.H., Govaert, L.E., Meijer, H.E.H., Localisation phenomena in glassy polymers: influence of thermal and mechanical history, *Polymer*, submitted.
- [21] Kramer, E.J., In: H.H. Kausch, Ed., *Adv. Pol. Sci.*, Springer-Verlag, Berlin, **52/53**, 1-56 (1983)
- [22] Kramer, E.J. and Berger, L.L., In: H.H. Kausch, Ed., *Adv. Pol. Sci.*, Springer-Verlag, Berlin, **91/92**, 1-68 (1990)
- [23] Donald, A.M.; Kramer, E.J., *J. Mat. Sci.*, **17**, 1871 (1982)
- [24] Wu, S., *Pol. Eng. Sci.*, **30**, 753 (1990)
- [25] Bucknall, C.B., In: R.N. Haward and R.J. Young, Eds., *The Physics of Glassy Polymers*, 2nd ed., Chapman & Hall, London, 363-412 (1997)
- [26] Bucknall, C.B. and Smith, R.R., *Polymer*, **6**, 437 (1965)
- [27] Donald, A.M.; Kramer, E.J., *J. Mat. Sci.*, **17**, 2351 (1982)
- [28] van der Sanden, M.C.M., de Kok, J.M.M., and Meijer, H.E.H., *Polymer*, **35**, 2995 (1994)
- [29] Magalhaes, A.M.L., and Borggreve, R.J.M., *Macromolecules*, **28**, 5841 (1995)
- [30] Jansen, B.J.P., Rastogi, S., Meijer, H.E.H., and Lemstra, P.J., *Macromolecules*, **34**, 3998 (2001)
- [31] Wu, S., *J. Appl. Pol. Sci.*, **35**, 549 (1988)
- [32] van der Sanden, M.C.M., Meijer, H.E.H., Lemstra, P.J., *Polymer*, **34**, 2148 (1993)
- [33] Keddie, J.L., Jones, R.A.L., and Cory, R.A., *Europhys. Lett.*, **27**, 59 (1994)
- [34] Forrest, J.A., and Mattsson, J., *Phys. Rev. E.*, **61**, R53 (2000)
- [35] Forrest, J.A., and Jones, R.A.L., In: A. Karim and S. Kumar Eds., *Polymer Surfaces, Interfaces, and Thin Films*, World Scientific Publishing, Singapore, 251-294 (2000)
- [36] van Melick, H.G.H., van Dijken, A.R., den Toonder, J.M.J., Govaert, L.E., Meijer, H.E.H., *Phil. Mag. A*, accepted
- [37] van der Aa, M.A.H., Schreurs, P.J.G., Baaijens, F.P.T., *Mech. of Mat.*, **33**, 555 (2001)
- [38] Ender, D.H. and Andrews, R.D., *Pol. Lett.*, **36**, 3057 (1965)
- [39] Meijer H.E.H., Govaert L.E., Smit R.J.M., A Multi-Level Finite Element Method for Modelling Rubber-Toughened Amorphous Polymers, In: R. Pearson, Ed., *Toughening of Plastics*, American Chemical Society, Boston, 50-70 (1999)

Chapter 8

Main conclusions

In this thesis the deformation and failure behaviour of glassy polymers is studied. The macroscopic response of this class of polymers is dominated by their intrinsic post-yield behaviour, i.e. strain softening and strain hardening. As was shown in chapter 2 the strain hardening modulus of glassy polymer proves to be proportional to the network density of the polymer irrespective of the nature of the network, physical entanglements or chemical cross-links. The large discrepancy between the strain hardening modulus and the rubber plateau modulus and the decreasing trend of the strain hardening modulus with temperature indicates that the strain hardening response differs from a purely rubber-elastic response. The fact that the increase of network density by cross-linking results in a proportional increase in strain hardening modulus suggests that the scale of cooperative motion after yielding is in the same order as the entanglement length and interferes with the concept of cohesive entanglements. It is discussed that the time-scale of the stress-induced segmental motion during deformation might be equal to the time-scale of the experiment, similar to the material being right at the glass-transition temperature. Since secondary interactions still play a significant role on this time-scale, this results in a higher strain hardening modulus. With increasing temperature the enhanced thermal mobility lowers this contribution and accounts for the negative temperature dependence.

In chapter 3 the transient deformation behaviour of mechanically rejuvenated polystyrene is investigated. The yield stress and strain softening recover on a time scale of days independent of molecular weight whereas the time-scale of re-embrittlement proves to be dependent on molecular weight. The molecular weight determines the tensile strength and hence the maximum load which can be transferred in a localised plastic zone. Since the recovered yield stress at which this strength is exceeded is different for the grades this provides an explanation for the different time-scales observed. The mechanically rejuvenated state can not be regarded as an ultimately quenched state, since the creep response of both materials proves to be quite different. The density of the mechanical rejuvenated material increased upon rejuvenation while strain softening was

eliminated. Since concept of free volume, in the (naive) definition of being directly related to the macroscopic density, is unable to account for this and other experimental observations another possible explanation for the physical origin of strain softening was discussed.

In chapter 4 the influence of the post-yield behaviour on the macroscopic deformation is demonstrated. Polycarbonate, with a moderate strain softening and strong strain hardening displays stable neck-growth during deformation. Increasing strain softening by an annealing treatment leads to more severe localisation of strain and even brittle fracture. The deformation modes can be analysed using a straight-forward stability analysis. It is shown that deformation of polystyrene with its pronounced strain softening and weak strain hardening results in extreme localisation of strain and generally brittle failure. Elimination of strain softening by mechanical rejuvenation results in a strongly enhanced ductility.

For the numerical prediction of crazing and brittle failure a failure criterion is required. In chapter 5 a hydrostatic stress-based void nucleation criterion is identified by a combination of micro-indentation experiments and numerical simulations. For polystyrene, a critical hydrostatic stress of 40 MPa proved to be the onset of void nucleation in a locally deformed plastic zone. This criterion was validated and proved to be independent of thermal history and strain rate. The value of the critical hydrostatic stress increased with increasing network density.

In several fields of polymer science an absolute length-scale is encountered experimentally. By means of micro- and nano-indentation experiments on various scales the force-displacements curves of polystyrene were recorded. Comparison with length-scale independent finite element simulations, using bulk properties, showed that for large indentation depth the simulation and experiments correlate well. At shallow indentation depths (100 nm) with a small indenter (2.2 μm) the resistance to indentation has decreased, suggesting that the mechanical properties near a free surface are indeed different from the bulk properties.

To conclude brittle-to-ductile transitions for polystyrene are predicted in chapter 7. An representative volume element (RVE) is deformed, while the craze initiation criterion identified in chapter 5 is evaluated. It is shown that by increasing the overall temperature a lowered stress level results and a transition from crazing to shear yielding is found at 70°C. Finally simulations are performed in which an absolute length-scale is incorporated, using the results of chapter 6. Below a interparticle distance of ca. 15 nm a brittle-to-ductile transition is observed. Both BDTs correlate well with experimental observations. These simulation show that a voided structure of small inclusions (20% voids, smaller than 40 nm) results in a lowered overall stress level (i.e. inhibiting crazing), but the localisation of strain within the ligaments is still quite severe. Delocalisation of strain could be achieved by applying adhering pre-cavitated core-shell rubbers which inhibit the build-up a hydrostatic stress and support the deforming ligaments to transfer more load and induce sequential yielding.

Samenvatting

Vooraf door hun makkelijke verwerkbaarheid en redelijke eigenschappen worden polymeren veelvuldig toegepast ook in structurele toepassingen. Het vooraf kunnen voorspellen, veelal met behulp van numerieke simulaties, van hun gedrag onder belasting is daarom belangrijk. In de laatste 20 jaar is dan ook veel werk geïnvesteerd in het ontwikkelen van numerieke methoden die, met name, het gedrag van glasachtige polymeren bij hoge rekken (*post-yield* gedrag) goed kunnen beschrijven. Het compressible Leonov model, ontwikkeld in onze groep, is goed in staat gebleken het intrinsieke gedrag, zoals reksnelheids- en temperatuursafhankelijke vloeï, strain softening en strain hardening, goed te beschrijven. Een faalcriterium, waarmee onderscheid tussen bros en taai gedrag gemaakt kan worden ontbreekt echter nog.

Uit eerdere studies is gebleken dat het macroscopisch deformatiegedrag wordt bepaald door het intrinsieke *post-yield* gedrag. Bijvoorbeeld het brose gedrag van polystyreen is het gevolg van de extreme rek-lokalisatie, geïnduceerd door de enorme strain softening en het gebrek aan strain hardening. Ductiliteitsverbetering zou daarom gericht moeten zijn op het reduceren of verwijderen van de strain softening en het versterken van de bijdrage van de strain-hardening. Hiervoor is kennis over wat zich afspeelt op moleculair niveau onontbeerlijk. Het is algemeen geaccepteerd dat de strain-hardening wordt bepaald door het fysische netwerk van de polymere ketens. Het grote verschil tussen de strain-hardeningsmodulus en de rubber-plateaumodulus en de sterk dalende modulus met toenemende temperatuur vraag echter om meer onderzoek. Over de fysische achtergrond van strain softening is veel minder bekend. Uit de literatuur blijkt wel dat het sterk gerelateerd is aan fysische veroudering, beïnvloed kan worden met warmtebehandelingen en na mechanische verjonging zelfs verdwenen is.

Een verminderde strain softening en versterkte strain hardening zijn echter geen garantie voor taai gedrag. Door een beperkte weerstand tegen cavitatie en de opbouw van hoge hydrostatische spanningen onder bepaalde belastingssituaties, b.v. onder een kerf, bezwijkt zelfs polycarbonaat aan *crazing* en heeft het een lage slagvastheid. Om een materiaal echt slagvast te maken moet de opbouw van deze hydrostatische spanningen voorkomen worden door het introduceren van een heterogene structuur, b.v. door het inmengen van rubberbolletjes. Hierdoor vindt er geen *crazing* meer plaats en resteert slecht *shear yielding* in materialen zoals polycarbonaat en polyamide en neemt hun slagvastheid sterk toe. Voor polystyreen neemt de slagvastheid ook iets toe omdat er meer crazes (*multiple crazing*) worden gevormd en dus een groter volume deformeert. Een

echte overgang van crazing naar shear yielding wordt echter pas bereikt als de polymereligaanten tussen de rubberbolletjes dunner zijn dan een bepaalde kritische dikte. Dit concept van een kritische dikte duidt erop dat de absolute lengteschaal van het materiaal een rol speelt. De in de literatuur gevonden verlaging van de glasovergangstemperatuur in dunne polystyreen films, die ook duidt op de aanwezigheid van een absolute lengteschaal, heeft dezelfde orde van grootte.

In de 6 artikelen waaruit dit proefschrift bestaat worden een aantal vragen en problemen zoals hierboven geschetst belicht en uitgediept. Om te beginnen is de relatie tussen de strain-hardeningsmodulus en de dichtheid van het polymere netwerk onderzocht. Het blijkt dat een toename van de netwerkdichtheid voor polystyreen, wat bereikt kan worden door cross-linken of blenden met polyphenyleen oxide (PPO), resulteert in een proportionele toename van de strain-hardeningsmodulus. In de hieropvolgende discussie wordt een mogelijke verklaring gegeven voor de grote afwijking tussen de strain-hardeningsmodulus en de rubber-plateaumodulus en voor de sterk dalende trend van deze modulus met toenemende temperatuur.

Zoals bekend kan door mechanische verjonging de strain-softening in polystyreen (tijdelijk) verwijderd worden, hetgeen resulteert in taai gedrag in trek. Het is gebleken dat het herstel van de vloeispanning en de strain-softening in de tijd een proces is dat onafhankelijk is van het molecuulgewicht. Door de toename van de treksterkte met het molecuulgewicht is de maximale spanning die door het polymeer kan worden gedragen wel afhankelijk van het molecuulgewicht. Daarom kan voor een polymeer met een relatief hoog molecuulgewicht de zich herstellende vloeispanning langer gedragen worden en zal het dus langer duren voor er weer brosse breuk optreedt. Kruipmetingen laten zien dat de toestand van mechanische verjonging anders is dan die van thermische verjonging. In de discussie zijn resultaten vergeleken met bestaande literatuur en wordt een mogelijke achtergrond van strain softening bediscussieerd.

Het intrinsieke post-yield gedrag, strain-softening en strain-hardening bepalen het macroscopisch deformatiegedrag van glasachtige polymeren. De lage strain softening en sterke strain hardening van polycarbonaat zorgen ervoor dat een trekproef een stabiele nek wordt gevormd. Wordt echter door een warmtebehandeling de vloeispanning en strain-softening verhoogd, dan heeft dit sterkere rek-lokalisatie tot gevolg en kan zelfs leiden tot brosse breuk in een laag-moleculaire polycarbonaat. De wijze van deformeren kan goed voorspeld worden met behulp van een nek-stabiliteitsanalyse. De hoge strain-softening en bijna ontbrekende strain-hardening heeft een extreme rek-lokalisatie tot gevolg voor polystyreen. Echter door mechanische verjonging kan de strain softening tijdelijk verwijderd worden, hetgeen in een trekproef vervolgens leidt tot een verhoogde ductiliteit.

Met numerieke simulaties gebruikmakend van het compressibel Leonov model kan het deformatiegedrag en rek-lokalisatie uitstekend beschreven worden. Door het ontbreken van een faalcriterium kan echter niet voorspeld worden of er taai of brosse breuk zal optreden. Door middel van micro-indentatie kunnen experimenteel op een reproduceerbare wijze crazes worden geïnitieerd in polystyreen. Met de eerder genoemde numerieke simulaties kan vervolgens lokaal de spanningstoestand geanalyseerd worden. Deze combinatie heeft geleid tot de identificatie van een craze-initiatie criterium. Bij een kritische hydrostatische spanning van 40 MPa, onder de voorwaarde dat dit wordt voorafgegaan door plastische deformatie, vindt cavitatie en holte-vorming plaats. Verdere validatie van dit criterium toont aan dat het onafhankelijk is van de thermische

geschiedenis en reksnelheid maar toeneemt met de netwerkdichtheid.

De aanwezigheid van een absolute lengteschaal is onderzocht door middel van indentatie. In micro- en nano-indentatie experimenten is op verschillende schalen de kracht-verplaatsingscurve en dus de weerstand tegen indentatie gemeten. Uit vergelijking met numerieke simulaties, waarin de lengteschaal geen rol speelt, blijkt dat voor grote indenters en grote indringdieptes de experimenten en simulaties met de bulk eigenschappen, goed overeenkomen. Voor de kleinste indenter ($2.2 \mu\text{m}$) en kleine indringdieptes (100 nm) is de weerstand tegen indentatie echter veel lager dan voorspeld in de simulatie. Dit duidt erop dat in een dunne laag aan een vrij oppervlak de mechanische eigenschappen anders kunnen zijn dan de bulkeigenschappen.

In het afsluitende hoofdstuk worden de numerieke simulaties gebruikt om bros-taai overgangen te voorspellen voor een representatief volume element (RVE) van polystyreen matrix met gaten. Hierbij wordt gebruikt gemaakt van het eerder bepaalde craze-initiatie criterium uit hoofdstuk 5. Een verhoging van de temperatuur leidt tot een dusdanige verlaging van het spanningniveau binnen het RVE dat bij een temperatuur van 70°C de kritische hydrostatische spanning niet meer wordt gehaald en dus een overgang van crazing naar shear-yielding is bereikt. Ook is getracht de invloed van een absolute lengteschaal mee te nemen in deze simulaties, gebruikmakend van de resultaten van hoofdstuk 6. Door een temperatuursgradient in de buurt van een vrij oppervlak aan te nemen wordt lokaal verhoging van segmentele mobiliteit bereikt. Dit leidt lokaal weer tot een verlaging van de vloeispanning en strain-softening. Het blijkt dat beneden een kritische ligamentdikte van ongeveer 15 nm polystyreen tussen de gaten geen crazing meer plaatsvindt en dus een bros-taai overgang is bereikt. Beide bros-taai overgangen komen goed overeen met experimentele observaties.

Dankwoord

Na 4,5 jaar werken, met dit boekje als doel, realiseer je je dat er in de loop van de tijd vele mensen zijn geweest die in meer of mindere mate, bewust of onbewust, een bijdrage hebben geleverd aan dit proefschrift. Allereerst wil ik natuurlijk Han Meijer en Leon Govaert bedanken voor hun begeleiding, de mogelijkheden die ze hebben geschept en de basis die ze hebben gelegd om dit werk te kunnen doen in een zeer goed uitgerust lab. Het nimmer aflatende enthousiasme van Leon was zeer inspirerend en geeft je vertrouwen in je werk; het zou tot de standaard uitrusting van een coach moeten behoren. De bijeenkomsten en discussies van het 'slagvastheidsclubje', en in latere fase, de discussies met Theo Tervoort heb ik ook zeer gewaardeerd.

Ik ben blij dat ik een gedeelte van dit werk heb kunnen doen in de 'industriële' omgeving van het Philips Natlab. Maarten Buijs bedankt voor het creëren van de gelegenheid, Jaap den Toonder, Auke van Dijken, Amar Mavinkurve en Dirk Brokken bedankt voor de (praktische) ondersteuning en de nodige discussie. Het spelen in Natlabvoetbalcompetitie en het behalen van het kampioenschap bracht daarbij ook nog de nodige ontspanning.

In dit werk zitten natuurlijk ook de nodige (on)zichtbare bijdragen van stagiaires en afstudeerders. Daarom gaat mijn dank ook uit naar He Li, David Carter, Nasser Ayoub, Christel Dona, Mark Neele, Bas Raas en, last but not least, Olaf Bressers voor z'n mooie werk bij Philips.

Om onderzoek te kunnen doen moeten de randvoorwaarden goed zijn. Dat deze goed zijn bij MaTe blijkt uit de goede technische ondersteuning van Patrick en Leo, wat computers betreft, en door Sjef, Toon, Rob en Ab wat experimenten betreft, waarvoor ik hen dan ook wil bedanken.

Hoewel de experimenten in de 'inspirerende' omgeving van het ESRF geen concrete resultaten opgeleverd hebben, heeft het verblijf in dit magnetische veld, waar je ieder gevoel voor tijd en richting verliest, toch het nodige inzicht verschaft. Naast het werkschema van 8 uur op en 8 uur af was het toch vooral gezellig, zeker als je bij onderhoud een dagje kunt gaan skiën. Bernard, Frank, Bas en de mensen van SKT bedankt. Van deze laatste groep wil ik Ilse van Casteren, Michael de Graaf, Jules Kierkels, Han Goossens en Sanjay Rastogi in het bijzonder bedanken voor hun hulp bij en doen van 'de meer scheikundige' experimenten.

Uit de meeste proefschriften blijkt wel dat je de nodige kamergenoten 'verslijt' gedurende je aio-loopbaan. Voor de zinnige en (on)zinnige discussies, gezelligheid en lunch-

ontspanning gaat mijn dank dan ook uit naar Nathan, Ad, Marco, Ron, Edwin, Jesus en Varvara. Ook het spelen met de in merendeel inmiddels gepromoveerde collega's bij AntILOpe was een zeer welkome afwisseling.

De inspannende ontspanning van sport was voor mij vrijwel onmisbaar. Hiervoor wil ik de spelers, trainer en begeleiders van 'het 1^{ste} van Berg' dan ook bedanken. Ondanks de wisselende prestaties en successen is 2 keer promoveren in 2 jaar niet slecht.

Mijn speciale dank gaat uit naar mijn familie en vrienden voor hun vertrouwen en steun gedurende de afgelopen jaren. Zeker mijn ouders die maar eens te meer bewijzen dat een sterke wil een doorzetttingsvermogen je uiteindelijk (dicht) bij je doel brengen.

Last but certainly not least wil ik Nanda bedanken. Niet alleen voor haar steun en vertrouwen, maar ook voor alle geduld en begrip toen het boekje 'bijna' af was.

Curriculum Vitae

The author was born on July 25th 1973 in Roermond and spent his youth in Lerop (St. Odiliënberg). After finishing his secondary education in 1991 at Bisschoppelijk College Schöndeln in Roermond, he studied mechanical engineering at Eindhoven University of Technology. He obtained his Masters' Degree in March 1997 after completion of his thesis 'Experimental validation of VIp RTM simulations' in the group of prof. Han Meijer. Before he started his PhD-study in October 1997, which resulted in this thesis, he did a short project on the influence of water absorption on the mechanical properties of flax/PP-composites. During the PhD-period the author completed the course Register Polymer Science (Register Polymeerkundige) organised by the National Dutch Research School (PTN).

